Emerging Soft Conductors for Bioelectronic Interfaces

Dace Gao, Kaushik Parida and Pooi See Lee*

D. Gao, Dr. K. Parida, Prof. P. S. Lee

School of Materials Science and Engineering

Nanyang Technological University

50 Nanyang Avenue, Singapore 639798, Singapore

E-mail: pslee@ntu.edu.sg

Abstract: *Bidirectional interfacing between electrode and biological system has enabled diagnostics and therapeutics in modern medicine, however the inherent dissimilarity between the soft, ion-rich, dynamic biological tissues and the rigid, dry, static electronic systems hinders the establishment of effective and reliable bioelectronic interfaces. In the past decade, the scope of flexible/stretchable electronics has been broadened into bioelectronics owing to the need of implementation of various biocompatible soft conductors. This review discusses the basic requirements for the construction of both epidermal and implantable bioelectronic interfaces utilizing soft materials, and summarizes the most recent progress in the development of soft conductors which are customized to interface with skin and other tissues. The conclusion provides an outlook on the remaining obstacles and outlines possible strategies to facilitate the technological advances in bioelectronics.*

1. Introduction

Bioelectronic interface is the general designation of miscellaneous bio-integrated electrodes that function to communicate with biological systems. Bioelectronic interfaces can be established either on human skin[1-3] or inside human body.[4-7] In terms of target applications, the interfaces are constructed for either physiological signal recording[1, 2] or electro-stimulation/modulation.[8-10] Despite the various modalities and form factors of existing bio-electrodes, the design and fabrication

of high-performance bioelectronic interfaces are guided by some universal principles,[5, 11] such as low interfacial impedance and intimate integration with curvilinear tissue surfaces. However, the inherent disparities between biological tissues and artificial electronics cannot be ignored. At epidermal interfaces, human skin is breathable, but electronics typically require stringent encapsulation for prolonged lifetimes. At implanted interfaces, tissues are soft, water-borne, and ionically conductive, but conventional electronics are rigid, water-exclusive and electronically conductive. As a result, significant challenges are encountered when coupling rigid electrodes with curved, complex and dynamic tissues of human body.

Recent advances in soft bioelectronics, with a focus in the development of flexible/stretchable conductors,[2, 7, 12] have brought on novel opportunities to eliminate physical and mechanical mismatches and enable compliant electrode coupling to biological tissues. Consequently, epidermal electronics utilizing soft conductors as electrodes can be deployed in seamless contact with the skin surface and hereby inhibit motion induced artifacts,[1] whilst soft electrodes/probes-based implants can accommodate dynamics of inner tissue and help to prevent scarring and inflammation.[5, 13] To this end, this review highlights the latest progress in soft bioelectronics, with a particular attention in the synthesis, preparation and integration of biocompatible soft conductors which have the potential to reshape nearly every aspect of clinical diagnostics and therapeutics in the near future. We firstly introduce the existing platforms for physiological recording and stimulation, based on which the rational guidelines are summarized for the fabrication of both epidermal and implantable soft bioelectronic interfaces respectively. Following that, recently developed soft conductors are categorized and discussed with different emphases. Finally, we conclude this account with an overview of unsolved difficulties and future research directions for soft bioelectronics.

2. Epidermal Bioelectronics

2.1. Epidermal Signal Recording

Being the largest organ of human body, our skin not only serves as a self-healable barrier against external stressors, but also permits the sensation of tactus, and regulates body temperature, peripheral circulation, as well as fluid balance. The realization of above-mentioned functionalities is enabled by the intricate anatomy (**Figure 1a**, left): capillary blood vessels, lymphatic vessels, peripheral nerves and sweat glands are densely distributed at different layers of the skin (epidermis, dermis and hypodermis); these plexuses are hierarchically connected to the central systems and substantially linked to remote organs deeply inside the body. Therefore, instead of being a static shielding layer, the skin is a dynamic and complex source providing a wide range of physiological signals that reflect the overall health and fitness conditions. Three primary types of physiological information, including physical, electrical and chemical signals (Figure 1a), can be measured by wearable or on-skin sensors.[1, 3]

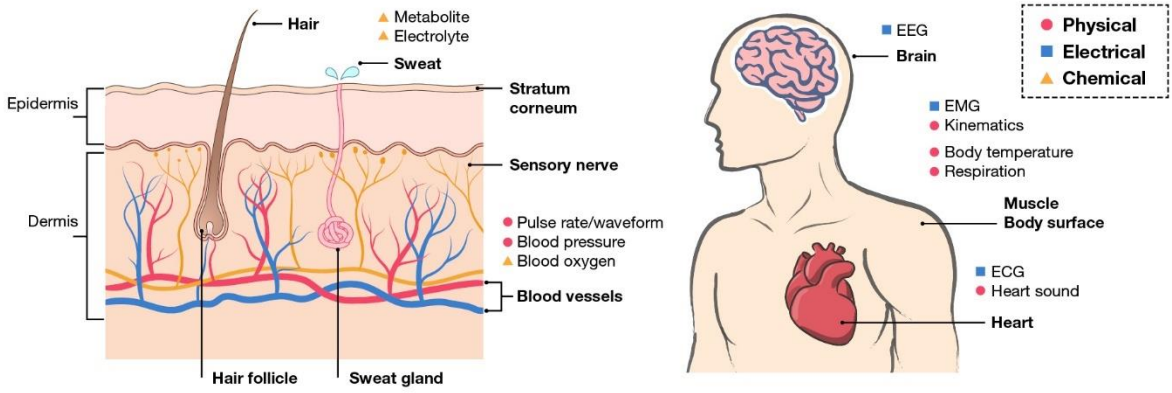

Figure 1. Schematic of skin anatomy and the summarization of various physiological signals accessible from epidermal sensors.

For physical signals, skin-conformal strain, pressure, optical and temperature sensors have been developed to monitor body movements (daily activity, essential tremor),[14] cardiovascular status (heart/pulse rate, blood pressure)[15-18] and other vital signs such as body temperature,[19-21] respiration conditions and skin mechanophysiology (**Figure 2a**). Apart from physical bio-feedbacks, electrical (electrophysiological) signals represent another class of measurable physiological information that is derived from action potentials generated across the membranes of activated neurons or muscle

cells.[11] The concurrent propagation of action potentials will superpose into tissue-scale potentials[22] and emanate to skin surface, which can then be captured by high-resolution electrogram methods in a noninvasive manner. Electrocardiography (ECG)[20, 23, 24] records the depolarization and repolarization of cardiac muscle cells in heartbeat cycles, with the spectrum of which providing detailed information about cardiac abnormalities like rhythm disturbances and inadequate blood flow in coronary artery. Electroencephalography (EEG)[25] measures the biopotential waveforms of brain via electrodes assembled on scalp surface. As human brain is a huge collection of neurons associated by synapses, the synchronized activation of thousands of neurons will generate detectable impulses of localized potential, which can be interpreted based on pulse frequency (alpha, beta, gamma waves, etc.) for the studies of cognitive processing, sleeping patterns,[26] neural diseases and so on. Similarly, electromyography (EMG)[9, 27-29] detects neurological activation of skeletal muscle by recording biopotential variation in muscle cells. The resulted electromyogram is used as a tool for diagnosing neuromuscular diseases and for controlling prostheses. Examples of recent progress in soft electrogram sensors are shown in figure 2b.

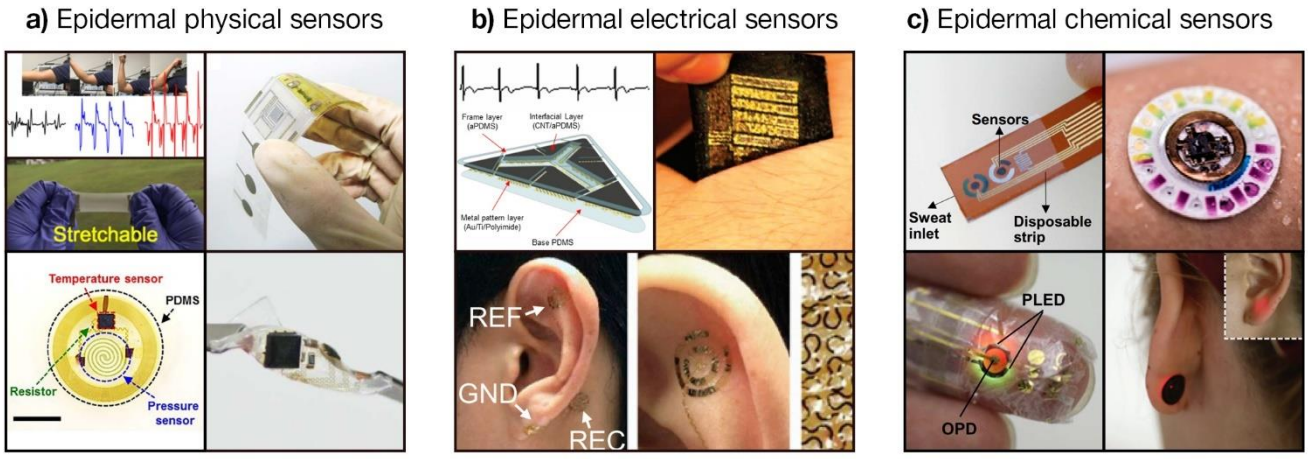

Figure 2. Epidermal bioelectronic sensors.

Wearable and skin-attachable chemical sensors for sweat analysis (Figure 2c, top) have been extensively studied in terms of epidermal chemical sensing.[30] Sweat is one of the most important secretions that contains a broad class of biomarkers,[31, 32] including various ions (sodium, calcium,

potassium and chloride), metabolic molecules (glucose, urea, lactate acid, uric acid) and even macromolecules like peptides and proteins.[33] As the widespread eccrine glands in dermis continuously and directly secrete sweat onto skin surface, sweat is featured as an ideal biofluid for target analytes sampling with easy accessibility and noninvasiveness. Most of the reported on-skin sweat sensors are generally based on electrochemical methods, wherein working electrodes are decorated with active materials that selectively respond to certain species. Specifically, enzymes (such as glucose oxidase and lactate oxidase) are widely used in molecular identification via amperometry,[34-38] whereas specially treated ion-selective membranes allow for ion concentration measurement via potentiometry.[39-42] Recent advances in this field include simultaneous screening[19] of multiple biomarkers by a multiplexed sweat sensing platform, the implementation of epidermal microfluidics[43-46] for enhanced sweat collection, routing and chrono-sampling, and the integration of colorimetric transduction techniques[47-50] for real-time analyte identification. Similar platforms, such as glucose sensing contact lenses[36] and tooth-mounted sensors,[51] have demonstrated potential applications in analyzing other external secretions like saliva and tear.

On-skin electronics for noninvasive blood monitoring has also emerged as a nascent area in healthcare. Blood glucose level has important clinical relevance to diabetes, while the oxygen saturation level is a critical indicator for the management of respiratory diseases.[52] Since blood flows in vessels with indirect accessibility, traditional blood testing always relies on invasive blood drawing process which causes pain and pinprick to patients. To reduce such discomforts during blood sampling, novel epidermal solutions have been developed based on soft optoelectronics. For example, a flexible pulse oximeter was fabricated based on soft organic photodiode (OPD) and organic light-emitting diode (OLED).[53] Hemoglobin in oxygenated or deoxygenated state yields different absorptivity to light at certain wavelength, therefore the device can accurately quantify oxygen level via optical tests. Similar epidermal oximeters (Figure 2c, bottom) are reported recently with improved skin conformability (3 μm in device thickness)[54] and miniaturized size (as small as a coin).[55]

2.2. Epidermal Stimulation

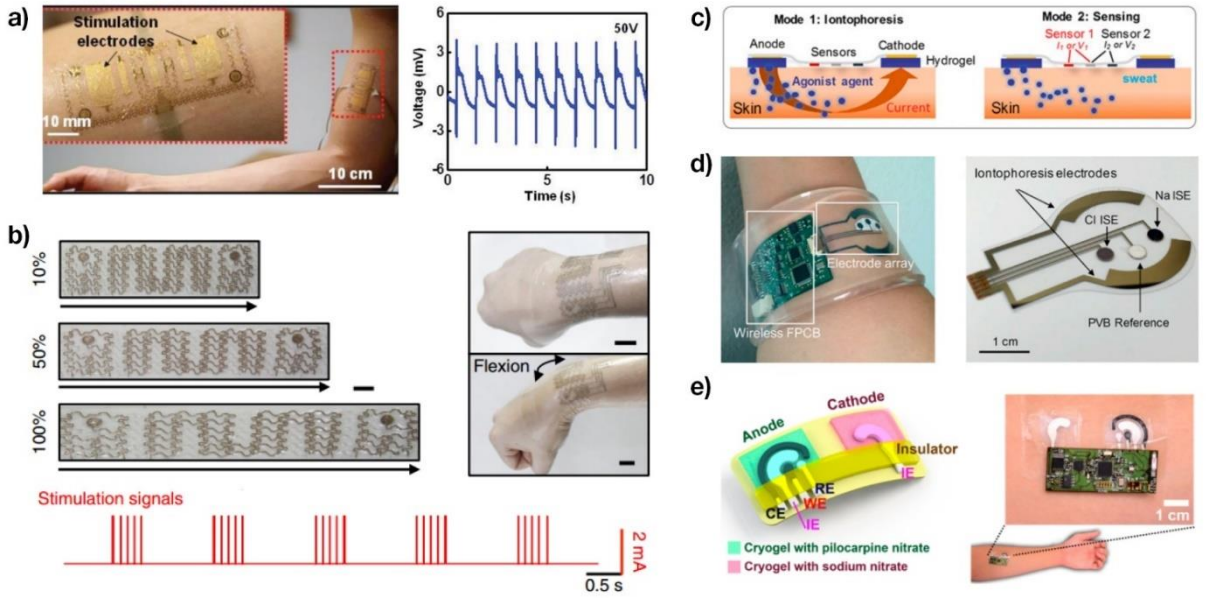

Figure 3. Epidermal stimulating devices.

Epidermal electronics can function not only as sensors, but also as actuating platforms for stimulations. Transcutaneous electrical nerve stimulation (TENS) is a classical and widely used epidermal stimulating method, and its application in electrotactile stimulation[9, 56, 57] emphasizes the usage of on-skin electrodes to inject small amplitude of current flow into skin, which stimulates the mechanoreceptors distributed throughout epidermis, dermis and subcutaneous tissue (hypodermis)[58] and elicits tactile sensations including light touch, pressure and vibration.[56] **Figure 3a** is the photograph of a multifunctional epidermal system that measures EMG, temperature, strain and delivers electrotactile stimulation simultaneously.[9] The coaxial stimulation electrode can supply constant-current pulse input (3 mA, 20 Hz and 0.2 ms pulse width) and yield in-phase voltage response in skin. Another recent device demonstrated by Choi *et al.* integrates thermal stimulation in conjunction with electrotactile stimulation and can operate under strain as large as 100% (Figure 3b). Such epidermal recording and stimulating technologies have been employed in neuromuscular rehabilitation,[59] pain relief[60] and fatigue prevention, and may find promising usefulness in bidirectional communicating with prostheses,[61] in which context an amputee is expected to exert

control to artificial limb via EMG, meanwhile experience tactile and proprioceptive feedbacks by applying electrotactile stimulation at the reinnervated skin sites.[9, 62]

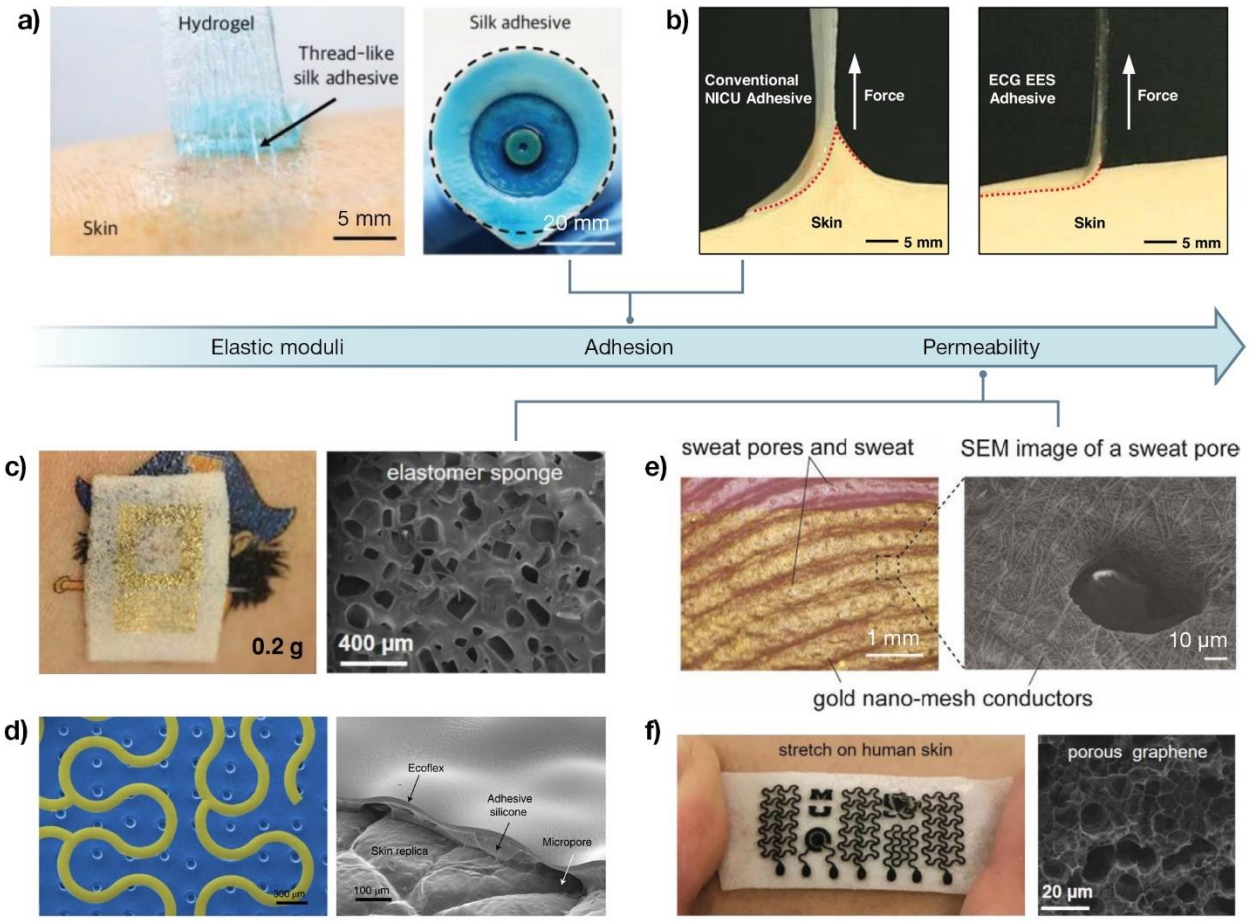

Figure 4. Material requirements for epidermal interfaces.

Epidermal stimulating platforms have also expedited the research progress in sweat sampling. Most of the above mentioned epidermal sweat sensors only perform properly when the volume of sweat sample reaches certain threshold (≥ 10 μL). The rate of sweat secretion in our daily life, in a circumstance where a person is not undergoing vigorous exercise, can be too low to sustain the requirement of on-demand and in situ sweat sampling. In this case, a well-developed on-skin stimulating method, namely iontophoresis,[34, 63, 64] provides the opportunity to control sweat excretion at specific time and targeted location. Figure 3c illustrates the mechanism of iontophoresis for sweat induction and on-site analysis.[63] Sweat stimulating agonists, such as pilocarpine, acetylcholine and methacholine, are applied between anode and epidermis. Injection of mild electrical

current assists the transdermal delivery of agonists so that the sweat glands are stimulated to secrete. Such sweat generating approach inspired the development of a fully integrated and autonomous wearable platform which can program the profile and interval of sweat extraction (Figure 3d).[63] In this device modality, agonists are loaded within a thin layer of hydrogel to supply long-term use, and the selection of different compound will lead to different patterns of sweat secretion. Electrochemical electrodes placed in between the stimulating electrodes provide on-site analysis of biomarkers immediately after iontophoresis. Similarly, a tattoo-based multifunctional system was also demonstrated with integrated iontophoresis and alcohol sensing functionalities (Figure 3e).[34]

2.3. Material Requirements for Epidermal Interfaces

Physiological diagnoses in conventional clinical practice always employ bulky and stationary instruments with a forest of wiring, meanwhile the sensing or stimulation electrodes attached to human skin tend to be stiff and nondeformable, which leads to significant mechanical mismatches at the bioelectronic interfaces. Hence, the impetus of developing epidermal bioelectronics (smart skin) is to provide comfort, mobile and continuous health monitoring or treatment in a noninvasive and wireless manner. The long-term intimate integration between abiotic-biotic systems addresses not only the importance of material properties and structural designs, but also the quality of interfaces concerning biocompatibility, adhesion, permeability and contact impedance, etc. Critical requirements for desired bio-integration are discussed as follow.

Studies in biomechanics indicate that human epidermis consists of a thin layer (50 - 100 μm) of soft tissue with an approximate modulus ranging from 20 kPa to a few hundred kPa,[65] and the skin can sustain up to 15% tensile strain in its elastic region.[66] Therefore, the formation of compliant contacts between electronics and epidermis emphasizes the usages of soft material systems, which may comprise polymeric substrates, conductive electrodes and active substances, with similar effective moduli and other physical properties in the preparation of epidermal electronic devices. Although plastics such as polyimide (PI),[43, 67, 68] polyethylene terephthalate (PET)[20] and

polyethylene naphthalate (PEN)[69] can render high flexibility by reducing thickness (< 5 μm), their high Young's moduli (> 1 GPa) and non-stretchable nature still lead to sub-optimal contact with the curvilinear and wrinkled epidermal surface, and make it impractical to accommodate skin's dynamic bend, stretch, and compression during body movements. The strategy of adopting intrinsically stretchable elastomers as thin-layer substrate is effective in reducing the modulus gap. Elastomers with Young's moduli similar to that of epidermis (< 200 kPa) have been widely exploited for epidermal interfacing and the representative examples are summarized in Table 1.

Table 1. Summary of representative soft elastomers used for epidermal integration.

Material	Elastic modulus	Commercial name	Manufacturer	Ref
Low-modulus silicone	~20 kPa	Solaris	Smooth-on	[25]
Low-modulus silicone	~60 kPa	Ecoflex 00-30	Smooth-on	[9, 16, 70]
Low-modulus silicone	~150 kPa	Dragon Skin 10	Smooth-on	[15]
Adhesive PDMS (aPDMS)	~27.5 kPa	MG 7-9850	Dow Corning	[24]
Ultrasoft silicone	~5 kPa	Silbione RT Gel 4717	Bluestar Silicones	[16, 29, 70]
Silicone sponge	~80 kPa	N/A	Mölnlycke Health Care AB	[48]
Porous silicone	~15 kPa	Dragon skin 10	Smooth-on	[28]
Modified polyester	~60 kPa	N/A	BASF	[66]

Apart from rational selection in the mechanical attributes of supportive substrates, adhesive coupling at epidermal interfaces should be further implemented to ensure reliable measurement and to prevent delamination. In electrophysiological diagnostics, the existence of small air gaps between epidermis and electronic patches is prone to artifacts and poor signal-to-noise ratio (SNR) because of increased contact impedance;[11, 71] in sweating sampling, the interspace can reduce sweat collecting efficiency and produce errors in analytical results. A simple approach to epidermal adhesion is based on van der Waals forces alone, as long as the patch is sufficiently thin and compliant.[25, 72] Several

biocompatible adhesives have also been developed to enhance long-term adhesion and remove the interfacial gaps, including microporous silicone,[73] adhesive polydimethylsiloxane (aPDMS),[24] polyvinyl alcohol (PVA) gel[74] and calcium-modified silk (**Figure 4a**).[23] Adhesion strength should be carefully modulated to mitigate peeling force during device removal (Figure 4b).[72]

With regards to the usability of skin-mounted electronics, gas permeability represents another critical consideration for the design and preparation of bio-integrated substrate and electrode materials. Most commercially available plastics or elastomers possess low gas permeability,[75] which blocks perspiration and increases the risk of skin allergies and inflammation. Recently, progress has been made in developing textile-based electronics,[29, 76, 77] and introducing porous structures into elastic silicone (figure 4c).[28, 48] Another work demonstrates the fabrication of microperforated soft silicone via microsphere-templated method (figure 4d),[73] wherein the breathability can be tuned by adjusting the density of pores. Besides, highly permeable and non-irritative conductors, such as conductive Au nanomesh (Figure 4e)[27] and laser-induced porous graphene (Figure 4f),[28] have also been developed and integrated into biocompatible sensors. Future epidermal electronics is expected to address the above-mentioned concerns simultaneously so as to deliver soft, inflammation-free and adhesive epidermal interfaces with low contact impedance and exceptional breathability.

3. Implantable Bioelectronics

3.1. Neural Interfaces for Signal Recording and Neuromodulation

Similar to the versatile physiological information collected by epidermal sensors, biosensing devices implanted in human body monitor the condition of our internal body from all physical, electrical and chemical aspects. For instance, physical signals such as intracranial pressure and temperature can be monitored in vivo by an optical sensing system,[78] while chemical information such as blood oxygen level can be detected by a subdermal oximetry.[79] Nevertheless, the most important aspect of implantable devices lies in neural signal recording and modulation via directly interfacing the nerve with invasive electrodes. Bidirectional communication between nerves and foreign electronics is

established by directly interfacing conductive electrodes with neural tissues or cells. These electrode-based neural interfaces can be classified depending on their implantation sites, the electrode geometries and the degree of invasiveness.[80] Generally speaking, central nervous system (CNS) of human consists of brain and spinal cord, while peripheral nervous system (PNS) describes the nerve network that spread throughout the body. Electrophysiological recording and stimulation in both CNS and PNS are crucial for diagnostics and therapy of neural diseases. The so far developed neural interfaces are configured either in plane format, such as the epidural/subdural flat electrodes[81, 82] enveloping cerebral cortex and the cuff electrodes[83] wrapping around PNS nerve fibers, or in needle-shaped geometry that penetrates tissue surface for high-resolution applications.[84, 85] More detailed discussion about neural anatomy and electrode configurations can be found in several comprehensive reviews.[13, 80]

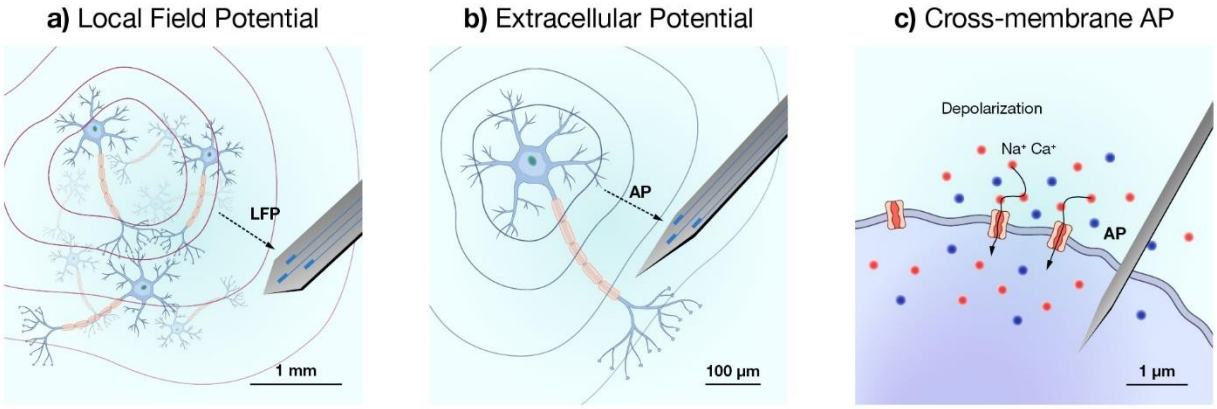

Figure 5. Neural signals recorded at different length scales.

The spatiotemporal resolution of neural signal recording depends on the length scale at which the interface is built. In cellular scale, action potentials or spikes generated from an individual neuron represent the elementary signal in neural activity. In tissue scale, the summation of action potentials from a large population of adjacent neurons generates local field potentials (LFPs).[86-88] Electrocorticogram (ECoG) is as an invasive alternative of EEG which monitors superficial LFPs of the brain in mm scale.[82, 89-91] Compared to EEG, ECoG exploits implanted epidural/subdural multielectrode arrays to eliminate noise from sources between dura and scalp, and hereby enhance

the SNR. The superficial signals acquired from ECoG contain low frequency oscillations (0.1 – 120 Hz) and provide limited information about deep brain neural activities. Moving towards deeper nerve region and higher spatiotemporal resolution, the wideband measurement of LFPs utilizing penetrating probes are employed (**Figure 5a**).[6] Such technology samples LFPs from a small cluster of subcortical neurons around the insertion site at higher frequency (> 300 Hz) to reflect more localized oscillatory signals, however it still cannot distinguish single neuron activities from the collection of LFPs. Further reducing the size of probing interfaces down to cellular and even subcellular scale makes it possible to isolate individual neuron action potentials. For example, extracellular potentials (~ kHz) from a specific neuron can be picked up at a distance smaller than 100 μm (Figure 5b),[84, 92] while action potentials across the cell membrane at nanometer scale are detectable by intracellular nano-probes (Figure 5c).[85]

While the neural recording platforms are commonly used as diagnostic tools, neuromodulation also finds great importance in neuronal activity manipulation, clinical treatment and neural prosthetics.[10, 93-95] Electrical stimulation at neural interfaces shares similar principles with neural signal recording but operates in a reverse manner. For signal recording, the action potentials or LFPs propagating in extracellular environment are captured by sensing electrodes via different mechanisms (capacitive, faradic and transistor, etc.). In the case of neuromodulation, external power source supply voltage to the interfacing electrodes to fire neuronal activities through charge injection. The faradic charge injection mode involves electrochemical reaction with direct electron transfer from an electrode to the electrolyte-filled extracellular region, while the more desired capacitive charge injection mode is a physical process which modulates the charging/discharging of electrical double layer (EDL) formed at the electrolyte-electrode interface. Detailed explanation and analysis about various neural sensing and stimulating mechanisms are elaborated in previous literature reviews.[7, 11]

3.2. Material Requirements for Neural Interfaces

Neural tissues are ultra-soft (< 10 kPa), compliant and constantly undergoing micro and macroscopic motions.[13] For instance, the seemingly static human brain is actually a pulsatile organ which continuously receives flow pulsation from the network of embedded blood vessels; the spinal cord, as well as the numerous peripheral nerves can experience up to 20% tensile strain during our daily activity.[13] Conventional implantable electrodes made out of noble metals and silicon (**Figure 6a**)[96] are chemically inert with favorable conductivity, yet their Young's moduli (~ 100 GPa) are orders of magnitude higher than that of the targeted neural tissue. Such mechanical mismatch will inevitably introduce tissue damage and neuroinflammatory during invasive implantation and subsequent chronic operation.[13, 97, 98] In the past decade, the fast growing research interest in soft electronics have inspired strategies to improve mechanical biocompatibility of neural interfaces. Pioneer studies in this field have proved that extreme flexibility can be achieved in ultrathin plastic films (epoxy,[82] parylene C,[89, 90] PI[67, 79] and PEN) despite their GPa-level Young's moduli. The reduced flexural rigidity makes it possible to establish coherent interfacing between ultrathin devices and wrinkled neural tissues (Figure 6b),[82] while the application of structural engineering, such as reconfiguring a continuous sheet into mesh structure,[81] can further enhance the compliance of thin film neural interfaces. The resultant ultrathin plastic electronics meet the requirement of conformability but still fail to accommodate the dynamic motions of our neural system. In recent progress, implants for use in vivo are manufactured with biocompatible elastomeric substrates to reversibly extend and relax following the micro and/or macroscopic motions of the neural tissues in direct contact. Several recently developed neural interfaces, such as a neural recording electrode grid (Figure 6c)[99] and a multimodal electronic dura meter,[100] are prepared to be stretchable by using silicone materials with ~ 1 MPa Young's moduli as substrates or matrices, but the moduli of these elastomers are still higher than the neural tissues and unable to serve as mechanically matched neural interfaces. Following this path, the development in hydrogel-based bioelectronics[11, 93, 101-104] may finally close the gap of mechanical mismatch at the electrode-tissue interfaces. Compared to dielectric elastomers, hydrogels are even softer with tissue-like modulus (in kPa range) and can preserve over 90 wt% of water to

mimic the living environment of neurons. By dissolving electrolytes[105] or blending conductive fillers[93, 106, 107] into hydrogels, ultra-soft ionic or electrical conductors (Figure 6d) can be fabricated as promising tissue interfacing electrodes for further implants. The advances of hydrogel bioelectronics will be discussed in detail in the later sections.

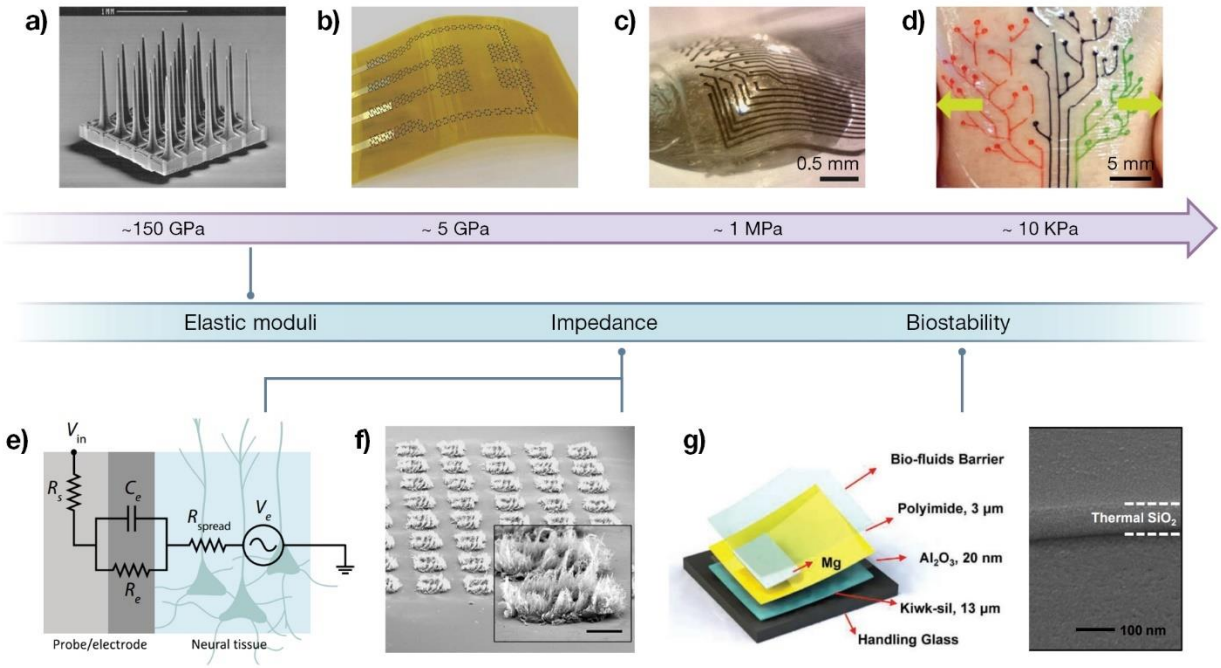

Figure 6. Material requirements for neural interfaces.

Impedance management is another key challenge confronted by high performance neural interfaces. The effective interfacial impedance between the neuron/neural tissue and the recording/stimulating electrode can be depicted by the equivalent circuit as shown in Figure 6e,[5] which contains the leakage resistance (R_e) and the EDL capacitance (C_e) in parallel at the electrode-tissue interface, and the resistance attributed to the intracellular/extracellular environment (R_{spread}). For both bioelectronic recording and stimulation, a low-impedance interface established with high C_e and low R_e is highly desirable for the purpose of reducing the operational voltage, avoiding irreversible electrochemical reactions and increasing the charge injection capacity (CIC). However, the pursuit in better signal sampling resolution and higher current injecting precision has led to a continuous reduction in electrode size with the side effect of increased R_e and reduced C_e. Therefore, the difficulty lies in how

to boost C_e while maintaining a minimized geometry in electrode footprint. To address this, modifying the surface of flat electrodes with porous nanomaterials[108, 109] or volumetric conductors[110, 111] can successfully translate C_e from a flat areal EDL into a volumetric EDL capacitance[112] and thus provide higher effective surface area. Figure 6f shows the morphology of an array of porous graphene electrodes in situ grown on PI substrate using laser pyrolysis[109]. After chemical doping, this flexible cortical microelectrode can achieve a small impedance of 519 Ω at 1 kHz (two orders of magnitude lower than a similar-size Au electrode) and a CIC as high as 3.1 mC cm^{-2}. Likewise, conductive polymer coating on flat electrodes also allows drastic reduction in the interfacial impedance ascribing to their porous nature and ion transporting capability.[110, 111]

A third material-related parameter worth considering is the long-term biostability of implantable bioelectronics. Chronically implanted devices are immersed in a wet, ion-rich and chemically reactive biological media. When implants become exposed to such a harsh internal environment, negative impacts including mechanical degradation, metallic oxidation/corrosion and impedance fluctuation will be triggered upon electrodes in lack of proper protection. Furthermore, the toxic by-products of biofouling can in turn exacerbate tissue damage and inflammation. Recent efforts in soft bioelectronics aim at improving the biostability of neural interfaces without compromising their intrinsic softness and neural recording/stimulating capabilities. The majority of these approaches involves adopting electrode materials with substantial resistance to biofluids,[90, 93, 110, 113] and developing soft and defect-free biofluid barriers with lifetime outlasting decades or more. A recent work exploits ultrathin SiO_2 layers grown at high temperature to encapsulate flexible electronics for chronic implants.[114] This thermal SiO_2 barrier excels previous encapsulation schemes in biofluids blocking performance owing to its low permeability to water and the elimination of defects. Capping the SiO_2 layer with 100 nm thick HfO_2 via atomic layer deposition (ALD) can further block ion diffusion and significantly reduce the hydrolysis rate of SiO_2 at high temperature (Figure 6g).[115] For further work, water- and ion-blocking elastomers with tissue-like Young's modulus are highly expected to be developed and applied in implantable bioelectronic devices.[101]

4. Metallic Materials and Composites for Bioelectronic Interfaces

4.1. Metallic Nanomembranes

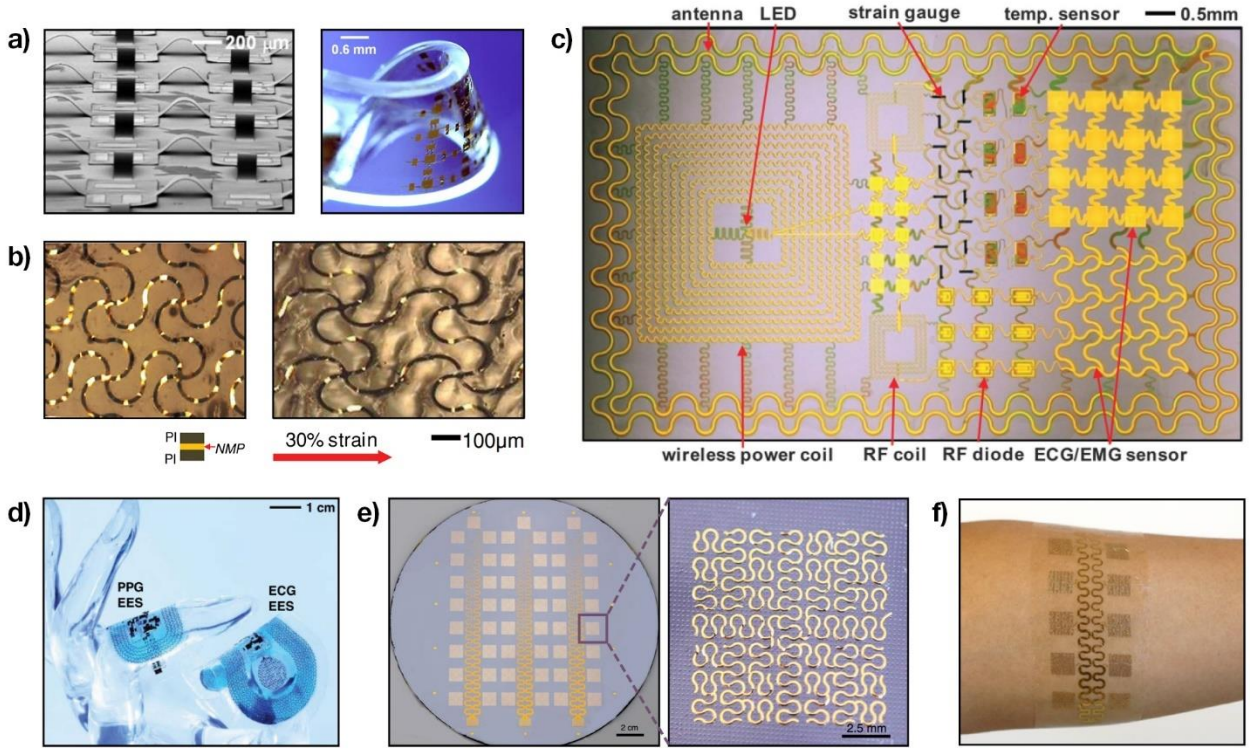

Figure 7. Metallic NMs based bioelectronic interfaces.

Other than developing intrinsically soft and stretchable conductive materials, engineering approaches that exploit micro/nanoscale forms of conventional inorganic conductors/semiconductors have also been widely studied and established to serve as bioelectronic interfacing electrodes.[116] The pivotal principle underlying these engineering methods is derived from structural mechanics: no matter how rigid a material is, it can always be rendered flexible in a sufficiently thin form as bending stiffness scales cubically with film thickness. Recent advances in microfabrication and thin film transferring processes have enabled the fabrication of ultra-flexible metallic nanomembranes (NMs) with 20 – 500 nm in thickness. Further configuring the NMs into "deterministic geometries" yields conductive systems that not only flex but also stretch and compress following the deformation of underneath elastomeric substrates or biological tissues. The "wavy" or "pop-up" structural NMs constructed

through a controlled bucking procedure is prevailing as stretchable conductors in wearables[117, 118] and soft robotics[119] (**Figure 7a**), whereas advanced designs in bio-integrated NMs commonly exploit filamentary serpentine (FS) mesh layouts without out-of-plane buckling for improved compliance and coherent lamination to epidermis and other tissue surfaces (Figure 7b).[120]

The fabrication of NMs-based stretchable electrodes is generally compatible with the state-of-the-art microfabrication techniques, wherein photolithography, electron beam deposition and reactive ion etching (RIE) are widely applied to achieve high resolution patterning and thickness control of the FS conductive traces. In the well-defined fabricating protocol developed by Rogers' group,[66] FS electrode (200 nm in thickness) in the open mesh layout involves 300 nm thick top and bottom PI encapsulating layers to place the NM layer at neutral plane, which helps to minimize bending induced strain. Au is commonly used for electrode deposition due to its biostability and good conductivity. The width of FS traces is assigned between 10 - 100 μm: while reduced width can significantly improve the conformability to skin topography and the mechanical robustness in integration,[121] it may adversely impair the electrodes' conductance at the same time. Therefore, the geometry of NMs electrode should be typically tailored for each target application. After being released from a supportive silicon wafer, the lithographically patterned FS electrodes can be transferred to thin (< 30 μm), low modulus elastomeric substrates for next-step epidermal bonding[25, 48, 122] or invasive implantation.[123, 124] For epidermal applications, the as formed NMs-on-elastomer composites serve as the basis of epidermal interfaces yielding skin-like effective moduli (< 150 kPa) and relatively large deformability up to 30% elastic strain,[125] which ensures conformal epidermal contact and robust on-skin operation at strains beyond the limit of skin (~ 15%). The resulting NMs can also be directly laminated onto skin without elastomeric substrates by direct printing, during which a thin layer (~200 nm) of adhesion (spray-on-bandage) is applied to facilitate transfer.[121] The substrate-free device has a total thickness of 800 nm, which is over 50 times thinner than the thinnest region of epidermis.[126] This ultrathin geometry further reduces bending stiffness and makes the device mechanically imperceptible to end users. The versatility of such systems has offered capabilities for

various types of physiological measurements, such as body temperature,[21, 68] strain,[121] pressure,[68] sweat analytes,[48] ECG,[16, 121] EEG[25, 73] and EMG,[121, 125] as well as electrostimulation for transcutaneous neuromodulation[123, 124] and electrotactile interactions.[9]

While other soft conductors for bioelectronic interfacing are still in their early stages of development, metallic NMs-based stretchable electrodes have enabled the construction of sophisticated embodiments which not only provide superior performance and reliability, but also integrate abundant functional modules to achieve highly autonomous and untethered multifunctional bioelectronics. Benefitted from their compatibility with microelectronic protocols, components to be integrated together can be developed in a same process flow and interconnected via stretchable FS traces. As an example, in the firstly reported NMs-based epidermal electronic system,[66] various modules including strain/temperature/physiological sensors, light-emitting diodes, thin film transistors (TFTs) constituted active circuits, signal amplifier, wireless powering and communicating coils are already seamlessly configured together in one single device (Figure 7c). The latest progress in NMs-based epidermal interfaces features an initial success in clinical practice. Chung *et al*. developed a binodal vital signs monitoring system (Figure 7d) and conducted pilot feasibility testing and validation in a neonatal intensive care unit (NICU).[72] The ultrathin, skin-like measurement modules are constructed on the basis of abovementioned FS circuits, and can noninvasively and gently interface with neonates' fragile, underdeveloped skin in replacement of conventional rigid electrodes and invasive artery probes. Moreover, these devices operate in a fully wireless and battery-free mode thanks to the incorporation of an NMs-based antenna in compliance with near-field communication (NFC) protocols,[50, 122, 127] which allows for simultaneous wireless data communication and energy delivery via an individual link. As a result, this epidermal technology not only bypasses the limitations of current wired systems, but also provides clinical-grade physiological monitoring capabilities in EEG, temperature and blood pressure sensing. Another research interest in this field is to break the limitation in overall sizes and deliver epidermal interfaces which are several orders of magnitudes larger than the previous embodiments. To fulfill this, a proof-of-concept large-

area epidermal electrodes array was developed through a contact-mode photolithographic method (Figure 7e, left).[73] In this construction, 17 square-shaped fractal mesh electrodes (figure 7e, right) are patterned in parallel with each electrode representing a typical physiological sensing site. After releasing from the processing wafer, the electrodes array (17 cm in length) can be intimately laminated over large regions of human body, such as the full circumference of the forearm (Figure 7f). For the application in prostheses, the increased device size and electrode quantity enable such epidermal system to acquire multi-channel EMG signals from a residual limb to manage exquisite prosthesis control. In another practice of full-scalp EEG monitoring, the array provides the capability to record electrical activities across the whole brain area during functional magnetic resonance imaging (fMRI), which facilitates the concurrent collection of both spatial fMRI and temporal EEG signals as complementary information of brain activity.[128, 129]

Metallic NMs are also widely utilized as soft conductors in implantable bioelectronic devices for subdermal oximetry,[79] optogenetics,[130-133] neural interfacing,[100] neuroregeneration[127] and many other target applications. In general, metallic NMs cater to three major functions in these implanted systems, including (i) serpentine conductive interconnects for the linkage between functional modules; (ii) interfacing electrodes for physiological signal recording and electrostimulation; and (iii) coil antenna for wireless energy harvesting and signal transmission. Despite the functional versatility of NMs in the aforementioned works, their capability to operate in the harsh, humid and often salty internal environment of human body is still uncertain and has rarely been demonstrated. Rapid penetration of biofluid into the active electronic regions may lead to current leakage, metal corrosion and biofouling. Compliant, ultrathin encapsulating layers which can intimately bond to NMs and serve as effective biofluid barriers must be developed to prolong the effective lifetime of the metallic NMs-based implanted biosensors and stimulators.

4.2. Metallic Nanowires and Their Analogues

Nanocomposites formed by imparting metallic nano-fillers into elastomeric polymer matrices offer an alternative for stretchable and tissue-compliant bioelectronic interfaces.[2, 134, 135] In these stretchable conductors, conductive pathways are established upon the percolation network formed by interconnected nano-fillers, which could be metallic flakes,[136-139] nanoparticles (NPs),[140] nanorods and nanowires (NWs),[141] etc. It is worth noting that a higher filler ratio increases the conductivity but deteriorates the softness and deformability of the composite at the same time. Therefore, for the preparation of nanocomposites requiring both high conductivity and large deformability, one dimensional (1D) metallic NWs are more favorable than the other options as their high-aspect-ratio nature helps to reduce the percolation threshold, resulting in optimal conductivity and minimized influence on the mechanical property of the original elastomer.

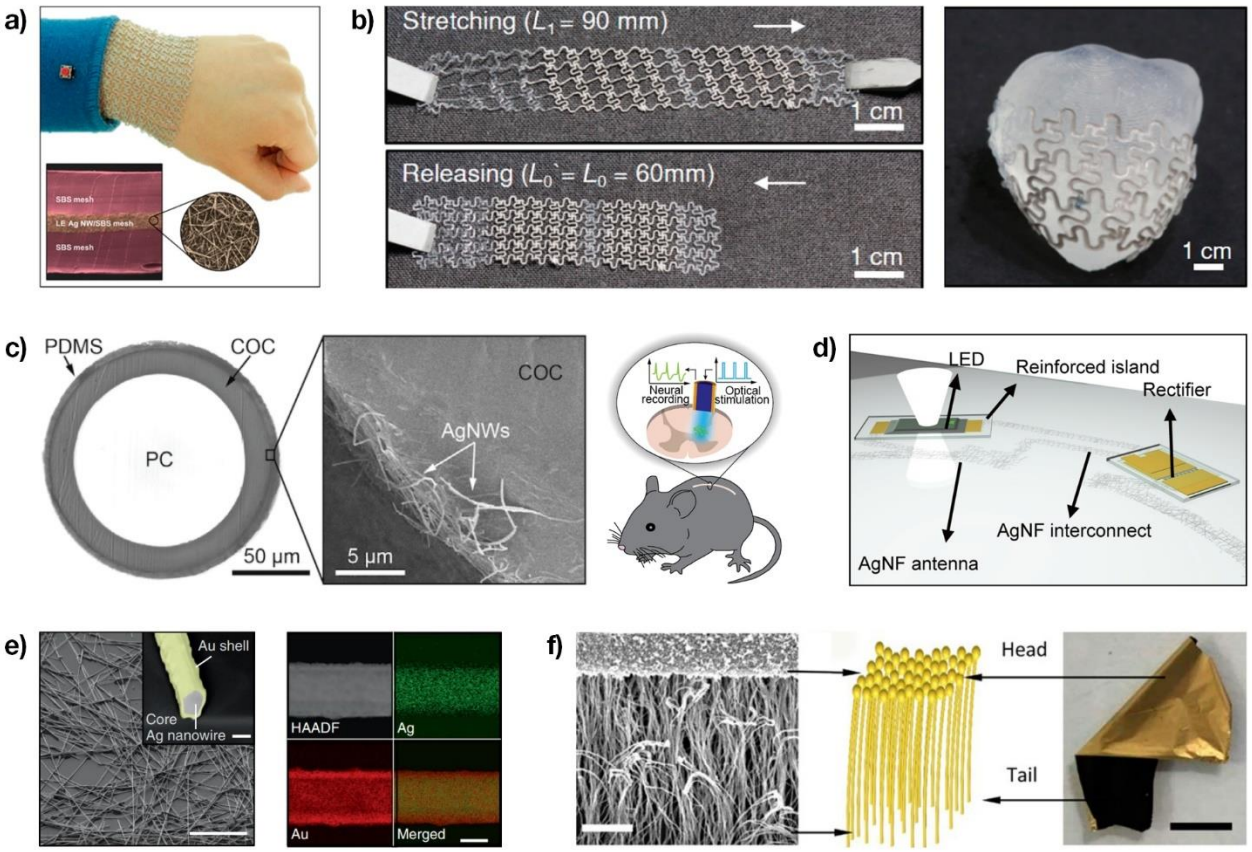

Figure 8. Metallic NWs and their analogues for bioelectronic interfaces.

Among all the representative metallic NWs, Ag nanowires (AgNWs) possess the highest intrinsic electrical conductivity and reasonable production costs. Several routes have been reported for the synthesis of AgNWs, among which the polyol approach is considered as the most efficient method due to its capability in mass production, low cost and ease of control.[142] As a result, AgNWs have been widely applied as conductive fillers in various elastomeric matrices. For example, a laminar AgNWs network embedded in the surface layer of PDMS reaches a pristine conductivity of ~ 8.1 × 10^3 S cm^{-1}. After several stretching/releasing cycles, the conductivity of the composite stabilizes at ~ 5.3 × 10^3 S cm^{-1} within 50% strain.[143] In another significant contribution, a AgNWs-based screen-printable ink was formulated to enable high-resolution patterning of stretchable conductor at a feature size of 50 μm.[144] The AgNW patterns inlaid in the shallow surface of polyurethane acrylate (PUA) exhibit rubbery stretchability and retains over 10^4 S cm^{-1} electrical conductivity at 70% strain. In light of their tunable mechanical property, outstanding conductivity and simple fabrication methods, AgNWs-elastomer composites are considered as ideal candidates for epidermal bioelectronics. For example, Choi *et al*. demonstrated a skin-mounted soft heater for articular thermal therapy (**Figure 8a**).[145] In this work, capping ligand bonded to the surface of AgNWs is modified by a ligand exchange reaction to facilitate homogeneous dispersion of AgNWs in nonpolar solvent (toluene) based styrene-butadiene-styrene (SBS) solution and enables one-step modelling of AgNWs-SBS elastic composite in the serpentine mesh design. Around 40 vol% of AgNWs loaded in the physically cross-linked SBS matrix yields an optimized conductivity of 1.1 × 10^4 S cm^{-1}, which allows for rapid temperature increase with only 1.0 V voltage being applied. Following up this work, the research group implemented the AgNWs-SBS composite in an implantable epicardial mesh to enable both ECG recording and cardiac electrostimulation (Figure 8b).[146] The composite mesh is configured as soft as cardiac tissue with a Young's modulus of ~ 44.7 kPa, therefore wrapping it around a moving rat heart for ECG measurement will not impede the heart's normal diastolic relaxation. When abnormal electrical conduction in diseased myocardium is detected, the therapeutic electrode can subsequently deliver electrostimulation to restore the global synchronous contractions. In another

example, Lu *et al*. developed resilient opto-electrophysiological neural probes by dip coating optical fibers with AgNWs then encapsulating with PDMS (Figure 8c, left).[147] The inherent stretchability of the probe permits deep implantation in the spinal cord of mouse, meanwhile the high conductivity of the AgNW network and low optical transmission loss at the PDMS-fiber interface can be maintained under spinal bending or stretching, allowing the probe to simultaneously deliver optical stimulations and record neural activities including single-neuron signals and LFPs (Figure 8c, right).

As an alternative to AgNW, one-dimensional, ultralong Ag nanofibers (AgNFs) could be directly electrospun into networks to produce stretchable and highly transparent conductors.[148-150] Park *et al*. demonstrated a wireless bio-sensing contact lens utilizing AgNFs-based electrodes as both antenna and interconnects of the functional modules (LED, glucose sensor and rectifier, Figure 8d).[36] The superior optoelectronic properties of the AgNFs network (~ 1.3 Ω sq^{-1} with 90% visible light transmittance) are beneficial for power transfer efficiency in the antenna and light transmission. In addition, the network exhibits good stretchability with less than 10% resistance increase under 30% tensile strain, making it both compliant to the curvilinear eye surface and mechanically durable for long-term wearing.

For chronically implanted bioelectronic devices, the usage of Ag nano-fillers as interfacing electrodes may introduce some negative effects. Due to the high tendency of being oxidized, Ag nanomaterials are prone to corrosion and biofouling in the biological environment.[151] On the other hand, Ag ions leached out from Ag are cytotoxic and potentially harmful to human health.[152] To tackle such issue, Choi *et al*. developed a Ag-Au core-sheath structured NW via galvanic-free deposition of Au on AgNWs (Figure 8e), wherein the Ag core confers high electrical conductivity, while the inert and bio-stable Au sheath ensures biostability and prevents ion leaching from the Ag core.[113] After the coating process, highly stretchable (~ 266 %) and conductive (~ 4.2×10^4 S cm^{-1}) (Ag-Au)-SBS nanocomposites could be produced following the procedure mentioned above with the assist of hexylamine ligand. To confirm the Au shell's capability of inhibiting the Ag core from ion leaching, both in vitro and in vivo experiments were performed. The in vitro results indicate that only

trace level (65 ppb) of Ag ions was detected in the artificial biofluids exposed to the Ag-Au nanocomposite for 3 days, which is ~ 80 times lower than the Ag ion level found in those exposed to bare AgNWs. The implantation of two different types of nanocomposites in rats further proves that the Au shell can effectively reduce Ag ions' accumulation in all organs.

Although Au nanowires (AuNWs) are costly in mass production and difficult to synthesize, the rationale to employ them in bioelectronics lies in their exceptional biostability and minimal cytotoxicity.[153-155] For example, AuNWs have been incorporated within alginate hydrogel to facilitate cell cultures.[106] For the cultivation of engineered cardiac patches, AuNWs in the composite help to electrically bridge adjacent cardiac cells and considerably reduce the overall film impedance compared to the pristine alginate film. As a result, the inclusion of AuNWs is advantageous to preparing high quality cardiac patches with stronger contractile strength. Recently, Wang *et al*. reported a success in the synthesis of vertically aligned AuNW films as extremely stretchable and biocompatible epidermal electrodes.[156] The "Janus" film contains a densely packed nanoparticle layer on top and a vertically aligned NW layer at the bottom (Figure 8f). Such unique feature promotes efficient electron hopping in the nanoparticle layer no matter how the NW layer deforms and helps to maintain sufficient conductivity even under 800% tensile strain. Based on this AuNW film, an intrinsically stretchable glucose biosensor was demonstrated by decorating the vertical AuNWs with glucose oxidase and Prussian blue nanoparticles.[37] The biosensor has a glucose sensing resolution of 10 μM and can provide a moderate sensitivity even under large deformation.

5. Low Dimensional Nanomaterials for Bioelectronic Interfaces

5.1. Carbon Nanotubes and Graphene

Carbon nanotubes (CNTs) are highly conductive, 1D nanomaterials which have received extensive research interests since discovery. CNTs are classified as single-walled carbon nanotubes (SWCNTs) and multi-walled carbon nanotubes (MWCNTs), and they can display either semiconducting or metallic charge transportation depending on the structural chirality. The utilization of CNTs in

biomedical applications was initially hindered by their short length (< 1 μm), poor dispersity in polar solvents, and the lack in purification methods.[157] Recent advances in CNT synthesis and morphology control has led to the preparation of ultralong SWCNTS (> 1 mm) with aligned spatial orientation during chemical vapor deposition (CVD) growth,[158, 159] meanwhile the improvements in chirality control, purification and functionalization have enhanced the biocompatibility of CNT-based bioelectronic interfaces.

CNT assemblies can achieve large surface area and volumetric capacitance while interfacing with biological tissues, therefore they have been actively investigated as functional coatings for implanted neural probes to reduce interfacial impedance and consequently improve the SNR of recorded neuron spikes.[7, 160, 161] CNT fibers fabricated through wet-spinning have been utilized as implanted microelectrodes with great softness, low impedance and chronic biocompatibility.[162] In vivo test by implanting the CNT fiber probe into rat cortex suggested an overall reduction in inflammation response compared with rigid metallic probes. For the construction of stretchable conductors, the high-aspect-ratio CNTs are ideal candidates to form percolation networks within elastomer matrices,[163] or they can be assembled as laminar composites[164] on the top surface of elastic substrates to provide superior conductivity even under large deformation. Thereby, the use of CNT-based stretchable conductors have also yielded many fundamental progresses in epidermal bioelectronics.[2] For instance, skin conformal CNT electrodes can be employed as ECG sensors for long-term health monitoring even under movements.[24] In another example, semiconducting CNTs are patterned as the channel material for stretchable TFTs to achieve robust operation under deformation. Such TFTs allow for the implementation of differential logic circuits which can nullify the strain-induced signal errors.[165] More recent work developed an autonomous self-repairing electronic skin by embedding a CNT percolation network in the shallow surface of a self-healable PDMS.[166] After bisected cut and self-healing at room temperature for 24 hours, the reconnected composite only increased slightly (~ 17%) in resistance, and could still sustain large tensile stretch. Such result suggests that the dynamic movement of the modified elastomer also enables the

reconstruction of CNT nanostructured networks. Based on this stretchable and self-healable composite, a multifunctional electronic skin system integrating the functions of ECG sensing, strain monitoring and light emitting was successfully demonstrated.

As a representative two dimensional (2D) carbon material, graphene has obtained significant attention for various bioelectronic devices[167] due to its fast electron transfer property, excellent chemical and thermal stability, high surface-to-volume ratio and superior mechanical properties such as being soft, intrinsically flexible, and mechanically robust. In recent years, graphene has achieved good yield production through CVD or reduction from graphene oxide.[168] Meanwhile, it has been used in several biomedical applications including bioimaging, drug delivery, anti-bacterial coating, tissue engineering, three-dimensional (3D) scaffolds for tissues, and DNA-sequencing.[169-171] Recently, it has also emerged as one of the most promising nanomaterials for epidermal and implantable bioelectronic devices for its excellent conductivity, biocompatibility, and mechanical compatibility with skin and tissues.[172, 173] The intrinsic biocompatibility of graphene is an interesting attribute for bioelectronic devices as it helps to reduce inflammatory responses and facilitates stable and long-term skin-mounting or implantation. The biocompatible of graphene can be effectively tuned via surface chemical functionalization to improve the interaction of graphene with biological tissue.[169, 174] Extensive work has been done to evaluate graphene's biocompatibility with cells and neural tissues.[175, 176] Park *et al*. found an increase in the density of neurons growth on monolayer graphene compared to that of glass substrates, due to the effective adhesion of human's neural stem cells with graphene.[177] Biocompatible 3D graphene scaffolds have also been developed for facilitating biological cell growth, proliferation, and differentiation.[178]

The amplitude of action potentials and LFPs generated from the brain is extremely low in the order of a few mV.[179] Thus, one of the most desirable properties of implanted electrodes is the high spatial and temporal resolution. This can be achieved by reducing the interfacial impedance of the electrodes with neural tissues to improve SNR and reduce baseline noise. Microelectrodes with extremely small footprints are essential for effective neural recording from single neuron at cellular level, yet

simultaneously reducing the size of the electrode and maintaining good SNR is still a huge challenge. To address this issue, Kuzum *et al*. developed a highly flexible graphene microelectrode with low baseline noise and improved SNR compared to that of Au electrodes for in vivo neural recording in an anaesthetized rat (**Figure 9a**, top).[180] The improved SNR can be credited to the high conductivity and low charge transfer resistance, which was improved by p-type doping, specifically by exposing the graphene to nitric acid to absorb electropositive nitrate groups (NO_3). The recording of spiking activity from brain using the doped-graphene electrodes exhibits a reduction in the noise level by 6 times compared to Au electrode (Figure 9a, bottom). The noise level can be further reduced by adopting other techniques such as surface functionalization, patterning to increase reactive sites, and alternative doping strategies to increase the density of active sites.[181]

Besides, the high charge storage capacity of structured graphene with high effective surface area can also increase the amount of interfacial charge transfer to improve SNR.[5, 11] The CIC of electrodes for neural stimulation needs to be above a certain level to trigger a functional response.[179] The amount of charge injection from the electrode depends on the EDL capacitance of the electrode in contact with neural tissues, however single/few-layer graphene has limited surface area and relatively low EDL capacitance. To increase EDL and reduce interfacial impedance, Lu *et al*. reported porous graphene electrodes (Figure 9b, right) with high surface area and EDL capacitance, making the SNR suitable for rodent cortical stimulation and sensing.[109] Figures 9b (left) shows the photograph of the highly flexible porous graphene electrodes array conformally mounted on the pial surface of mouse cortex for in vivo cortical recording. Cyclic voltammetry of the porous graphene electrode demonstrates higher charge transfer capacity compared to Au electrode (Figure 9c). Even after a million biphasic stimulation cycles, there was no significant degradation in the device performance, thus indicating a stable electrode for bioelectronics. Apollo *et al*. used laser induced reduced-graphene oxide (rGO) embedded in parylene-C as high CIC electrode for stimulating retinal ganglion cells and recording neural activity from cat visual cortex.[182] Extensive work has been done to improve the capacitance of graphene-based materials in the active research domain of batteries and

supercapacitors, therefore inspiration can be derived from other research fields for the development of high capacitance graphene electrodes for implantable bioelectronics.[183, 184]

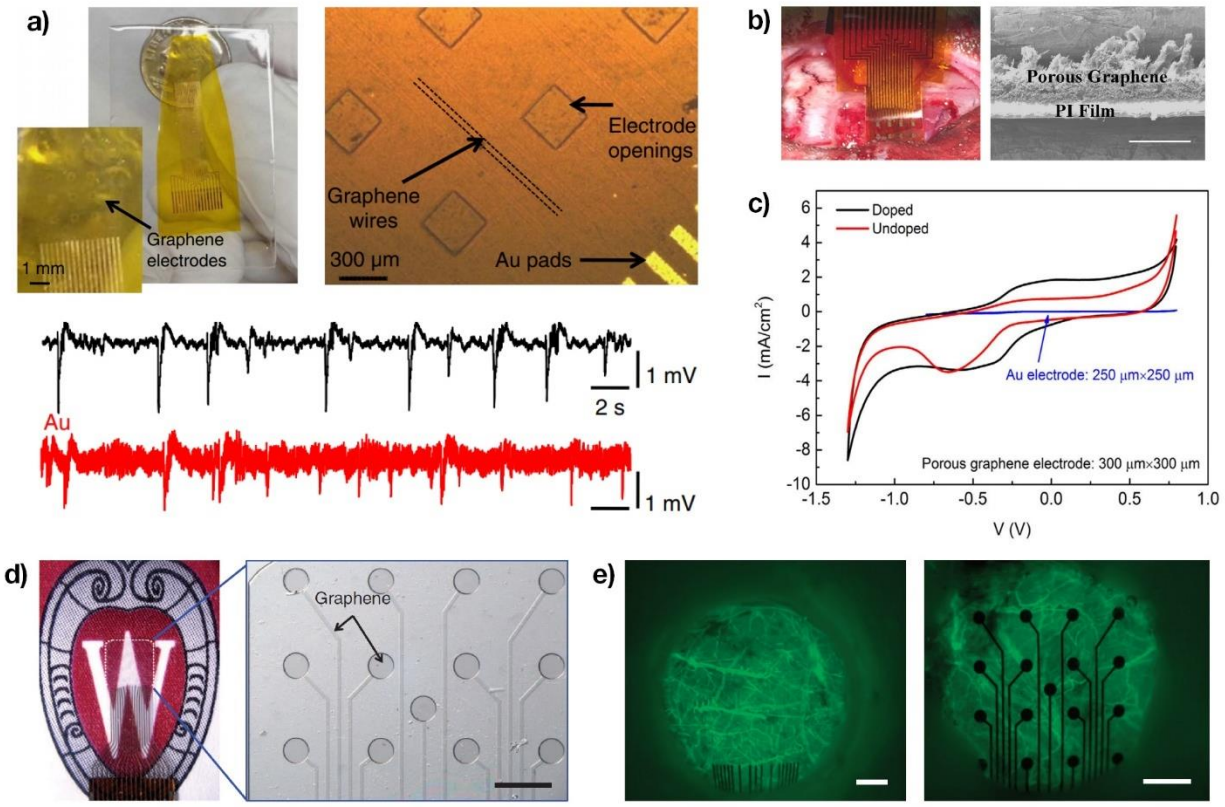

Figure 9. Graphene based bioelectronic interfaces.

Simultaneously recording electrical signals and optogenetically stimulating the nerve tissues is of great significance for neural treatment and recovery.[185] Furthermore, obtaining in vivo image of neural activities during implantation is beneficial for obtaining information of both the interface and the neural tissues surrounding it, which can significantly improve the process of implantation.[186] However, traditional metallic-based implanted electrodes fail to provide in vivo imaging and optical simulation due to its opacity. Thus, it is extremely important to develop transparent electrodes for neural interfacing. Indium tin oxide (ITO) material is the most commonly used transparent conductor, but it is brittle, rigid, and mechanically incompatible with neural tissues. To address this issue, Park *et al*. developed a transparent and flexible electrodes array based on graphene for neural interfacing, optogenetical simulation and imaging.[90] The transparent electrodes were fabricated by CVD and

deposited on a parylene substrate, which leads to an over 90% transparency over a wide range of spectrum, from infrared to ultraviolet. Figure 9d shows the high transparency of the graphene microelectrodes. Besides, the electrodes have excellent mechanical properties such as being ultrathin, flexible, and conformal to neural brain tissues. Figures 9e (left) shows the fluorescence image of the transparent graphene microelectrodes conformally mounted onto the cerebral cortex of the mouse for simultaneous neural signal detection and optogenetical stimulation. Furthermore, Kuzum *et al*. developed a highly transparent and flexible graphene electrode used to record cortical electrophysiological signals and image the cortical area simultaneously.[180] These works demonstrate that graphene electrodes can be effectively utilized for optogenetic stimulation and in vivo imaging of the nerve tissues, along with recording and stimulating electrical signals due to their transparency combined with excellent mechanical and electrical properties.

Another important factor for ensuring long-term stability of the implanted electrodes is the chemical stability of the electrodes in biofluids. Metallic electrodes corrode in biological fluids, which increases the impedance over a period of time, thus degrading the electrodes' performance.[187] Kuzum *et al*. used graphene to improve the corrosion resistance of Au electrode by hindering the diffusion of molecules and faradic reactions at the interface between metal and biofluids.[180] The electrode showed stable performance even after 6 months in a phosphate-buffered saline environment, indicating that graphene can effectively act as a corrosion protective layer for metallic electrodes to ensure their chronic usage in harsh environments. Alternatively, another approach to reduce inflammatory reactions at the neural interface is to utilize the bio-functionality of the graphene to release biologically active anti-inflammatory molecules, for reducing immunochemical rejections interface.[188] Various biomolecules can be loaded onto graphene utilizing π-π stacking interactions, hydrogen bonding and hydrophobic interactions, to be delivered at the neural interface.[160, 189] Graphene can also be modified by incorporating functional groups such as hydroxyl, carboxyl, and amino to further increase the loading capacity of biomolecules.[190]

5.2. MXenes

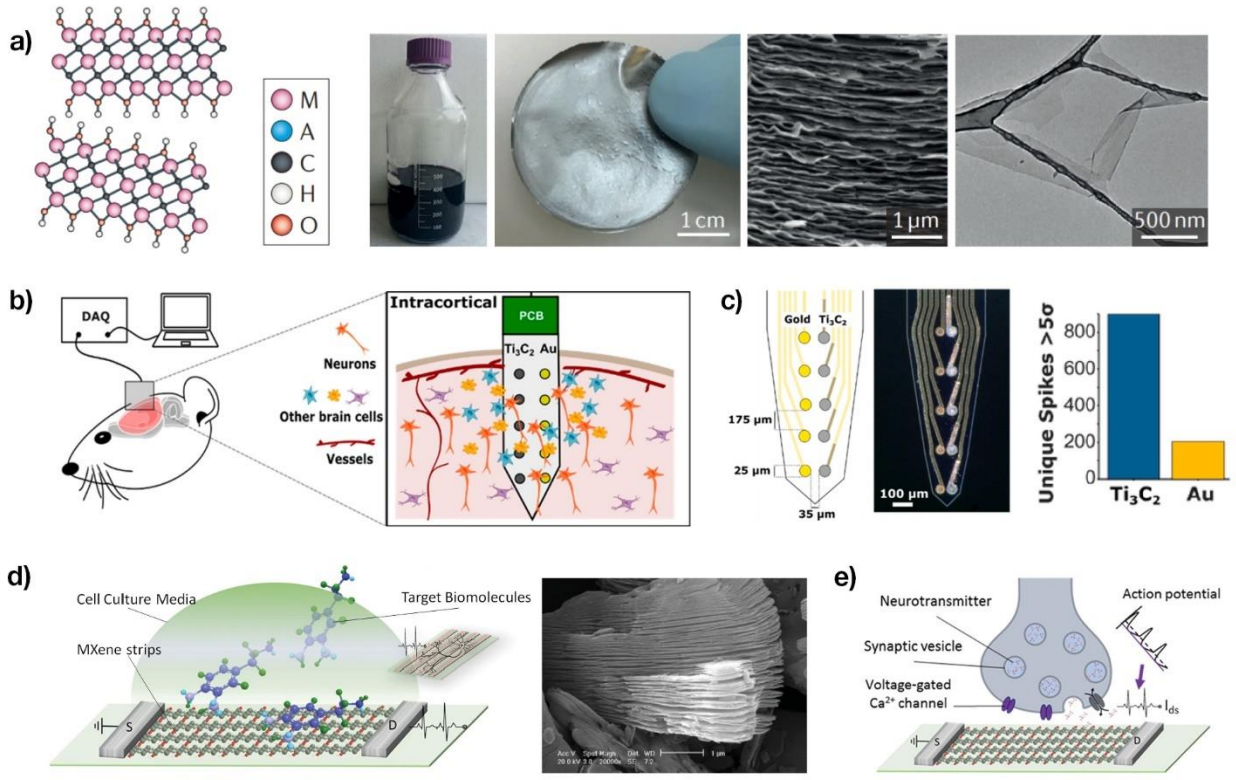

Figure 10. MXene based bioelectronic interfaces.

Encouraged by the discovery of atomic nanosheet of graphene, the intensive research interests in the 2D field have expedited the synthesis of many novel 2D materials.[191] Recently, MXenes, a new class of 2D layered materials, have gained significant focus due to their diverse physical and chemical properties.[192] MXenes are synthesized by etching sp-group elements from MAX phases, which are a cluster of 3D layered materials (metal carbides, carbonitrides, and nitrides) with a general formula of $M_{n+1}AX_n$ (n = 1 - 3). In this formulation, M is the d-block transition metal element such as titanium, chromium, vanadium and so on, A is the sp-group element such as groups 13 and 14 elements, and X is either carbon or nitrogen. Till date, more than 60 varieties of MXenes have been synthesized with a myriad of different properties.[193] **Figure 10a** shows the schematic of MXene's atomic structure, digital photo of delaminated MXene dispersed in water, digital photo of freestanding MXene film prepared by vacuum filtration, SEM image of a Mxene film's cross-section, and TEM image of a single-layer MXene flake. Hydrophilicity is an uncommon characteristic of carbon-based

nanomaterials, which hinders their aqueous solution processability. However, MXenes are hydrophilic due to the abundant functional groups on their surfaces. Therefore, simple and scalable solution processes can be adopted to fabricate MXene electrodes. Owing to their excellent metallic conductivity (~10,000 S cm^{-1}), high volumetric capacitance (1,500 F cm^{-3}), favorable biocompatibility and superior mechanical properties, MXenes have been recently explored for various biomedical and bioelectronic applications such as biosensing,[194] diagnostic imaging,[195] cancer theranostics,[196] and neural implantations.

Recently, the biocompatibility of MXene with biological cells was established by systemic injection of MXene for cancer theranostic applications.[196, 197] Furthermore, the biocompatibility of MXene with neural tissues was evaluated by studying the cytotoxicity of the in vitro growth of cortical neurons on MXene electrodes.[198] Even after 1 week, there was no obvious difference in neuronal viability and neurite outgrowth per neuron compared to the polystyrene-based control sample. Although neural tissues are highly sensitive to environmental conditions and interactions, MXene does not affect their bioactivity. The neuron tissues grew, formed neural networks and adhered to the MXene substrate, indicating that MXene can effectively interface with neural tissues. MXene coating on implanted metal electrodes can inhibit surface oxidation and provide a mechanically compliant neural interface between implants and surrounding neural tissues.[199] Driscoll *et al*. reported a Ti_3C_2-based MXene electrode with high resolution, high SNR, low baseline noise, and low susceptibility to high-frequency interference for bioelectronic devices.[198] The electrode was implanted into the brain of an anesthetized rat to record signals at various spatial and temporal scales (Figure 10b). Schematic diagram and microscopy image of the MXene/Au intracortical electrode array is shown in Figure 10c (left). Spiking activity generated by the same neuron were recorded by adjacent MXene and Au electrodes. The MXene electrode demonstrated better SNR compared to that of Au electrode (Figure 10c, right) attributing to the high electrical conductivity, low interfacial impedance, and high volumetric capacitance of the 2D MXene electrode.

The detection of electrolytes, metabolites and pH value in biofluids can effectively predict the health condition of human.[167, 194, 200] Recently, MXenes have become potential candidates for biochemical sensors as their large surface-to-volume ratio and fast electron transfer feature facilitate fast response in biomolecule sensing.[167] For example, Lei *et al*. designed and fabricated a stretchable epidermal sweat sensor by incorporating a novel Ti_3C_2 MXene/Prussian blue composite.[201] Attributing to the exceptional conductivity and unique 2D morphology of MXene, this biosensor outperforms the previous ones with higher electrochemical sensitivity, sensing accuracy and larger linear detection range. In another work, Ti_3C_2 MXene was utilized to develop a flexible and highly sensitive transistor-based biosensor (Figure 10d, left) for the detection of dopamine.[202] The multi-layered structure of Ti_3C_2 MXene provides a high surface area for the interaction with biomolecules, leading to high sensitivity (Figure 10d, right). The MXene transistor can also be used for monitoring real-time spiking activities in primary hippocampal neurons (Figure 10e). When the action potential was fired, neurotransmitters are released and bound with MXene to induce a change in the electrical signal. Furthermore, Nafion solubilized Au/MXene nanocomposite was used to detect enzymatic glucose for the diagnosis of diabetes.[194] Owing to its high specific surface area, the device demonstrates high sensitivity (4.2 μA mM^{-1} cm^{-2}), excellent linearity (in the range from 0.1 mM to 18 mM), and low detection limit (5.9 μM). The superior in-plane electrical conductivity of MXene is further enhanced by incorporating Au nanoparticles on its surface, which improves the enzyme immobilization and increases the device sensitivity. Nafion with negative surface charge helps to eliminate the penetration of similarly charged species, thus improving the selectivity of the biosensor. Additionally, Song *et al*. developed a ratiometric pH sensor using Ti_3C_2 MXene quantum dots (QDs) to monitor intracellular pH values.[203] The surface of the Ti_3C_2 is functionalized with polyethylenimine (PEI) which exhibits blue photoluminescence attributing to surface defect emissions and bandgap transitions. Due to the protonation or deprotonation of the Ti_3C_2 QDs, it exhibits a pH-dependent luminescence behavior. There is a 10% decrease in the intensity of absorption spectra with a change of pH value from 5 to 9, thus indicating a highly sensitive pH sensor.

Several works have reported the development of gas sensors for monitoring health conditions.[200, 203-205] The mechanism of gas sensing is based on changing the conductivity of MXene by modulating the charge transfer process during the adsorption and desorption of gas molecules on its surface. Kim *et al*. reported using MXene for ammonia sensing. When ammonia molecules are absorbed on the oxygen-terminated MXene surface, excessive electrons will be injected into the electrode.[200] Kim *et al*. reported a MXene-based volatile organic compounds (VOC) gas sensor with extremely high SNR by utilizing the high metallic conductivity and the high functionalized surface of MXene.[205] We have recently shown that MXene can be used to adsorb and control release of aroma small molecules using efficient resistive heating due to its good thermal conductivity.[204]

5.3. Transition-metal Dichalcogenides

Apart from graphene and MXenes, 2D transition-metal dichalcogenides (TMDCs) constitute another important category in the family of 2D materials. TMDCs are described by a common formula of MX_2, wherein M is an optional transition metal and X is an element from chalcogen (S, Se, or Te). The arbitrary combination of transition metals and chalcogens delivers various TMDCs possessing a wide spectrum of electronic, optical, chemical and mechanical properties,[206, 207] meanwhile the enriched polymorphs and tunable electronic energy band of each TMDC material provide the possibility to cater for many intended biomedical applications. TMDCs could be synthesized by either top-down or bottom-up approaches.[207-209] The top-down method refers to mechanical exfoliation of bulky precursors to generate high-quality monolayers, however the yield is low, and precise control in flake size and shape is difficult to achieve. The bottom-up method, typically CVD growth, allows for the preparation of well size-controlled and single-crystalline TMDCs without the appearance of residue compounds, which is beneficial for the usage as bioelectronic interfaces.[209, 210] Recently, a molten-salt-assisted CVD process was developed to synthesize a wide variety of TMDCs whose precursors are of high melting points.[211] Besides, pure TMDCs are considered biocompatible with little cytotoxicity compared with many other nanomaterials, and the surface of TMDCs is free of

dangling bonds,[212] making them highly stable on skin and even in biofluids during long period of implantation.

Molybdenum disulfide (MoS_2) is one of the most extensively studied semiconducting TMDCs with a direct bandgap of ~ 1.9 eV.[213] Due to its remarkable chemical stability, optical transparency and high charge mobility,[214] MoS_2 has been regarded as a promising candidate for future flexible electronic systems. For example, MoS_2 can be patterned onto ultrathin and flexible epoxy substrate to form a skin conformal pressure sensor array,[215] and a more recent work demonstrates a highly flexible active-matrix tactile sensor using MoS_2 as backplane circuity and strain sensing module.[216] For biomedical applications, MoS_2 is mainly exploited for biochemical sensing in the modality of either TFTs or electrochemical transducers. In the first modality, MoS_2 serves as an ideal channel material with excellent switching characteristics and sensitive response to biomolecules (e.g. proteins and DNA) immobilized on the channel surface.[213, 214, 217-219] These TFT-based biosensors are preliminarily fabricated on rigid substrates and only applicable for in vitro biomarkers sampling. Recently, MoS_2 based TFTs have been processed on flexible PI substrate through a scalable method.[219] The sensor array exhibits a picomolar-level sensitivity to a typical type of matrix protein, and reveals impressive flexibility and durability by withstanding severe mechanical deformations. In the second modality, MoS_2 is employed as working electrodes in electrochemical systems. Wu *et al*. firstly presented the preparation of reduced MoS_2 with fast electron transfer rate in selected redox system,[220] which was successfully used to detect glucose and dopamine. A more recent work features a flexible glucose sensor by incorporating MoS_2 in the composite working electrode.[221] The detection limit of glucose is as low as 10 nM owing to the improved electron transfer rate facilitated by MoS_2. These initial successes in MoS_2-based biosensors pave the way for the integration of biologically benign TMDCs into advanced epidermal and implantable bioelectronic systems.

6. Organic Conductors for Bioelectronic Interfaces

6.1. Conductive Polymers

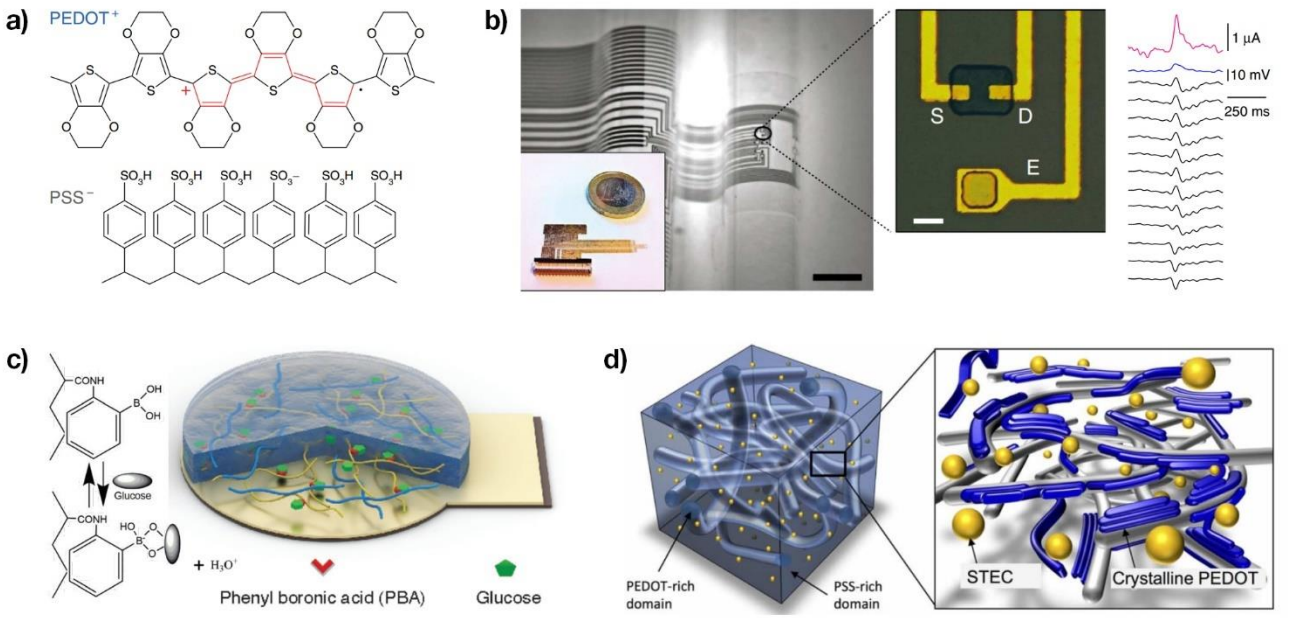

Figure 11. Conductive polymer based bioelectronic interfaces.

Conductive polymers such as poly(3,4-ethylenedioxythiophene) (PEDOT), polypyrrole (PPy) and polyaniline (PANI) have attracted great attention in bioelectronics considering their mechanical compliance, facile processability and synthetic tunability for targeted applications. The electrical conductivity of these polymers is originated from their conjugated backbones where delocalized electrons/holes exist. Further incorporating ionic dopants such as polyelectrolytes can introduce more charge transportation sites and hereby boost their electrical conductivity to a higher level. A prototypical conductive polymer being widely used is poly(3,4-ethylenedioxythiophene) doped with poly(styrene sulfonate); (PEDOT:PSS, **Figure 11a**). This compound is a heavily p-doped organic conductor with exceptional electrical conductivity (> 1,000 S cm^{-1}), biocompatibility and readily commercial availability as a solution-processible dispersion.[222] With sufficient hydration, PEDOT:PSS exhibits a mixed electronic and ionic conductivity[223, 224] as the electronic carriers are highly mobile in the polymer chains while ion-transporting pathways are established in the water-rich soft polymer matrix. Such unique feature of PEDOT:PSS has been leveraged in a variety of bioelectronic interfaces which can benefit from the mixed electronic/ionic conduction.[225-227] For

example, PEDOT:PSS coating has long been exploited for increasing the capacitance of miniaturized neural probes.[110, 228, 229] Since the coating layer is porous and possesses high ion-drift mobility, ions in the extracellular fluid can promptly penetrate the polymer matrix and create molecular-level EDL at the electrolyte/PEDOT chain interface. The resulted volumetric capacitance is orders of magnitude higher than the capacitance of areal EDL because C_e in this context is proportional to electrode volume instead of area.[112] As a result, the high volumetric capacitance can significantly reduce the interfacial impedance for both neural recording and stimulation with a small probe footprint.

The mixed electronic/ionic conductivity in PEDOT:PSS also enables other biosensing functions in the modality of organic electrochemical transistor (OECT).[230-234] OECTs share a similar device configuration with conventional field effect transistors (FET) wherein the source and drain electrodes are bridged with a channel. The major difference is that, instead of being gated across a dielectric layer, the organic channel material in an OECT is directly exposed to an electrolyte, which can be various biofluids in the context of in vivo and in vitro biological sensing applications. State-of-the-art OECTs utilizing PEDOT:PSS as channel material work in depletion mode: when excessive cations are injected from the electrolyte into the channel to affect the doping state (redox state in the language of electrochemistry) of PEDOT, electrical conductivity of the channel is impaired due to a decreased carrier density.[230] Such ionic-to-electronic signal transducing mechanism makes OECT an ideal candidate to monitor electrophysical signals associated with ion movements. The first in vivo application of flexible OECT recording cortex ECoG was demonstrate by Khodagholy *et al*.[233] As shown in Figure 11b (left), the transistor array was prepared on a 2 μm thick parylene thin film to render extreme flexibility and compliance to neural tissues. In vivo ECoG measurements on the somatosensory cortex of rats were performed concurrently using a PEDOT:PSS surface electrode, a penetrating silicon probe and an OECT, respectively. The superior SNR (44 dB) acquired from OECT was twice larger than that obtained from surface electrode (Figure 11b, right), revealing that the local signal amplifying capability of OECT is a key advantage in neural interfacing and ECoG recording. OECTs can also perform as noninvasive biosensors for the detection of biomarkers in human

secretions. For the detection of metabolites, the early-generation OECTs are fabricated on rigid substrates and rely predominantly on the interaction between the target molecule and its redox enzyme to achieve selectivity.[235, 236] Moving forward, soft and enzyme-free OECTs are developed recently as wearable biosensors. For example, an all-PEDOT:PSS-based textile OECT was prepared through screen printing and subsequent thermal annealing, wherein PEDOT:PSS modified fabrics are utilized as both channel and gate electrodes to detect oxidizable compounds (adrenaline, dopamine and ascorbic) without the assist of enzyme.[237] In a separate study, Wustoni *et al*. synthesized an enzyme-free conductive gel via a one-step electropolymerization procedure on flexible PI substrate (Figure 11c).[238] The gel electrode contains phenylboronic acid as an alternative to glucose oxidase and serves as the planar gate for a glucose selective OECT.

The organic bioelectronic devices introduced above are flexible yet non-stretchable since the high Young's modulus of PEDOT:PSS (on the order of GPa) merely allows for 5% strain before rupture.[239] Blending PEDOT:PSS with plasticizing additives can effectively impart deformability to the inherently stiff polymer. For example, the addition of a fluorosurfactant (Zonyl FS-300) at 1% volume ratio endows PEDOT:PSS with 30% reversible stretchability when bonded to a UV/ozone-treated PDMS substrate.[240] Triton X-100 is another nonionic surfactant which shows strong plasticizing effect when excessively added into PEDOT:PSS.[241] The as formed viscoelastic rubber with 0.7 wt% Triton X-100 reported by Oh *et al*. exhibits a maximum rupture strain at around 60%, however the insulating nature of surfactant harms the intrinsic conductivity of PEDOT:PSS. To avoid such drawback, Wang *et al*. incorporated ionic liquids into PEDOT:PSS to assist both extensibility and electrical conductivity simultaneously.[242] This impressive result was explained as a synergistic effect: the addition of ionic liquid weakens electrostatic force between PEDOT and PSS, allowing the formation of "hard" PEDOT conductive paths and a "soft" PSS matrix (figure 11d). The softened PSS region leads to higher fracture strain, meanwhile the PEDOT region with higher crystallinity enhances the electrical conductivity. Thus, the resulting PEDOT:PSS film has a high conductivity of 4,100 S cm^{-1} under 100% strain, and the maximum endurable strain is 800% before substrate fracture.

However, the cytotoxicity of fluorosurfactants and ionic liquids prevents the utilization of highly stretchable PEDOT:PSS as biocompatible interfacing electrodes. To tackle such issue, the same team followed up on the previous work and developed an implantable PEDOT:PSS-based neural interface by removing the ionic liquid additive through water exchange.[93] The resulted PEDOT:PSS hydrogel exhibits remarkable aqueous stability and biocompatibility, yet at a cost of decayed electrical conductivity and stretchability. Therefore, strategies that simultaneously boost the biological, mechanical and electrical performances of PEDOT:PSS should be developed with great attention for future conductive polymer-based bioelectronics.

6.2. Ionically Conductive Hydrogels

Traditionally, microfabricated silicon and metals are used as electrode in bioelectronic devices due to its chemical stability and non-toxicity.[5, 13] However, there exists a huge mismatch in Young's modulus (approximately in the order of 10^6 times) between conventional rigid bioelectronic electrodes and neural tissues. This leads to inflammatory response,[243, 244] scarring[245, 246] and immunochemical rejection in biological tissues, and results in the degradation in the device performance, depleting the life-time and reducing the safety margin of its operation. For effective integration of the implanted electronic devices with the biological tissues, one of the key criteria is Young's modulus matching between the interfacing materials and the surrounding biological tissues.

Hydrogels are compatible with the biological tissues due to their similar mechanical, chemical and ionically conductive properties, thus they are considered as suitable candidates for both epidermal and implantable bioelectronic devices.[251] Hydrogel mostly comprises 70 - 90 wt% of water, which is very similar to the water content of biological tissues.[252] Hydrogels are soft material with its mechanical modulus in the range of a few kPa (similar to that of neural tissues), in which the polymer matrix provides the required mechanical strength. The formation of the polymer matrix could be facilitated by chemical crosslinking, ionotropic crosslinking and physical interactions such as hydrogen bonding. Representative hydrogels with Young's modulus similar to biological tissues are

categorized in Table 2 with their synthesis methods, electrical and mechanical properties summarized. Recently, a few works have reported tough hydrogels formed by dense and robust hydrogel bonding with Young's modulus in the range of 1.3 - 5.4 MPa and fracture energy in the range of 600 - 4,500 J m^{-2}.[253] Furthermore, by utilizing the strategy of crack bridging by covalent crosslinks and unzipping the network of ionic crosslinks, extremely tough hydrogels have been reported with a fracture energy of 9,000 J m^{-2}.[254] Thus, mechanical properties of hydrogel can be effectively tuned for a variety of different applications.

Table 2. Representative ionically conductive hydrogels.

Polymer network	Charge carriers	Synthesis method	Ionic conductivity (S cm^{-1})	Young's modulus	Ref
PEG	Various salts	Chemical crosslinking	N/A	45 Pa	[103]
PEG	Na_2HPO_4/Na_2SO_4	Chemical crosslinking	7.71×10^{-3}	N/A	[105]
PAAm[a)]	LiCl	Chemical crosslinking	N/A	12 kPa	[247]
Silk fiber	$CaCl_2$	Metal ligand crosslinking	5.99×10^{-3}	160 kPa	[23]
PAAm	Polyelectrolyte	Chemical/ionotropic crosslinking	3.5×10^{-2}	N/A	[248]
PAA-co-DMAPS[b)]	NaCl	Dynamic ionotropic crosslinking	2×10^{-5}	27.6 kPa	[249]
PVA	$Na_2B_4O_7$	Dynamic hydrogel bond	2.9×10^{-5}	15 kPa	[250]

[a)] PAAm = polyacrylamide; [b)] DMAPS = 3-dimethyl (methacryloyloxyethyl) ammonium propane sulfonate

Hydrogels have been broadly used in many biomedical applications such as cell culture,[255] organ replacement, wound healing patches,[256] neural implantations, tissue engineering scaffolds,[257] and soft tissue adhesives.[258] There have been several reports on the use of hydrogels as a coating on existing rigid electrodes to increase their biocompatibility. Spencer *et al*. coated polyethylene glycol-dimethacrylate (PEG-DMA) hydrogel on glass capillaries electrodes (**Figure 12a**).[259] The Young's modulus of the PEG-DMA hydrogel was controlled by tuning the molecular weight and concentration of the macromer. After implanting the electrode into the rodent brain for eight weeks, the PEG-DMA

hydrogel coated sample showed a significant reduction in the reactivity of glial fibrillary acidic protein (GFAP). However, the glass capillaries-based electrodes are still rigid, making it unsuitable for long term implantation. To address this issue, Rao *et al*. coated polyethylene glycol-containing polyurethane (PU) hydrogel on soft PDMS rods.[260] After implanting the probes into the cortex of rat for six weeks, they observed a reduction in the neuronal cell loss and glial scarring at the location of implantation.

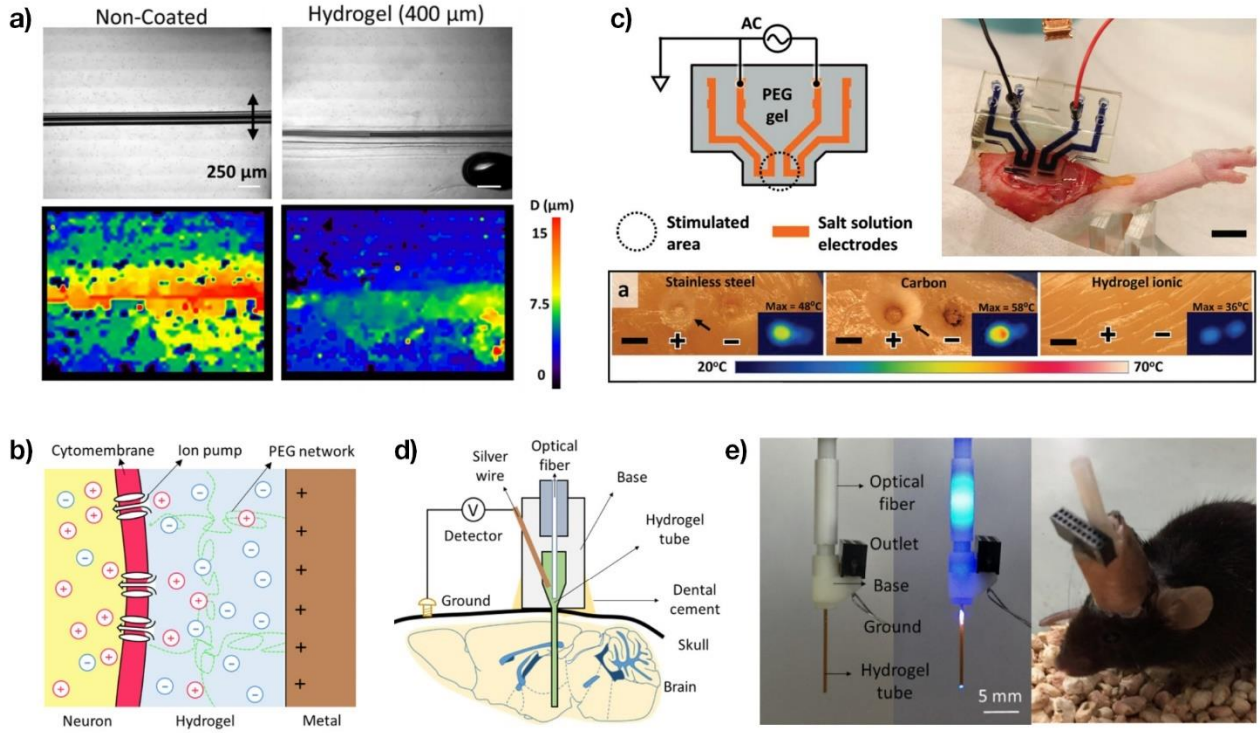

Figure 12. Ionically conductive hydrogel based bioelectronic interfaces.

Other issues associated with interfacing the bioelectronics devices (electrode array) with the nervous system is the electrode array degradation, and charge imbalance caused by the prolonged high-frequency stimulation.[261, 262] Typically, to restore charge balance, direct current (DC) is prevented from being transduced to the surrounding tissue by using a capacitor. However, capacitors are not effective at high frequency. Thus, the effective way is to develop electrode materials which prevents charge imbalance. Hydrogels provide a very high surface area which can effectively resolve the charge imbalance across electrode in electrical therapy-based nerve block applications. Gilmour

et al. evaluated the performance of hydrogel coated electrodes with commercially available bare Pt-Ir electrode for high-frequency nerve stimulation.[263] They observed that for both in vivo and in vitro conditions, the hydrogel coating on the nerve cuff electrode array improves the electrochemical properties and significantly reduced the impedance across the electrode and the nerve tissues at high frequencies. The hydrogel electrodes significantly increase the CIC of the electrode at lower voltage and power compared to metallic electrodes. This ensures safe operation and enables smaller and more spatially selective electrodes in implanted devices. Thus, the hydrogel-based electrodes are most suitable for high-frequency electrode stimulation for nerve block therapies.

Biological tissues are ionically conductive with a relatively low level of electrical conductivity (in the range of 0.1 to 1 S m^{-1},[11, 87] while metallic electrodes conduct electricity due to the flow of electrons. To stimulate the biological tissues, the electronic current in the metallic electrodes is converted to ionic current at the interface between ionically conductive tissues and electrically conductive electrodes through faradic charge injection or capacitive coupling. When the voltage drop across this interface exceeds a certain threshold, it causes localized heating, formation of chemically reactive species, and changes in the pH, thus leading to the degradation of the electrodes and severe immunochemical reactions that damage the biological tissues. Ionically conductive hydrogels can be used to partially alleviate the abovementioned issues. The conductivity of hydrogel is based on ionic current due to the transport of mobile ions, thus facilitating safe, seamless, and effective integration between electrodes and tissues by eliminating the conversion of electronic current to ionic current. Furthermore, the water content in the hydrogel electrodes helps to dissipate heat associated with current injection, thereby inhibiting burns and pains caused by conventional metallic electrodes.[105] The working mechanism of the hydrogel electrode is associated with the formation of an EDL capacitor across the hydrogel-metal interface (Figure 12b). The metallic electrode acts as the electronic conductor and hydrogel acts as the ionic conductor. Charge flow across the EDL is based on capacitive coupling, where no electrochemical reaction takes place at the EDL interface. The hydrogel electrode acts as a buffer layer between the metallic electrode and the biological tissue.[264]

During neural recording, action potentials fired by the neurons will simultaneously trigger ions' migration in the ionically conductive hydrogel, and subsequently induce current flow in metal. During neural stimulations, the applied electrical potential couples across the EDL at the hydrogel-metal interface and drives an ionic current in the hydrogel towards the neural tissue, which creates an electrical potential at the outer membrane of the targeted neural tissue, thus stimulating the neurons.[265]

Hydrogel-based ionic conductors typically possess relatively low ionic conductivity (10^{-4} - 10^{-3} S cm^{-1}) and slow response time due to the sluggish nature of mobile ions. Therefore, they are not suitable for certain applications such as monitoring high-frequency (>1,000 Hz) single neuron spikes. Low conductivity also leads to high interfacial impedance which can degrade the SNR during neural signal recording. Thus, it is essential to further improve the ionic conductivity of the ionic hydrogels. To address this issue, Zhao *et al*. fabricated a salt/poly(ethylene glycol) aqueous two-phase system (salt/PEG ATPS) based hydrogel which is compatible and stable in aqueous and living environments (Figure12c, top).[105] The PEG rich phase has low conductivity due to the low salt content and the salt-rich phase is highly conductive due to the high salt content. The high resistance contrast between the two-phase of the hydrogel facilitates the concentration of the ionic current in the salt phase, thus reducing the leakage current via PEG, which is desirable for the delivery of localized current. Based on this ATPS, ionic circuits were developed using UV-assisted bonding and micro molding. Owing to the low mechanical stiffness of the salt/PEG ATPS-based hydrogel, the dimension and shape of the ionic channels can be modified by external mechanical force. This hydrogel was implanted onto rat tibialis anterior (TA) muscle for electrical stimulation of muscle tissues. Various experimental results demonstrate that the developed hydrogel-based ionic stimulator is suitable for the transmission of sub-tetanic signals to skeletal muscle with reduced local heating and tissue damage compared with carbon and metal electrodes (Figure 12c, bottom).

In certain applications, achieving simultaneous neural stimulation and recording is essential. The conventional setup uses glass fibers to transmit light to neurons for neural stimulations, and employs

metal wires to record electrophysiological signals.[266] However, using two different materials/devices for stimulation and recording increases the degree of invasiveness and cannot locate the exact site of implantation. To address this issue, Sheng *et al*. reported a single fiber-based polyethylene glycol (PEG) hydrogel neural probe (Figure 12 d-e) that functions both as an ionic conductor (for electrical recordings) and as an optical fiber (for co-locating the site of laser stimulations) in the brain of a mouse.[103] After implantation, the PEG hydrogel acts as an interface between the metallic electrode of the detector and the cytomembrane of the neurons, and mimics the extracellular environment chemically by exchanging matter (such as ions, molecules, and water) with the neurons. The hydrogel in the frozen state is stiff, which facilitates its insertion into the soft brain tissue. After the insertion, it will become soft and mechanically compatible with the brain tissues. The PEG hydrogel as a neural interface shows less immunochemical rejections compared to metallic electrodes, thus enabling chronic operation in both in vivo and in vitro conditions.

6.3. Electrically Conductive Hydrogels

To further improve the interfacing performance of hydrogel-based bio-electrodes, enhancing both ionic and electronic conductivity without compromising the biocompatibility and the soft mechanical characteristics of hydrogel is becoming important. Electrical conductivity can be introduced to hydrogel by incorporating electrically conductive fillers. Polymer-based electrically conductive hydrogel is a hybrid material comprising interpenetrating hydrogel network and conductive polymer, such as PEDOT:PSS, PPy and PANI. The hydrogel network provides the required mechanical properties, and the conductive polymer provides the electrical conductivity.[225-227] Various approaches, including direct blending, in-situ and in-growth polymerization methods, have been devoted to develop electrically conductive hydrogels.[267-273] Table 3 summarizes the representative electrically conductive hydrogels including their formulations, synthesis methods, electrical and mechanical properties.

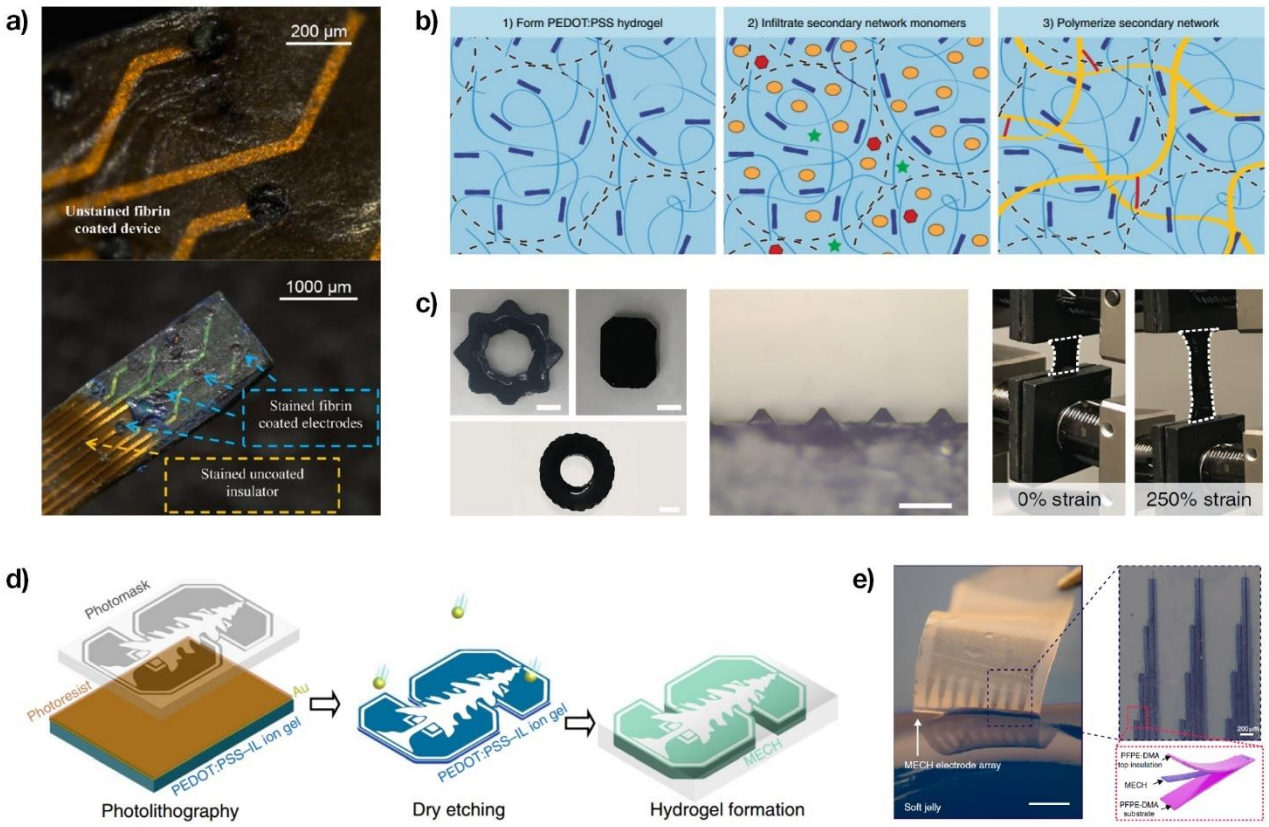

Figure 13. Electrically conductive hydrogel based bioelectronic interfaces.

Among all the conductive polymers, PEDOT:PSS-based hydrogels have gained significant attention in various bioelectronic devices.[226, 274] Kim *et al*. reported developing a conductive hydrogel coating to improve the neural recording capability of the electrodes.[272] Sodium alginate is used as the hydrogel matrix and PEDOT is used as the conductive material. The PEDOT significantly improves the recording functionality of the hydrogel electrode and helps to restore interfered electrical signals. Castagnola *et al*. also demonstrated a fibrin hydrogel coating with nanocomposite of carbon nanotube (CNT) and PEDOT nanocomposite to improve the neural recording capability (**Figure 13a**).[275] The electrode was coated with PEDOT-CNT nanocomposite by electrodeposition and successfully reduced the contact impedance by 2 orders of magnitude. To boost the mechanical matching with the surrounding tissues, the electrodes were further encapsulated with human fibrin-

based hydrogel which prevents the direct exposure of the nanocoating with the brain tissues. The electrode was used to record neural signals from rat somatosensory cortex.

Table 3. Representative electrically conductive hydrogels.

Polymer network	Charge carriers	Synthesis method	Electrical conductivity (S cm^{-1}) / Impedance	Young's modulus	Ref
PEDOT:PSS	PEDOT:PSS	Anneal and reswell	40	2 MPa	[276]
PEDOT:PSS	PEDOT:PSS	Water exchange	47.4 ± 1.2	32 ± 5.1 kPa	[93]
PAA	PEDOT:PSS	Infiltration of secondary polymer	$2.4 \pm 0.5 \times 10^{-1}$	8 - 374 kPa	[277]
PAAm	PANI	In situ polymerization	5×10^{-2}	125 kPa	[268]
PNIPAM	PANI	In situ polymerization	$8.4 \pm 0.2 \times 10^{-3}$	66.1 Pa	[269]
PAAm	PANI	In situ polymerization	3.9×10^{-1}	N/A	[267]
Agarose	PPy	In situ polymerization	1.95×10^{-1}	46 kPa	[273]
Alginate	PPy	In situ polymerization	$1.1 \pm 0.3 \times 10^{-4}$	20 – 200 kPa	[278]
Alginate	PPy	Electrochemical deposition	7 kΩ at 1 kHz	N/A	[271]
PVA-taurine	PEDOT/pTS	Photopolymerization and electrodeposition	N/A	N/A	[263]
Alginate	PEDOT	Electrochemical deposition	2.5 ± 0.5 kΩ at 1 kHz	N/A	[228]
Human fibrin	PEDOT-CNT	Electrochemical deposition	4.4 kΩ at 100 Hz	N/A	[275]

Feig *et al*. reported an interpenetrating hydrogel network, formed by infiltrating a loosely crosslinked PEDOT:PSS network with a polyacrylic acid (PAA) based secondary polymer scaffold (Figure 13b).[277] A record-high conductivity of 0.23 S cm^{-1} was achieved by improving the connectivity of the PEDOT:PSS network through controlled gelation of the conductive PEDOT:PSS polymer. The interpenetrating electrically conductive polymer matrix and the ionically conductive hydrogel matrix leads to the formation of EDL at molecular level, resulting in a significant increase in capacitance compared to that of the metal and ionic conductor interactions. The high volumetric capacitance leads to a significant decrease in the interfacial impedance, resulting in improved

bioelectronic performance in terms of both stimulation and recording. Due to the low solid concentration of PEDOT:PSS (around 1.1 wt%) in the hydrogel, its Young's modulus can be effectively controlled (in the range of 8 - 374 kPa) by tuning the secondary polymer network without affecting the conductivity (>10 S m^{-1}) and stretchability (> 100%). Additionally, due to its tunable mechanical properties, the hydrogel can be easily molded into various geometries (Figure 13c) to meet the demands of specific applications.

Miniaturization of conductive hydrogel electrodes is challenging due to the lack of micropatterning methods for hydrogel at sub-100-μm resolution. Traditional photolithographic patterning process is incompatible with general hydrogels because of their high water inclusion and porous microstructure. To address this issue, Liu et al. developed a hydrogel precursor formed by blending PEDOT:PSS with ionic liquids. Such PEDOT:PSS ionogel can be patterned at a feature resolution of 5 μm via photolithography and dry etching, then transform into a micropatterned PEDOT:PSS conductive hydrogel by subsequent water exchange (Figure 13d).[93] Based on this method, conductive hydrogel in the form of microelectrode arrays for sciatic nerve stimulation in mice was prepared (Figure 13e). The developed electrode demonstrated stable electrical behavior when subjected to mechanical strain, and showed a significant reduction in the interfacial impedance, resulting in a higher current density compared to Pt base electrodes. For effective integration of the bioelectronic devices with biological tissues, Young's modulus of both conductors and passivating/insulating polymers should be similar to that of biological tissues to reduce mechanical mismatch. In order to achieve this, a stretchable (up to 200%) UV-crosslinked dimethacrylate-functionalized perfluoropolyether (PFPE-DMA) polymer was prepared with a tunable Young's modulus < 30 kPa. The stability and biocompatibility were evaluated by implanting the electrode array consisting of PEDOT:PSS hydrogel as the electrode and PFPE-DMA as the insulating layer in live mice for localized, low-voltage electrically stimulated muscle movements. After 6 weeks period, no severe inflammation was found and a good electrode connection with the surrounding nerves was maintained.

7. Conclusion and Future Outlook

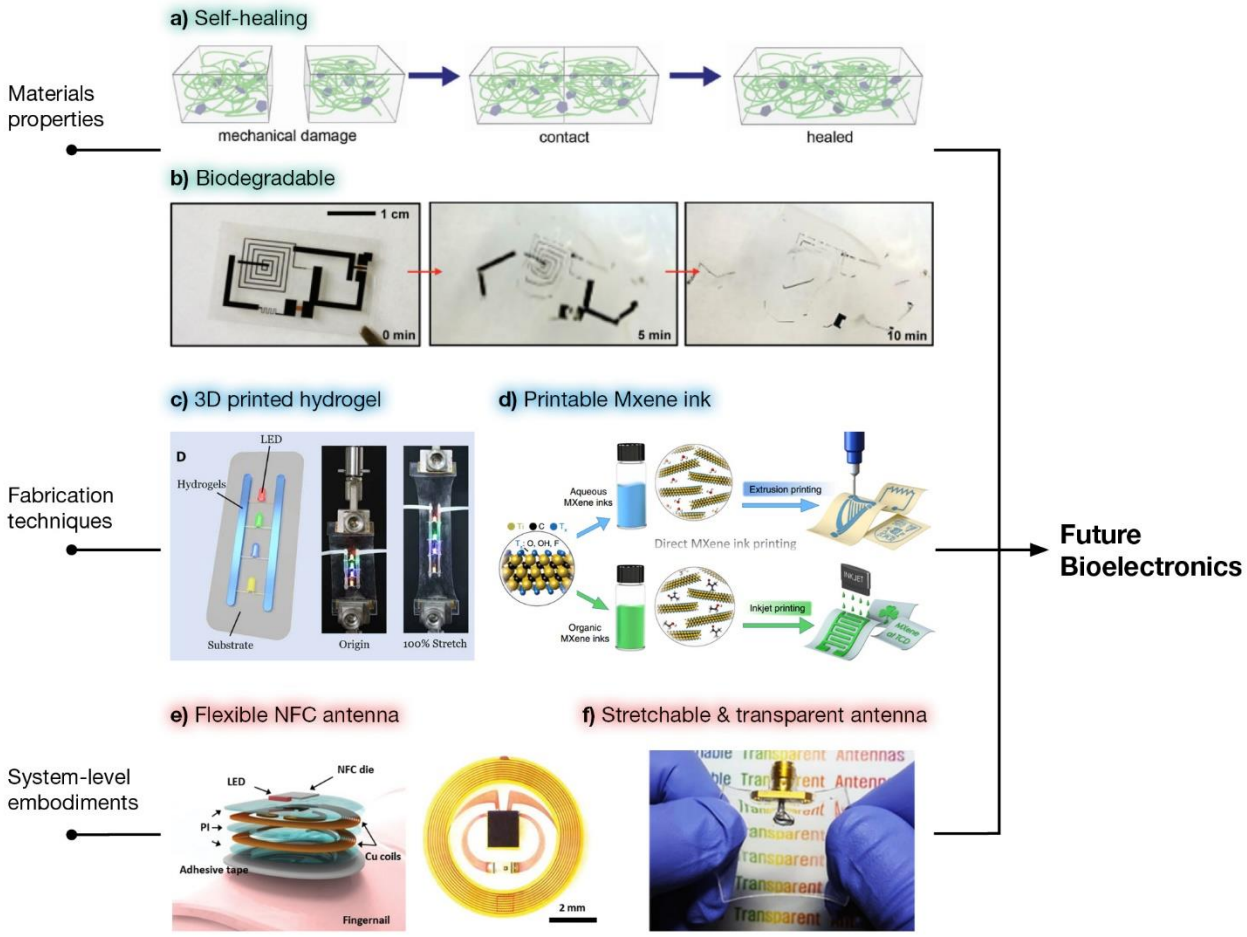

Figure 14. Research trends for future soft bioelectronic interfaces.

In the realm of advanced health care, the endeavors to replace rigid epidermal electrodes/implants with compliant, imperceptible bio-integrated devices have triggered the inception and rapid development of soft bioelectronics over the past decade. In view of the complex physical and mechanical interaction at the coupled abiotic-biotic interfaces, researchers are motivated to infuse flexible/stretchable materials with novel features which could improve biocompatibility. With immense amount of efforts being made, soft conductors ranging from metallic and carbonaceous nanomaterials, to conductive polymers and many hydrogels have been successfully tailored to meet the demand of seamless integration and chronic operation as bioelectronic interfaces, thereby serving as a powerful foundation for next-generation epidermal/implantable systems. The soft conductor-

based interfaces summarized in this review represent the recent and cutting-edge strategies attempted to push the boundary of diagnostic and therapeutic technologies. However, profound challenges still need to be solved before fulfilling the vision of a "soft" future from bench to bedside, translating laboratory demonstrations to real world settings. As an example, symptoms detection of many chronic neural diseases requires the capability to track physiological signals over months and even years, yet the lifetime, long-term stability in mechanical robustness and sensing performance of the so far reported soft implants have seldom been testified in vivo. Besides, toxicity of some new materials is still questionable due to the lack in strict evaluation, therefore cautions must be exercised when adopting them as bioelectronic interfaces, especially in invasive applications. The path towards clinical translation could only progress through many iterations before the final authentication of their biostability and non-toxicity.

A separate consideration lies in the approach to incorporate unusual characteristics into these soft bioelectronic interfaces through molecular design and material chemistry engineering. For instance, self-healable materials,[279] including ionic conductors (Figure 14a),[250, 280, 281] CNT composites[166] and multiple dielectric elastomers,[139, 282-285] have been developed and benefited from the emerging self-healing chemistry to mimic the restorative capability of human skin. By integrating the individual self-healing modules into a functional epidermal bioelectronic system, attractive breakthroughs will be achieved in the near future to make compliant and ultrathin epidermal interfaces mechanically and electrically robust against unexpected damages. Transient bioelectronics[286] represent another aspect where materials chemistry can bring about significant impacts in the next generation implants. Conventional implanted biomedical devices are non-bioresorbable and inevitably require secondary device removal surgery with the risk of unwanted tissue trauma or infection during the surgical procedure. Implantable bioelectronic interfaces constructed entirely out of biodegradable materials can avoid the aforementioned problem owing to their capability to dissolve, degrade or disintegrate in biofluids after a controlled period of device lifetime (Figure 14b).[287-290] Fundamental research in materials chemistry will be essential to advance this emerging aspect. One imperative challenge to be

addressed is how to actively control the materials' lifetime without being affected by physiological conditions such as pH, ion concentration and temperature.[291] The biocompatibility and cytotoxicity of byproducts after degradation should also be carefully studied before in vivo tests.

In addition, the development of precise and high-yield fabrication techniques is also essential for soft bioelectronic interfaces at the stage of industrialization. Firstly, manufacturing processes in current electronic industry must be improved to accommodate unconventional soft substrates and conductors; next, mass productivity with quality control should be ensured for the sake of cost efficiency; furthermore, inexpensive, rapid and high-resolution patterning techniques are highly desired to deliver miniaturized electrode footprint for certain bioelectronic applications. Conventional electronics are primarily developed through reliable photolithography and vacuum deposition procedures, which are however time-consuming, costly and generate large amount of chemical wastes. Printing technologies, including roll-to-roll/gravure printing, screening printing,[292] additive inkjet printing[293-295] and 3D printing,[296] are considered promising candidates for scalable, eco-friendly and low-cost manufacturing methods of bioelectronic devices. The low processing temperature of these printing methods is beneficial for most plastic/elastomer substrates, meanwhile they are inherently compatible with solution-processable organic conductors such as conductive polymers[242, 297-300] and ionically/electrically conductive hydrogels (Figure 14c).[301-303] Besides, a broad variety of inorganic nanomaterials, such as metallic flakes,[136] nanowires,[144, 304] CNTs[163, 305, 306] and 2D nanosheets (Figure 14d),[307, 308] have been successfully dispersed in liquid phase to formulate printable inks with on-demand rheological and chemical properties. Novel encapsulating materials such as anti-biofouling coatings may also be required in implanted bioelectronic probes, and aerosol jet printing method for high quality and conformable coating could be utilized.[309] While most examples listed here are not targeted at biomedical applications, we believe that the establishment of high-throughput production lines for printable devices will represent a milestone in the roadmap of soft bioelectronics towards medical diagnosis and treatment.

From the perspective of system-level embodiments, maturation of wireless powering and signal transmitting protocols will definitely help to untether future medical systems from massive wirings. Meanwhile, powering solutions including in vivo energy storage and energy harvesting technologies, should be extensively studied to support long-time functioning of integrated sensors, stimulators and other functional components. Among all the wireless strategies, inductive resonant antenna-based NFC technology represents one of the most promising solutions for energy harvesting and data transfer in a compact, ultrathin and skin-like form factor.[310] Miniaturized and flexible/stretchable NFC antennae are typically fabricated using metallic NMs (Figure 14e) as introduced in section 4.1.[55, 311-313] Recent works have demonstrated antennas-based on 3D helical NMs,[314] liquid metal[315] and nanomaterial composites[316] to achieve novel properties such as improved quality factor, stretchability and transparency (Figure 14f). However, current soft NFC modules have unavoidable limitations including the short communicating distance and unstable operation under extreme deformations, which should be adequately addressed before implementation. Besides, soft epidermal/implantable devices that harvest electrical energy from light[317] or mechanical motions[318-320] may offer alternative approaches to power bioelectronic devices. In conclusion, there is still a wide room for innovation, design, fabrication, and development of biocompatible soft bioelectronics with improved properties for effective bioelectronic integration. For future progress, interdisciplinary collaborations between material scientists, electronic engineers and medical specialists will be pivotal to yield broader impact in soft bioelectronic interfaces.

Acknowledgements

This work was supported by the Competitive Research Program (NRF-CRP13-2014-02) and NRF Investigatorship (Award No. NRF-NRFI2016-05) under the National Research Foundation, Prime Minister's Office, Singapore. D. Gao acknowledges the research scholarships awarded by Nanyang Technological University, Singapore.

Conflict of Interest

The authors declare no conflict of interest.

Key Words

bioelectronics, soft conductors, epidermal interfaces, neural interfaces

Received: ((will be filled in by the editorial staff))
Revised: ((will be filled in by the editorial staff))
Published online: ((will be filled in by the editorial staff))

References

[1] T. Someya, M. Amagai, *Nat. Biotechnol.* **2019**, *37*, 382.

[2] T. R. Ray, J. Choi, A. J. Bandodkar, S. Krishnan, P. Gutruf, L. Tian, R. Ghaffari, J. A. Rogers, *Chem. Rev.* **2019**, *119*, 5461.

[3] Y. Liu, M. Pharr, G. A. Salvatore, *ACS Nano* **2017**, *11*, 9614.

[4] S. M. Won, E. Song, J. Zhao, J. Li, J. Rivnay, J. A. Rogers, *Adv. Mater.* **2018**, *30*, e1800534.

[5] J. Rivnay, H. Wang, L. Fenno, K. Deisseroth, G. G. Malliaras, *Sci. Adv.* **2017**, *3*, e1601649.

[6] M. Lee, H. J. Shim, C. Choi, D. H. Kim, *Nano Lett.* **2019**, *19*, 2741.

[7] M. D. Ferro, N. A. Melosh, *Adv. Funct. Mater.* **2018**, *28*, 1704335.

[8] A. Chortos, J. Liu, Z. Bao, *Nat. Mater.* **2016**, *15*, 937.

[9] B. Xu, A. Akhtar, Y. Liu, H. Chen, W. H. Yeo, S. I. Park, B. Boyce, H. Kim, J. Yu, H. Y. Lai, S. Jung, Y. Zhou, J. Kim, S. Cho, Y. Huang, T. Bretl, J. A. Rogers, *Adv. Mater.* **2016**, *28*, 4462.

[10] E. Marder, *Neuron* **2012**, *76*, 1.

[11] H. Yuk, B. Lu, X. Zhao, *Chem. Soc. Rev.* **2019**, *48*, 1642.

[12] S. Choi, H. Lee, R. Ghaffari, T. Hyeon, D. H. Kim, *Adv. Mater.* **2016**, *28*, 4203.

[13] S. P. Lacour, G. Courtine, J. Guck, *Nat. Rev. Mater.* **2016**, *1*, 16063.

[14] X. Chen, K. Parida, J. Wang, J. Xiong, M. F. Lin, J. Shao, P. S. Lee, *ACS Appl. Mater. Interfaces* **2017**, *9*, 42200.

[15] S. Z. Guo, K. Qiu, F. Meng, S. H. Park, M. C. McAlpine, *Adv. Mater.* **2017**, *29*, 1701218.

[16] Y. Liu, J. J. Norton, R. Qazi, Z. Zou, K. R. Ammann, H. Liu, L. Yan, P. L. Tran, K. I. Jang, J. W. Lee, D. Zhang, K. A. Kilian, S. H. Jung, T. Bretl, J. Xiao, M. J. Slepian, Y. Huang, J. W. Jeong, J. A. Rogers, *Sci. Adv.* **2016**, *2*, e1601185.

[17] C. M. Boutry, A. Nguyen, Q. O. Lawal, A. Chortos, S. Rondeau-Gagne, Z. Bao, *Adv. Mater.* **2015**, *27*, 6954.

[18] M.-F. Lin, J. Xiong, J. Wang, K. Parida, P. S. Lee, *Nano Energy* **2018**, *44*, 248.

[19] W. Gao, S. Emaminejad, H. Y. Y. Nyein, S. Challa, K. Chen, A. Peck, H. M. Fahad, H. Ota, H. Shiraki, D. Kiriya, D. H. Lien, G. A. Brooks, R. W. Davis, A. Javey, *Nature* **2016**, *529*, 509.

[20] Y. Yamamoto, S. Harada, D. Yamamoto, W. Honda, T. Arie, S. Akita, K. Takei, *Sci. Adv.* **2016**, *2*, e1601473.

[21] R. C. Webb, A. P. Bonifas, A. Behnaz, Y. Zhang, K. J. Yu, H. Cheng, M. Shi, Z. Bian, Z. Liu, Y. S. Kim, W. H. Yeo, J. S. Park, J. Song, Y. Li, Y. Huang, A. M. Gorbach, J. A. Rogers, *Nat. Mater.* **2013**, *12*, 938.

[22] P. Malmivuo, J. Malmivuo, R. Plonsey, *Bioelectromagnetism: principles and applications of bioelectric and biomagnetic fields*, Oxford University Press, USA, **1995**.

[23] J.-W. Seo, H. Kim, K. Kim, S. Q. Choi, H. J. Lee, *Adv. Funct. Mater.* **2018**, *28*, 1800802.

[24] S. M. Lee, H. J. Byeon, J. H. Lee, D. H. Baek, K. H. Lee, J. S. Hong, S. H. Lee, *Sci. Rep.* **2014**, *4*, 6074.

[25] J. J. Norton, D. S. Lee, J. W. Lee, W. Lee, O. Kwon, P. Won, S. Y. Jung, H. Cheng, J. W. Jeong, A. Akce, S. Umunna, I. Na, Y. H. Kwon, X. Q. Wang, Z. Liu, U. Paik, Y. Huang, T. Bretl, W. H. Yeo, J. A. Rogers, *Proc. Natl. Acad. Sci. U. S. A.* **2015**, *112*, 3920.

[26] V. K. Somers, M. E. Dyken, M. P. Clary, F. M. Abboud, *J. Clin. Invest.* **1995**, *96*, 1897.

[27] A. Miyamoto, S. Lee, N. F. Cooray, S. Lee, M. Mori, N. Matsuhisa, H. Jin, L. Yoda, T. Yokota, A. Itoh, M. Sekino, H. Kawasaki, T. Ebihara, M. Amagai, T. Someya, *Nat. Nanotechnol.* **2017**, *12*, 907.

[28] B. Sun, R. N. McCay, S. Goswami, Y. Xu, C. Zhang, Y. Ling, J. Lin, Z. Yan, *Adv. Mater.* **2018**, *30*, e1804327.

[29] K. I. Jang, S. Y. Han, S. Xu, K. E. Mathewson, Y. Zhang, J. W. Jeong, G. T. Kim, R. C. Webb, J. W. Lee, T. J. Dawidczyk, R. H. Kim, Y. M. Song, W. H. Yeo, S. Kim, H. Cheng, S. I. Rhee, J. Chung, B. Kim, H. U. Chung, D. Lee, Y. Yang, M. Cho, J. G. Gaspar, R. Carbonari, M. Fabiani, G. Gratton, Y. Huang, J. A. Rogers, *Nat. Commun.* **2014**, *5*, 4779.

[30] Y. Yang, W. Gao, *Chem. Soc. Rev.* **2019**, *48*, 1465.

[31] K. Wilke, A. Martin, L. Terstegen, S. S. Biel, *Int. J. Cosmet. Sci.* **2007**, *29*, 169.

[32] M. Bariya, H. Y. Y. Nyein, A. Javey, *Nat. Electron.* **2018**, *1*, 160.

[33] M. M. Raiszadeh, M. M. Ross, P. S. Russo, M. A. Schaepper, W. Zhou, J. Deng, D. Ng, A. Dickson, C. Dickson, M. Strom, C. Osorio, T. Soeprono, J. D. Wulfkuhle, E. F. Petricoin, L. A. Liotta, W. M. Kirsch, *J. Proteome Res.* **2012**, *11*, 2127.

[34] J. Kim, I. Jeerapan, S. Imani, T. N. Cho, A. Bandodkar, S. Cinti, P. P. Mercier, J. Wang, *ACS Sens.* **2016**, *1*, 1011.

[35] H. Lee, C. Song, Y. S. Hong, M. S. Kim, H. R. Cho, T. Kang, K. Shin, S. H. Choi, T. Hyeon, D. H. Kim, *Sci. Adv.* **2017**, *3*, e1601314.

[36] J. Park, J. Kim, S. Y. Kim, W. H. Cheong, J. Jang, Y. G. Park, K. Na, Y. T. Kim, J. H. Heo, C. Y. Lee, J. H. Lee, F. Bien, J. U. Park, *Sci. Adv.* **2018**, *4*, eaap9841.

[37] Q. Zhai, S. Gong, Y. Wang, Q. Lyu, Y. Liu, Y. Ling, J. Wang, G. P. Simon, W. Cheng, *ACS Appl. Mater. Interfaces* **2019**, *11*, 9724.

[38] W. Jia, A. J. Bandodkar, G. Valdes-Ramirez, J. R. Windmiller, Z. Yang, J. Ramirez, G. Chan, J. Wang, *Anal. Chem.* **2013**, *85*, 6553.

[39] A. J. Bandodkar, D. Molinnus, O. Mirza, T. Guinovart, J. R. Windmiller, G. Valdes-Ramirez, F. J. Andrade, M. J. Schoning, J. Wang, *Biosens. Bioelectron.* **2014**, *54*, 603.

[40] J. Kim, W. R. de Araujo, I. A. Samek, A. J. Bandodkar, W. Jia, B. Brunetti, T. R. L. C. Paixão, J. Wang, *Electrochem. Commun.* **2015**, *51*, 41.

[41] D. P. Rose, M. E. Ratterman, D. K. Griffin, L. Hou, N. Kelley-Loughnane, R. R. Naik, J. A. Hagen, I. Papautsky, J. C. Heikenfeld, *IEEE Trans. Biomed. Eng.* **2015**, *62*, 1457.

[42] T. Guinovart, A. J. Bandodkar, J. R. Windmiller, F. J. Andrade, J. Wang, *Analyst* **2013**, *138*, 7031.

[43] A. J. Bandodkar, J. Choi, S. P. Lee, W. J. Jeang, P. Agyare, P. Gutruf, S. Wang, R. A. Sponenburg, J. T. Reeder, S. Schon, T. R. Ray, S. Chen, S. Mehta, S. Ruiz, J. A. Rogers, *Adv. Mater.* **2019**, *31*, 1902109.

[44] A. Martin, J. Kim, J. F. Kurniawan, J. R. Sempionatto, J. R. Moreto, G. Tang, A. S. Campbell, A. Shin, M. Y. Lee, X. Liu, J. Wang, *ACS Sens.* **2017**, *2*, 1860.

[45] H. Y. Y. Nyein, L. C. Tai, Q. P. Ngo, M. Chao, G. B. Zhang, W. Gao, M. Bariya, J. Bullock, H. Kim, H. M. Fahad, A. Javey, *ACS Sens.* **2018**, *3*, 944.

[46] J. T. Reeder, J. Choi, Y. Xue, P. Gutruf, J. Hanson, M. Liu, T. Ray, A. J. Bandodkar, R. Avila, W. Xia, S. Krishnan, S. Xu, K. Barnes, M. Pahnke, R. Ghaffari, Y. Huang, J. A. Rogers, *Sci. Adv.* **2019**, *5*, eaau6356.

[47] A. Koh, D. Kang, Y. Xue, S. Lee, R. M. Pielak, J. Kim, T. Hwang, S. Min, A. Banks, P. Bastien, M. C. Manco, L. Wang, K. R. Ammann, K. I. Jang, P. Won, S. Han, R. Ghaffari, U. Paik, M. J. Slepian, G. Balooch, Y. Huang, J. A. Rogers, *Sci. Transl. Med.* **2016**, *8*, 366ra165.

[48] X. Huang, Y. Liu, K. Chen, W. J. Shin, C. J. Lu, G. W. Kong, D. Patnaik, S. H. Lee, J. F. Cortes, J. A. Rogers, *Small* **2014**, *10*, 3083.

[49] V. F. Curto, C. Fay, S. Coyle, R. Byrne, C. O'Toole, C. Barry, S. Hughes, N. Moyna, D. Diamond, F. Benito-Lopez, *Sens. Actuators, B* **2012**, *171-172*, 1327.

[50] A. J. Bandodkar, P. Gutruf, J. Choi, K. Lee, Y. Sekine, J. T. Reeder, W. J. Jeang, A. J. Aranyosi, S. P. Lee, J. B. Model, R. Ghaffari, C. J. Su, J. P. Leshock, T. Ray, A. Verrillo, K. Thomas, V. Krishnamurthi, S. Han, J. Kim, S. Krishnan, T. Hang, J. A. Rogers, *Sci. Adv.* **2019**, *5*, eaav3294.

[51] P. Tseng, B. Napier, L. Garbarini, D. L. Kaplan, F. G. Omenetto, *Adv. Mater.* **2018**, *30*, e1703257.

[52] N. D. Giardino, L. Chan, S. Borson, *Appl. Psychophysiol. Biofeedback* **2004**, *29*, 121.

[53] C. M. Lochner, Y. Khan, A. Pierre, A. C. Arias, *Nat. Commun.* **2014**, *5*, 5745.

[54] T. Yokota, P. Zalar, M. Kaltenbrunner, H. Jinno, N. Matsuhisa, H. Kitanosako, Y. Tachibana, W. Yukita, M. Koizumi, T. Someya, *Sci. Adv.* **2016**, *2*, e1501856.

[55] J. Kim, P. Gutruf, A. M. Chiarelli, S. Y. Heo, K. Cho, Z. Xie, A. Banks, S. Han, K. I. Jang, J. W. Lee, K. T. Lee, X. Feng, Y. Huang, M. Fabiani, G. Gratton, U. Paik, J. A. Rogers, *Adv. Funct. Mater.* **2017**, *27*, 1604373.

[56] K. A. Kaczmarek, J. G. Webster, P. Bach-y-Rita, W. J. Tompkins, *IEEE Trans. Biomed. Eng.* **1991**, *38*, 1.

[57] M. Ying, A. P. Bonifas, N. Lu, Y. Su, R. Li, H. Cheng, A. Ameen, Y. Huang, J. A. Rogers, *Nanotechnology* **2012**, *23*, 344004.

[58] J. Dargahi, S. Najarian, *Int. J. Med. Robot. Comp.* **2004**, *01*, 23.

[59] J. A. Downey, S. J. Myers, E. G. Gonzalez, *The physiological basis of rehabilitation medicine*, Butterworth-Heinemann, Stoneham, MA **2013**.

[60] M. V. Hurley, L. M. Bearne, *Best. Pract. Res. Clin. Rheumatol.* **2008**, *22*, 419.

[61] C. Antfolk, M. D'alonzo, B. Rosen, G. Lundborg, F. Sebelius, C. Cipriani, *Expert Rev. Med. Devices* **2013**, *10*, 45.

[62] B. Peerdeman, D. Boere, H. Witteveen, H. Hermens, S. Stramigioli, H. Rietman, P. Veltink, S. Misra, *J. Rehabil. Res. Dev.* **2011**, *48*, 719.

[63] S. Emaminejad, W. Gao, E. Wu, Z. A. Davies, H. Yin Yin Nyein, S. Challa, S. P. Ryan, H. M. Fahad, K. Chen, Z. Shahpar, S. Talebi, C. Milla, A. Javey, R. W. Davis, *Proc. Natl. Acad. Sci. U. S. A.* **2017**, *114*, 4625.

[64] L. E. Gibson, R. E. Cooke, *Pediatrics* **1959**, *23*, 545.

[65] X. Liang, S. A. Boppart, *IEEE Trans. Biomed. Eng.* **2009**, *57*, 953.

[66] D. H. Kim, N. Lu, R. Ma, Y. S. Kim, R. H. Kim, S. Wang, J. Wu, S. M. Won, H. Tao, A. Islam, K. J. Yu, T. I. Kim, R. Chowdhury, M. Ying, L. Xu, M. Li, H. J. Chung, H. Keum, M. McCormick, P. Liu, Y. W. Zhang, F. G. Omenetto, Y. Huang, T. Coleman, J. A. Rogers, *Science* **2011**, *333*, 838.

[67] E. Song, C. H. Chiang, R. Li, X. Jin, J. Zhao, M. Hill, Y. Xia, L. Li, Y. Huang, S. M. Won, K. J. Yu, X. Sheng, H. Fang, M. A. Alam, Y. Huang, J. Viventi, J. K. Chang, J. A. Rogers, *Proc. Natl. Acad. Sci. U. S. A.* **2019**, *116*, 15398.

[68] S. Han, J. Kim, S. M. Won, Y. Ma, D. Kang, Z. Xie, K. T. Lee, H. U. Chung, A. Banks, S. Min, S. Y. Heo, C. R. Davies, J. W. Lee, C. H. Lee, B. H. Kim, K. Li, Y. Zhou, C. Wei, X. Feng, Y. Huang, J. A. Rogers, *Sci. Transl. Med.* **2018**, *10*, eaan4950.

[69] M. Kaltenbrunner, T. Sekitani, J. Reeder, T. Yokota, K. Kuribara, T. Tokuhara, M. Drack, R. Schwodiauer, I. Graz, S. Bauer-Gogonea, S. Bauer, T. Someya, *Nature* **2013**, *499*, 458.

[70] C. H. Lee, Y. Ma, K.-I. Jang, A. Banks, T. Pan, X. Feng, J. S. Kim, D. Kang, M. S. Raj, B. L. McGrane, B. Morey, X. Wang, R. Ghaffari, Y. Huang, J. A. Rogers, *Adv. Funct. Mater.* **2015**, *25*, 3698.

[71] Y. M. Chi, T. P. Jung, G. Cauwenberghs, *IEEE Rev. Biomed. Eng.* **2010**, *3*, 106.

[72] H. U. Chung, B. H. Kim, J. Y. Lee, J. Lee, Z. Xie, E. M. Ibler, K. Lee, A. Banks, J. Y. Jeong, J. Kim, C. Ogle, D. Grande, Y. Yu, H. Jang, P. Assem, D. Ryu, J. W. Kwak, M. Namkoong, J. B. Park, Y. Lee, D. H. Kim, A. Ryu, J. Jeong, K. You, B. Ji, Z. Liu, Q. Huo, X. Feng, Y. Deng, Y. Xu, K. I. Jang, J. Kim, Y. Zhang, R. Ghaffari, C. M. Rand, M. Schau, A. Hamvas, D. E. Weese-Mayer, Y. Huang, S. M. Lee, C. H. Lee, N. R. Shanbhag, A. S. Paller, S. Xu, J. A. Rogers, *Science* **2019**, *363*, eaau0780.

[73] L. Tian, B. Zimmerman, A. Akhtar, K. J. Yu, M. Moore, J. Wu, R. J. Larsen, J. W. Lee, J. Li, Y. Liu, B. Metzger, S. Qu, X. Guo, K. E. Mathewson, J. A. Fan, J. Cornman, M. Fatina, Z. Xie, Y. Ma, J. Zhang, Y. Zhang, F. Dolcos, M. Fabiani, G. Gratton, T. Bretl, L. J. Hargrove, P. V. Braun, Y. Huang, J. A. Rogers, *Nat. Biomed. Eng.* **2019**, *3*, 194.

[74] S. Lee, Y. Inoue, D. Kim, A. Reuveny, K. Kuribara, T. Yokota, J. Reeder, M. Sekino, T. Sekitani, Y. Abe, T. Someya, *Nat. Commun.* **2014**, *5*, 5898.

[75] T. Ebrahimi, Fannir, Nguyen, Plesse, Vidal, Madden, *Robotics* **2019**, *8*, 60.

[76] J. Xiong, P. Cui, X. Chen, J. Wang, K. Parida, M. F. Lin, P. S. Lee, *Nat. Commun.* **2018**, *9*, 4280.

[77] J. S. Heo, J. Eom, Y. H. Kim, S. K. Park, *Small* **2018**, *14*, 1703034.

[78] J. Shin, Z. Liu, W. Bai, Y. Liu, Y. Yan, Y. Xue, I. Kandela, M. Pezhouh, M. R. MacEwan, Y. Huang, W. Z. Ray, W. Zhou, J. A. Rogers, *Sci. Adv.* **2019**, *5*, eaaw1899.

[79] H. Zhang, P. Gutruf, K. Meacham, M. C. Montana, X. Zhao, A. M. Chiarelli, A. Vazquez-Guardado, A. Norris, L. Lu, Q. Guo, C. Xu, Y. Wu, H. Zhao, X. Ning, W. Bai, I. Kandela, C. R. Haney, D. Chanda, R. W. t. Gereau, J. A. Rogers, *Sci. Adv.* **2019**, *5*, eaaw0873.

[80] J. H. Lee, H. Kim, J. H. Kim, S. H. Lee, *Lab Chip* **2016**, *16*, 959.

[81] D. H. Kim, J. Viventi, J. J. Amsden, J. Xiao, L. Vigeland, Y. S. Kim, J. A. Blanco, B. Panilaitis, E. S. Frechette, D. Contreras, D. L. Kaplan, F. G. Omenetto, Y. Huang, K. C. Hwang, M. R. Zakin, B. Litt, J. A. Rogers, *Nat. Mater.* **2010**, *9*, 511.

[82] J. Viventi, D. H. Kim, L. Vigeland, E. S. Frechette, J. A. Blanco, Y. S. Kim, A. E. Avrin, V. R. Tiruvadi, S. W. Hwang, A. C. Vanleer, D. F. Wulsin, K. Davis, C. E. Gelber, L. Palmer, J. Van der Spiegel, J. Wu, J. Xiao, Y. Huang, D. Contreras, J. A. Rogers, B. Litt, *Nat. Neurosci.* **2011**, *14*, 1599.

[83] F. J. Rodriguez, D. Ceballos, M. Schuttler, A. Valero, E. Valderrama, T. Stieglitz, X. Navarro, *J. Neurosci. Methods* **2000**, *98*, 105.

[84] L. Luan, X. Wei, Z. Zhao, J. J. Siegel, O. Potnis, C. A. Tuppen, S. Lin, S. Kazmi, R. A. Fowler, S. Holloway, A. K. Dunn, R. A. Chitwood, C. Xie, *Sci. Adv.* **2017**, *3*, e1601966.

[85] J. T. Robinson, M. Jorgolli, A. K. Shalek, M. H. Yoon, R. S. Gertner, H. Park, *Nat. Nanotechnol.* **2012**, *7*, 180.

[86] Y. Kajikawa, C. E. Schroeder, *Neuron* **2011**, *72*, 847.

[87] G. Buzsaki, C. A. Anastassiou, C. Koch, *Nat. Rev. Neurosci.* **2012**, *13*, 407.

[88] S. Katzner, I. Nauhaus, A. Benucci, V. Bonin, D. L. Ringach, M. Carandini, *Neuron* **2009**, *61*, 35.

[89] D. Khodagholy, J. N. Gelinas, T. Thesen, W. Doyle, O. Devinsky, G. G. Malliaras, G. Buzsaki, *Nat. Neurosci.* **2015**, *18*, 310.

[90] D. W. Park, A. A. Schendel, S. Mikael, S. K. Brodnick, T. J. Richner, J. P. Ness, M. R. Hayat, F. Atry, S. T. Frye, R. Pashaie, S. Thongpang, Z. Ma, J. C. Williams, *Nat. Commun.* **2014**, *5*, 5258.

[91] D. Khodagholy, J. N. Gelinas, Z. Zhao, M. Yeh, M. Long, J. D. Greenlee, W. Doyle, O. Devinsky, G. Buzsaki, *Sci. Adv.* **2016**, *2*, e1601027.

[92] M. Radivojevic, D. Jackel, M. Altermatt, J. Muller, V. Viswam, A. Hierlemann, D. J. Bakkum, *Sci. Rep.* **2016**, *6*, 31332.

[93] Y. Liu, J. Liu, S. Chen, T. Lei, Y. Kim, S. Niu, H. Wang, X. Wang, A. M. Foudeh, J. B. Tok, Z. Bao, *Nat. Biomed. Eng.* **2019**, *3*, 58.

[94] D. Farina, I. Vujaklija, M. Sartori, T. Kapelner, F. Negro, N. Jiang, K. Bergmeister, A. Andalib, J. Principe, O. C. Aszmann, *Nat. Biomed. Eng.* **2017**, *1*, 0025.

[95] K. Ashkan, P. Rogers, H. Bergman, I. Ughratdar, *Nat. Rev. Neurol.* **2017**, *13*, 548.

[96] P. J. Rousche, R. A. Normann, *IEEE Trans. Rehabil. Eng.* **1999**, *7*, 56.

[97] A. A. Sharp, A. M. Ortega, D. Restrepo, D. Curran-Everett, K. Gall, *IEEE Trans. Biomed. Eng.* **2008**, *56*, 45.

[98] H. Lee, R. V. Bellamkonda, W. Sun, M. E. Levenston, *J. Neural. Eng.* **2005**, *2*, 81.

[99] K. Tybrandt, D. Khodagholy, B. Dielacher, F. Stauffer, A. F. Renz, G. Buzsaki, J. Voros, *Adv. Mater.* **2018**, *30*, e1706520.

[100] I. R. Minev, P. Musienko, A. Hirsch, Q. Barraud, N. Wenger, E. M. Moraud, J. Gandar, M. Capogrosso, T. Milekovic, L. Asboth, R. F. Torres, N. Vachicouras, Q. Liu, N. Pavlova, S. Duis, A. Larmagnac, J. Voros, S. Micera, Z. Suo, G. Courtine, S. P. Lacour, *Science* **2015**, *347*, 159.

[101] C. Yang, Z. Suo, *Nat. Rev. Mater.* **2018**, *3*, 125.

[102] H. R. Lee, C. C. Kim, J. Y. Sun, *Adv. Mater.* **2018**, *30*, e1704403.

[103] H. Sheng, X. Wang, N. Kong, W. Xi, H. Yang, X. Wu, K. Wu, C. Li, J. Hu, J. Tang, J. Zhou, S. Duan, H. Wang, Z. Suo, *Extreme Mech. Lett.* **2019**, *30*, 100510.

[104] X. Liu, H. Yuk, S. Lin, G. A. Parada, T. C. Tang, E. Tham, C. de la Fuente-Nunez, T. K. Lu, X. Zhao, *Adv. Mater.* **2018**, *30*, 1704821.

[105] S. Zhao, P. Tseng, J. Grasman, Y. Wang, W. Li, B. Napier, B. Yavuz, Y. Chen, L. Howell, J. Rincon, F. G. Omenetto, D. L. Kaplan, *Adv. Mater.* **2018**, *30*, 1800598.

[106] T. Dvir, B. P. Timko, M. D. Brigham, S. R. Naik, S. S. Karajanagi, O. Levy, H. Jin, K. K. Parker, R. Langer, D. S. Kohane, *Nat. Nanotechnol.* **2011**, *6*, 720.

[107] Y. Liu, A. F. McGuire, H. Y. Lou, T. L. Li, J. B. Tok, B. Cui, Z. Bao, *Proc. Natl. Acad. Sci. U. S. A.* **2018**, *115*, 11718.

[108] E. W. Keefer, B. R. Botterman, M. I. Romero, A. F. Rossi, G. W. Gross, *Nat. Nanotechnol.* **2008**, *3*, 434.

[109] Y. Lu, H. Lyu, A. G. Richardson, T. H. Lucas, D. Kuzum, *Sci. Rep.* **2016**, *6*, 33526.

[110] T. D. Kozai, K. Catt, Z. Du, K. Na, O. Srivannavit, R. U. Haque, J. Seymour, K. D. Wise, E. Yoon, X. T. Cui, *IEEE Trans. Biomed. Eng.* **2016**, *63*, 111.

[111] K. A. Ludwig, J. D. Uram, J. Yang, D. C. Martin, D. R. Kipke, *J. Neural. Eng.* **2006**, *3*, 59.

[112] C. M. Proctor, J. Rivnay, G. G. Malliaras, *J. Polym. Sci., Part B: Polym. Phys.* **2016**, *54*, 1433.

[113] S. Choi, S. I. Han, D. Jung, H. J. Hwang, C. Lim, S. Bae, O. K. Park, C. M. Tschabrunn, M. Lee, S. Y. Bae, J. W. Yu, J. H. Ryu, S. W. Lee, K. Park, P. M. Kang, W. B. Lee, R. Nezafat, T. Hyeon, D. H. Kim, *Nat. Nanotechnol.* **2018**, *13*, 1048.

[114] H. Fang, J. Zhao, K. J. Yu, E. Song, A. B. Farimani, C. H. Chiang, X. Jin, Y. Xue, D. Xu, W. Du, K. J. Seo, Y. Zhong, Z. Yang, S. M. Won, G. Fang, S. W. Choi, S. Chaudhuri, Y. Huang, M. A. Alam, J. Viventi, N. R. Aluru, J. A. Rogers, *Proc. Natl. Acad. Sci. U. S. A.* **2016**, *113*, 11682.

[115] E. Song, Y. K. Lee, R. Li, J. Li, X. Jin, K. J. Yu, Z. Xie, H. Fang, Y. Zhong, H. Du, J. Zhang, G. Fang, Y. Kim, Y. Yoon, M. A. Alam, Y. Mei, Y. Huang, J. A. Rogers, *Adv. Funct. Mater.* **2018**, *28*, 1702284.

[116] J. A. Rogers, T. Someya, Y. Huang, *Science* **2010**, *327*, 1603.

[117] D. H. Kim, J. Song, W. M. Choi, H. S. Kim, R. H. Kim, Z. Liu, Y. Y. Huang, K. C. Hwang, Y. W. Zhang, J. A. Rogers, *Proc. Natl. Acad. Sci. U. S. A.* **2008**, *105*, 18675.

[118] X. Hu, P. Krull, B. de Graff, K. Dowling, J. A. Rogers, W. J. Arora, *Adv. Mater.* **2011**, *23*, 2933.

[119] R. H. Kim, D. H. Kim, J. Xiao, B. H. Kim, S. I. Park, B. Panilaitis, R. Ghaffari, J. Yao, M. Li, Z. Liu, V. Malyarchuk, D. G. Kim, A. P. Le, R. G. Nuzzo, D. L. Kaplan, F. G. Omenetto, Y. Huang, Z. Kang, J. A. Rogers, *Nat. Mater.* **2010**, *9*, 929.

[120] J. A. Fan, W. H. Yeo, Y. Su, Y. Hattori, W. Lee, S. Y. Jung, Y. Zhang, Z. Liu, H. Cheng, L. Falgout, M. Bajema, T. Coleman, D. Gregoire, R. J. Larsen, Y. Huang, J. A. Rogers, *Nat. Commun.* **2014**, *5*, 3266.

[121] W. H. Yeo, Y. S. Kim, J. Lee, A. Ameen, L. Shi, M. Li, S. Wang, R. Ma, S. H. Jin, Z. Kang, Y. Huang, J. A. Rogers, *Adv. Mater.* **2013**, *25*, 2773.

[122] J. Kim, A. Banks, H. Cheng, Z. Xie, S. Xu, K. I. Jang, J. W. Lee, Z. Liu, P. Gutruf, X. Huang, P. Wei, F. Liu, K. Li, M. Dalal, R. Ghaffari, X. Feng, Y. Huang, S. Gupta, U. Paik, J. A. Rogers, *Small* **2015**, *11*, 906.

[123] L. Xu, S. R. Gutbrod, A. P. Bonifas, Y. Su, M. S. Sulkin, N. Lu, H. J. Chung, K. I. Jang, Z. Liu, M. Ying, C. Lu, R. C. Webb, J. S. Kim, J. I. Laughner, H. Cheng, Y. Liu, A. Ameen, J. W. Jeong, G. T. Kim, Y. Huang, I. R. Efimov, J. A. Rogers, *Nat. Commun.* **2014**, *5*, 3329.

[124] L. Xu, S. R. Gutbrod, Y. Ma, A. Petrossians, Y. Liu, R. C. Webb, J. A. Fan, Z. Yang, R. Xu, J. J. Whalen, 3rd, J. D. Weiland, Y. Huang, I. R. Efimov, J. A. Rogers, *Adv. Mater.* **2015**, *27*, 1731.

[125] J. W. Jeong, W. H. Yeo, A. Akhtar, J. J. Norton, Y. J. Kwack, S. Li, S. Y. Jung, Y. Su, W. Lee, J. Xia, H. Cheng, Y. Huang, W. S. Choi, T. Bretl, J. A. Rogers, *Adv. Mater.* **2013**, *25*, 6839.

[126] Y. Takema, Y. Yorimoto, M. Kawai, G. Imokawa, *Br. J. Dermatol.* **1994**, *131*, 641.

[127] J. Koo, M. R. MacEwan, S. K. Kang, S. M. Won, M. Stephen, P. Gamble, Z. Xie, Y. Yan, Y. Y. Chen, J. Shin, N. Birenbaum, S. Chung, S. B. Kim, J. Khalifeh, D. V. Harburg, K. Bean, M. Paskett, J. Kim, Z. S. Zohny, S. M. Lee, R. Zhang, K. Luo, B. Ji, A. Banks, H. M. Lee, Y. Huang, W. Z. Ray, J. A. Rogers, *Nat. Med.* **2018**, *24*, 1830.

[128] M. Ullsperger, S. Debener, *Simultaneous EEG and fMRI: recording, analysis, and application*, Oxford University Press, New York **2010**.

[129] P. Ritter, A. Villringer, *Neurosci. Biobehav. Rev.* **2006**, *30*, 823.

[130] Y. Zhang, A. D. Mickle, P. Gutruf, L. A. McIlvried, H. Guo, Y. Wu, J. P. Golden, Y. Xue, J. G. Grajales-Reyes, X. Wang, S. Krishnan, Y. Xie, D. Peng, C. J. Su, F. Zhang, J. T. Reeder, S. K. Vogt, Y. Huang, J. A. Rogers, R. W. t. Gereau, *Sci. Adv.* **2019**, *5*, eaaw5296.

[131] A. D. Mickle, S. M. Won, K. N. Noh, J. Yoon, K. W. Meacham, Y. Xue, L. A. McIlvried, B. A. Copits, V. K. Samineni, K. E. Crawford, D. H. Kim, P. Srivastava, B. H. Kim, S. Min, Y. Shiuan, Y. Yun, M. A. Payne, J. Zhang, H. Jang, Y. Li, H. H. Lai, Y. Huang, S. I. Park, R. W. t. Gereau, J. A. Rogers, *Nature* **2019**, *565*, 361.

[132] P. Gutruf, V. Krishnamurthi, A. Vázquez-Guardado, Z. Xie, A. Banks, C.-J. Su, Y. Xu, C. R. Haney, E. A. Waters, I. Kandela, S. R. Krishnan, T. Ray, J. P. Leshock, Y. Huang, D. Chanda, J. A. Rogers, *Nat. Electron.* **2018**, *1*, 652.

[133] S. I. Park, D. S. Brenner, G. Shin, C. D. Morgan, B. A. Copits, H. U. Chung, M. Y. Pullen, K. N. Noh, S. Davidson, S. J. Oh, J. Yoon, K. I. Jang, V. K. Samineni, M. Norman, J. G. Grajales-Reyes, S. K.

Vogt, S. S. Sundaram, K. M. Wilson, J. S. Ha, R. Xu, T. Pan, T. I. Kim, Y. Huang, M. C. Montana, J. P. Golden, M. R. Bruchas, R. W. t. Gereau, J. A. Rogers, *Nat. Biotechnol.* **2015**, *33*, 1280.

[134] J. Wang, M.-F. Lin, S. Park, P. S. Lee, *Mater. Today* **2018**, *21*, 508.

[135] S. Choi, S. I. Han, D. Kim, T. Hyeon, D. H. Kim, *Chem. Soc. Rev.* **2019**, *48*, 1566.

[136] J. Wang, G. Cai, S. Li, D. Gao, J. Xiong, P. S. Lee, *Adv. Mater.* **2018**, *30*, 1706157.

[137] N. Matsuhisa, D. Inoue, P. Zalar, H. Jin, Y. Matsuba, A. Itoh, T. Yokota, D. Hashizume, T. Someya, *Nat. Mater.* **2017**, *16*, 834.

[138] S. Park, G. Thangavel, K. Parida, S. Li, P. S. Lee, *Adv. Mater.* **2019**, *31*, 1805536.

[139] K. Parida, G. Thangavel, G. Cai, X. Zhou, S. Park, J. Xiong, P. S. Lee, *Nat. Commun.* **2019**, *10*, 2158.

[140] Y. Kim, J. Zhu, B. Yeom, M. Di Prima, X. Su, J. G. Kim, S. J. Yoo, C. Uher, N. A. Kotov, *Nature* **2013**, *500*, 59.

[141] S. Gong, W. Cheng, *Adv. Electron. Mater.* **2017**, *3*, 1600314.

[142] Y. Sun, Y. Xia, *Adv. Mater.* **2002**, *14*, 833.

[143] F. Xu, Y. Zhu, *Adv. Mater.* **2012**, *24*, 5117.

[144] J. Liang, K. Tong, Q. Pei, *Adv. Mater.* **2016**, *28*, 5986.

[145] S. Choi, J. Park, W. Hyun, J. Kim, J. Kim, Y. B. Lee, C. Song, H. J. Hwang, J. H. Kim, T. Hyeon, D. H. Kim, *ACS Nano* **2015**, *9*, 6626.

[146] J. Park, S. Choi, A. H. Janardhan, S. Y. Lee, S. Raut, J. Soares, K. Shin, S. X. Yang, C. Lee, K. W. Kang, H. R. Cho, S. J. Kim, P. Seo, W. Hyun, S. Jung, H. J. Lee, N. Lee, S. H. Choi, M. Sacks, N. S. Lu, M. E. Josephson, T. Hyeon, D. H. Kim, H. J. Hwang, *Sci. Transl. Med.* **2016**, *8*, 344ra86.

[147] C. Lu, S. Park, T. J. Richner, A. Derry, I. Brown, C. Hou, S. Rao, J. Kang, C. T. Mortiz, Y. Fink, P. Anikeeva, *Sci. Adv.* **2017**, *3*, e1600955.

[148] J. Jang, B. G. Hyun, S. Ji, E. Cho, B. W. An, W. H. Cheong, J.-U. Park, *NPG Asia Mater.* **2017**, *9*, e432.

[149] S. Ji, J. Jang, E. Cho, S. H. Kim, E. S. Kang, J. Kim, H. K. Kim, H. Kong, S. K. Kim, J. Y. Kim, J. U. Park, *Adv. Mater.* **2017**, *29*.

[150] B. W. An, S. Heo, S. Ji, F. Bien, J. U. Park, *Nat. Commun.* **2018**, *9*, 2458.

[151] M. Yang, Z. D. Hood, X. Yang, M. Chi, Y. Xia, *Chem. Commun.* **2017**, *53*, 1965.

[152] D. McShan, P. C. Ray, H. Yu, *J. Food Drug Anal.* **2014**, *22*, 116.

[153] S. Gong, D. T. Lai, Y. Wang, L. W. Yap, K. J. Si, Q. Shi, N. N. Jason, T. Sridhar, H. Uddin, W. Cheng, *ACS Appl. Mater. Interfaces* **2015**, *7*, 19700.

[154] S. Gong, Y. Zhao, L. W. Yap, Q. Shi, Y. Wang, J. A. P. B. Bay, D. T. H. Lai, H. Uddin, W. Cheng, *Adv. Electron. Mater.* **2016**, *2*, 1600121.

[155] M. D. Ho, Y. Ling, L. W. Yap, Y. Wang, D. Dong, Y. Zhao, W. Cheng, *Adv. Funct. Mater.* **2017**, *27*, 1700845.

[156] Y. Wang, S. Gong, D. Gomez, Y. Ling, L. W. Yap, G. P. Simon, W. Cheng, *ACS Nano* **2018**, *12*, 8717.

[157] C. M. Voge, J. P. Stegemann, *J. Neural. Eng.* **2011**, *8*, 011001.

[158] L. X. Zheng, M. J. O'Connell, S. K. Doorn, X. Z. Liao, Y. H. Zhao, E. A. Akhadov, M. A. Hoffbauer, B. J. Roop, Q. X. Jia, R. C. Dye, D. E. Peterson, S. M. Huang, J. Liu, Y. T. Zhu, *Nat. Mater.* **2004**, *3*, 673.

[159] Z. Liu, L. Jiao, Y. Yao, X. Xian, J. Zhang, *Adv. Mater.* **2010**, *22*, 2285.

[160] A. A. John, A. P. Subramanian, M. V. Vellayappan, A. Balaji, H. Mohandas, S. K. Jaganathan, *International journal of nanomedicine* **2015**, *10*, 4267.

[161] S. M. Wellman, J. R. Eles, K. A. Ludwig, J. P. Seymour, N. J. Michelson, W. E. McFadden, A. L. Vazquez, T. D. Y. Kozai, *Adv. Funct. Mater.* **2018**, *28*, 1701269.

[162] F. Vitale, S. R. Summerson, B. Aazhang, C. Kemere, M. Pasquali, *ACS Nano* **2015**, *9*, 4465.

[163] T. Sekitani, H. Nakajima, H. Maeda, T. Fukushima, T. Aida, K. Hata, T. Someya, *Nat. Mater.* **2009**, *8*, 494.

[164] D. J. Lipomi, M. Vosgueritchian, B. C. Tee, S. L. Hellstrom, J. A. Lee, C. H. Fox, Z. Bao, *Nat. Nanotechnol.* **2011**, *6*, 788.

[165] C. Zhu, A. Chortos, Y. Wang, R. Pfattner, T. Lei, A. C. Hinckley, I. Pochorovski, X. Yan, J. W. F. To, J. Y. Oh, J. B. H. Tok, Z. Bao, B. Murmann, *Nat. Electron.* **2018**, *1*, 183.

[166] D. Son, J. Kang, O. Vardoulis, Y. Kim, N. Matsuhisa, J. Y. Oh, J. W. To, J. Mun, T. Katsumata, Y. Liu, A. F. McGuire, M. Krason, F. Molina-Lopez, J. Ham, U. Kraft, Y. Lee, Y. Yun, J. B. Tok, Z. Bao, *Nat. Nanotechnol.* **2018**, *13*, 1057.

[167] Y. Chen, C. Tan, H. Zhang, L. Wang, *Chem. Soc. Rev.* **2015**, *44*, 2681.

[168] H. Kim, J.-H. Ahn, *Carbon* **2017**, *120*, 244.

[169] C. Cheng, S. Li, A. Thomas, N. A. Kotov, R. Haag, *Chem. Rev.* **2017**, *117*, 1826.

[170] D. Bitounis, H. Ali-Boucetta, B. H. Hong, D. H. Min, K. Kostarelos, *Adv. Mater.* **2013**, *25*, 2258.

[171] X. Ding, H. Liu, Y. Fan, *Adv. Healthcare Mater.* **2015**, *4*, 1451.

[172] A. Bendali, L. H. Hess, M. Seifert, V. Forster, A. F. Stephan, J. A. Garrido, S. Picaud, *Adv. Healthcare Mater.* **2013**, *2*, 929.

[173] F. Veliev, A. Briançon-Marjollet, V. Bouchiat, C. Delacour, *Biomaterials* **2016**, *86*, 33.

[174] P. Kang, M. C. Wang, S. Nam, *Microelectron. Eng.* **2016**, *161*, 18.

[175] S. Syama, P. V. Mohanan, *Int. J. Biol. Macromol.* **2016**, *86*, 546.

[176] C. Liao, Y. Li, S. Tjong, *Int. J. Mol. Sci.* **2018**, *19*, 3564.

[177] S. Y. Park, J. Park, S. H. Sim, M. G. Sung, K. S. Kim, B. H. Hong, S. Hong, *Adv. Mater.* **2011**, *23*, H263.

[178] C. Martin, S. Merino, J. M. Gonzalez-Dominguez, R. Rauti, L. Ballerini, M. Prato, E. Vazquez, *Sci. Rep.* **2017**, *7*, 10942.

[179] K. Kostarelos, M. Vincent, C. Hebert, J. A. Garrido, *Adv. Mater.* **2017**, *29*, 1700909.

[180] D. Kuzum, H. Takano, E. Shim, J. C. Reed, H. Juul, A. G. Richardson, J. de Vries, H. Bink, M. A. Dichter, T. H. Lucas, D. A. Coulter, E. Cubukcu, B. Litt, *Nat. Commun.* **2014**, *5*, 5259.

[181] M. S. Mannoor, H. Tao, J. D. Clayton, A. Sengupta, D. L. Kaplan, R. R. Naik, N. Verma, F. G. Omenetto, M. C. McAlpine, *Nat. Commun.* **2012**, *3*, 763.

[182] N. V. Apollo, M. I. Maturana, W. Tong, D. A. X. Nayagam, M. N. Shivdasani, J. Foroughi, G. G. Wallace, S. Prawer, M. R. Ibbotson, D. J. Garrett, *Adv. Funct. Mater.* **2015**, *25*, 3551.

[183] K. Parida, V. Bhavanasi, V. Kumar, J. Wang, P. S. Lee, *J. Power Sources* **2017**, *342*, 70.

[184] V. Kumar, S. Park, K. Parida, V. Bhavanasi, P. S. Lee, *Materials Today Energy* **2017**, *4*, 41.

[185] L. Fenno, O. Yizhar, K. Deisseroth, *Annu. Rev. Neurosci.* **2011**, *34*, 389.

[186] A. A. Schendel, S. Thongpang, S. K. Brodnick, T. J. Richner, B. D. Lindevig, L. Krugner-Higby, J. C. Williams, *J. Neurosci. Methods* **2013**, *218*, 121.

[187] A. Norlin, J. Pan, C. Leygraf, *J. Electrochem. Soc.* **2005**, *152*, J7.

[188] H. S. Jung, T. Lee, I. K. Kwon, H. S. Kim, S. K. Hahn, C. S. Lee, *ACS Appl. Mater. Interfaces* **2015**, *7*, 9598.

[189] V. Georgakilas, J. N. Tiwari, K. C. Kemp, J. A. Perman, A. B. Bourlinos, K. S. Kim, R. Zboril, *Chem. Rev.* **2016**, *116*, 5464.

[190] Y. Chen, A. Star, S. Vidal, *Chem. Soc. Rev.* **2013**, *42*, 4532.

[191] S. Z. Butler, S. M. Hollen, L. Cao, Y. Cui, J. A. Gupta, H. R. Gutierrez, T. F. Heinz, S. S. Hong, J. Huang, A. F. Ismach, E. Johnston-Halperin, M. Kuno, V. V. Plashnitsa, R. D. Robinson, R. S. Ruoff, S. Salahuddin, J. Shan, L. Shi, M. G. Spencer, M. Terrones, W. Windl, J. E. Goldberger, *ACS Nano* **2013**, *7*, 2898.

[192] B. Anasori, M. R. Lukatskaya, Y. Gogotsi, *Nat. Rev. Mater.* **2017**, *2*, 16098.

[193] J. Pang, R. G. Mendes, A. Bachmatiuk, L. Zhao, H. Q. Ta, T. Gemming, H. Liu, Z. Liu, M. H. Rummeli, *Chem. Soc. Rev.* **2019**, *48*, 72.

[194] R. Rakhi, P. Nayak, C. Xia, H. N. Alshareef, *Sci. Rep.* **2016**, *6*, 36422.

[195] C. Dai, Y. Chen, X. Jing, L. Xiang, D. Yang, H. Lin, Z. Liu, X. Han, R. Wu, *ACS nano* **2017**, *11*, 12696.

[196] H. Lin, Y. Wang, S. Gao, Y. Chen, J. Shi, *Adv. Mater.* **2018**, *30*, 1703284.

[197] X. Han, J. Huang, H. Lin, Z. Wang, P. Li, Y. Chen, *Adv. Healthcare Mater.* **2018**, *7*, 1701394.

[198] N. Driscoll, A. G. Richardson, K. Maleski, B. Anasori, O. Adewole, P. Lelyukh, L. Escobedo, D. K. Cullen, T. H. Lucas, Y. Gogotsi, *ACS nano* **2018**, *12*, 10419.

[199] M. Soleymaniha, M. A. Shahbazi, A. R. Rafieerad, A. Maleki, A. Amiri, *Adv. Healthcare Mater.* **2019**, *8*, 1801137.

[200] B. Xiao, Y.-c. Li, X.-f. Yu, J.-b. Cheng, *Sens. Actuators, B* **2016**, *235*, 103.

[201] Y. Lei, W. Zhao, Y. Zhang, Q. Jiang, J. H. He, A. J. Baeumner, O. S. Wolfbeis, Z. L. Wang, K. N. Salama, H. N. Alshareef, *Small* **2019**, *15*, e1901190.

[202] B. Xu, M. Zhu, W. Zhang, X. Zhen, Z. Pei, Q. Xue, C. Zhi, P. Shi, *Adv. Mater.* **2016**, *28*, 3333.

[203] X. Chen, X. Sun, W. Xu, G. Pan, D. Zhou, J. Zhu, H. Wang, X. Bai, B. Dong, H. Song, *Nanoscale* **2018**, *10*, 1111.

[204] J. H. Ciou, S. Li, P. S. Lee, *Small* **2019**, *15*, 1903281.

[205] S. J. Kim, H. J. Koh, C. E. Ren, O. Kwon, K. Maleski, S. Y. Cho, B. Anasori, C. K. Kim, Y. K. Choi, J. Kim, Y. Gogotsi, H. T. Jung, *ACS Nano* **2018**, *12*, 986.

[206] X. Xu, W. Yao, D. Xiao, T. F. Heinz, *Nature Physics* **2014**, *10*, 343.

[207] S. Manzeli, D. Ovchinnikov, D. Pasquier, O. V. Yazyev, A. Kis, *Nat. Rev. Mater.* **2017**, *2*, 17033.

[208] R. Kurapati, K. Kostarelos, M. Prato, A. Bianco, *Adv. Mater.* **2016**, *28*, 6052.

[209] K. Kalantar-zadeh, J. Z. Ou, T. Daeneke, M. S. Strano, M. Pumera, S. L. Gras, *Adv. Funct. Mater.* **2015**, *25*, 5086.

[210] Y. Hayamizu, C. R. So, S. Dag, T. S. Page, D. Starkebaum, M. Sarikaya, *Sci. Rep.* **2016**, *6*, 33778.

[211] J. Zhou, J. Lin, X. Huang, Y. Zhou, Y. Chen, J. Xia, H. Wang, Y. Xie, H. Yu, J. Lei, D. Wu, F. Liu, Q. Fu, Q. Zeng, C. H. Hsu, C. Yang, L. Lu, T. Yu, Z. Shen, H. Lin, B. I. Yakobson, Q. Liu, K. Suenaga, G. Liu, Z. Liu, *Nature* **2018**, *556*, 355.

[212] W. Zhao, R. M. Ribeiro, G. Eda, *Acc. Chem. Res.* **2015**, *48*, 91.

[213] C. P. Lu, G. Li, J. Mao, L. M. Wang, E. Y. Andrei, *Nano Lett.* **2014**, *14*, 4628.

[214] J. Zhao, N. Li, H. Yu, Z. Wei, M. Liao, P. Chen, S. Wang, D. Shi, Q. Sun, G. Zhang, *Adv. Mater.* **2017**, *29*, 1702076.

[215] M. Park, Y. J. Park, X. Chen, Y. K. Park, M. S. Kim, J. H. Ahn, *Adv. Mater.* **2016**, *28*, 2556.

[216] Y. J. Park, B. K. Sharma, S. M. Shinde, M. S. Kim, B. Jang, J. H. Kim, J. H. Ahn, *ACS Nano* **2019**, *13*, 3023.

[217] H. Li, Z. Yin, Q. He, H. Li, X. Huang, G. Lu, D. W. Fam, A. I. Tok, Q. Zhang, H. Zhang, *Small* **2012**, *8*, 63.

[218] D. Sarkar, W. Liu, X. Xie, A. C. Anselmo, S. Mitragotri, K. Banerjee, *ACS Nano* **2014**, *8*, 3992.

[219] P. Zhang, S. Yang, R. Pineda-Gomez, B. Ibarlucea, J. Ma, M. R. Lohe, T. F. Akbar, L. Baraban, G. Cuniberti, X. Feng, *Small* **2019**, *15*, 1901265.

[220] S. Wu, Z. Zeng, Q. He, Z. Wang, S. J. Wang, Y. Du, Z. Yin, X. Sun, W. Chen, H. Zhang, *Small* **2012**, *8*, 2264.

[221] J. Yoon, S. N. Lee, M. K. Shin, H. W. Kim, H. K. Choi, T. Lee, J. W. Choi, *Biosens. Bioelectron.* **2019**, *140*, 111343.

[222] A. Elschner, S. Kirchmeyer, W. Lovenich, U. Merker, K. Reuter, *PEDOT: principles and applications of an intrinsically conductive polymer*, CRC Press, **2010**.

[223] J. Rivnay, S. Inal, B. A. Collins, M. Sessolo, E. Stavrinidou, X. Strakosas, C. Tassone, D. M. Delongchamp, G. G. Malliaras, *Nat. Commun.* **2016**, *7*, 11287.

[224] E. Stavrinidou, P. Leleux, H. Rajaona, D. Khodagholy, J. Rivnay, M. Lindau, S. Sanaur, G. G. Malliaras, *Adv. Mater.* **2013**, *25*, 4488.

[225] M. R. Abidian, K. A. Ludwig, T. C. Marzullo, D. C. Martin, D. R. Kipke, *Adv. Mater.* **2009**, *21*, 3764.

[226] M. Berggren, A. Richter-Dahlfors, *Adv. Mater.* **2007**, *19*, 3201.

[227] R. Green, M. R. Abidian, *Adv. Mater.* **2015**, *27*, 7620.

[228] M. R. Abidian, D. C. Martin, *Adv. Funct. Mater.* **2009**, *19*, 573.

[229] H. C. Tian, J. Q. Liu, D. X. Wei, X. Y. Kang, C. Zhang, J. C. Du, B. Yang, X. Chen, H. Y. Zhu, Y. N. Nuli, C. S. Yang, *Biomaterials* **2014**, *35*, 2120.

[230] J. Rivnay, S. Inal, A. Salleo, R. M. Owens, M. Berggren, G. G. Malliaras, *Nat. Rev. Mater.* **2018**, *3*, 17086.

[231] W. Lee, D. Kim, N. Matsuhisa, M. Nagase, M. Sekino, G. G. Malliaras, T. Yokota, T. Someya, *Proc. Natl. Acad. Sci. U. S. A.* **2017**, *114*, 10554.

[232] A. Williamson, M. Ferro, P. Leleux, E. Ismailova, A. Kaszas, T. Doublet, P. Quilichini, J. Rivnay, B. Rozsa, G. Katona, C. Bernard, G. G. Malliaras, *Adv. Mater.* **2015**, *27*, 4405.

[233] D. Khodagholy, T. Doublet, P. Quilichini, M. Gurfinkel, P. Leleux, A. Ghestem, E. Ismailova, T. Herve, S. Sanaur, C. Bernard, G. G. Malliaras, *Nat. Commun.* **2013**, *4*, 1575.

[234] J. Rivnay, P. Leleux, M. Ferro, M. Sessolo, A. Williamson, D. A. Koutsouras, D. Khodagholy, M. Ramuz, X. Strakosas, R. M. Owens, C. Benar, J. M. Badier, C. Bernard, G. G. Malliaras, *Sci. Adv.* **2015**, *1*, e1400251.

[235] D. A. Bernards, D. J. Macaya, M. Nikolou, J. A. DeFranco, S. Takamatsu, G. G. Malliaras, *J. Mater. Chem.* **2008**, *18*, 116.

[236] H. Tang, F. Yan, P. Lin, J. Xu, H. L. W. Chan, *Adv. Funct. Mater.* **2011**, *21*, 2264.

[237] I. Gualandi, M. Marzocchi, A. Achilli, D. Cavedale, A. Bonfiglio, B. Fraboni, *Sci. Rep.* **2016**, *6*, 33637.

[238] S. Wustoni, A. Savva, R. Sun, E. Bihar, S. Inal, *Adv. Mater. Interfaces* **2018**, *6*, 1800928.

[239] D. Tahk, H. H. Lee, D.-Y. Khang, *Macromolecules* **2009**, *42*, 7079.

[240] D. J. Lipomi, J. A. Lee, M. Vosgueritchian, B. C. K. Tee, J. A. Bolander, Z. Bao, *Chem. Mater.* **2012**, *24*, 373.

[241] J. Y. Oh, S. Kim, H. K. Baik, U. Jeong, *Adv. Mater.* **2016**, *28*, 4455.

[242] Y. Wang, C. Zhu, R. Pfattner, H. Yan, L. Jin, S. Chen, F. Molina-Lopez, F. Lissel, J. Liu, N. I. Rabiah, Z. Chen, J. W. Chung, C. Linder, M. F. Toney, B. Murmann, Z. Bao, *Sci. Adv.* **2017**, *3*, e1602076.

[243] P. J. Rousche, D. S. Pellinen, D. P. Pivin, J. C. Williams, R. J. Vetter, D. R. Kipke, *IEEE Trans. Biomed. Eng.* **2001**, *48*, 361.

[244] J. Leach, A. K. H. Achyuta, S. K. Murthy, *Front. Neuroeng.* **2010**, *2*, 18.

[245] P. Moshayedi, G. Ng, J. C. Kwok, G. S. Yeo, C. E. Bryant, J. W. Fawcett, K. Franze, J. Guck, *Biomaterials* **2014**, *35*, 3919.

[246] E. Castagnola, A. Ansaldo, E. Maggiolini, T. Ius, M. Skrap, D. Ricci, L. Fadiga, *Front. Neuroeng.* **2014**, *7*.

[247] C. C. Kim, H. H. Lee, K. H. Oh, J. Y. Sun, *Science* **2016**, *353*, 682.

[248] Y. Yang, L. Guan, X. Li, Z. Gao, X. Ren, G. Gao, *ACS Appl. Mater. Interfaces* **2018**, *11*, 3428−3437.

[249] Z. Lei, P. Wu, *Nat. Commun.* **2018**, *9*, 1134.

[250] K. Parida, V. Kumar, W. Jiangxin, V. Bhavanasi, R. Bendi, P. S. Lee, *Adv. Mater.* **2017**, *29*, 1702181.

[251] D. Seliktar, *Science* **2012**, *336*, 1124.

[252] S. Kalia, *Polymeric hydrogels as smart biomaterials*, Springer, **2016**.

[253] X. N. Zhang, Y. J. Wang, S. Sun, L. Hou, P. Wu, Z. L. Wu, Q. Zheng, *Macromolecules* **2018**, *51*, 8136.

[254] J. Y. Sun, X. Zhao, W. R. Illeperuma, O. Chaudhuri, K. H. Oh, D. J. Mooney, J. J. Vlassak, Z. Suo, *Nature* **2012**, *489*, 133.

[255] S. R. Caliari, J. A. Burdick, *Nat. Methods* **2016**, *13*, 405.

[256] B. Sharma, S. Fermanian, M. Gibson, S. Unterman, D. A. Herzka, B. Cascio, J. Coburn, A. Y. Hui, N. Marcus, G. E. Gold, J. H. Elisseeff, *Sci. Transl. Med.* **2013**, *5*, 167ra6.

[257] H. W. Kang, S. J. Lee, I. K. Ko, C. Kengla, J. J. Yoo, A. Atala, *Nat. Biotechnol.* **2016**, *34*, 312.

[258] H. Yuk, T. Zhang, S. Lin, G. A. Parada, X. Zhao, *Nat. Mater.* **2016**, *15*, 190.

[259] K. C. Spencer, J. C. Sy, K. B. Ramadi, A. M. Graybiel, R. Langer, M. J. Cima, *Sci. Rep.* **2017**, *7*, 1952.

[260] L. Rao, H. Zhou, T. Li, C. Li, Y. Y. Duan, *Acta Biomater.* **2012**, *8*, 2233.

[261] L. Guo, *Front. Neurosci.* **2016**, *10*, 599.

[262] R. A. Green, N. H. Lovell, G. G. Wallace, L. A. Poole-Warren, *Biomaterials* **2008**, *29*, 3393.

[263] N. A. Staples, J. A. Goding, A. D. Gilmour, K. Y. Aristovich, P. Byrnes-Preston, D. S. Holder, J. W. Morley, N. H. Lovell, D. J. Chew, R. A. Green, *Front. Neurosci.* **2018**, *11*, 748.

[264] B. Song, Y. Gu, J. Pu, B. Reid, Z. Zhao, M. Zhao, *Nat. Protoc.* **2007**, *2*, 1479.

[265] M. H. Histed, V. Bonin, R. C. Reid, *Neuron* **2009**, *63*, 508.

[266] M. R. Warden, J. A. Cardin, K. Deisseroth, *Annu. Rev. Biomed. Eng.* **2014**, *16*, 103.

[267] G.-P. Hao, F. Hippauf, M. Oschatz, F. M. Wisser, A. Leifert, W. Nickel, N. Mohamed-Noriega, Z. Zheng, S. Kaskel, *ACS nano* **2014**, *8*, 7138.

[268] J. Duan, X. Liang, J. Guo, K. Zhu, L. Zhang, *Adv. Mater.* **2016**, *28*, 8037.

[269] Y. Shi, C. Ma, L. Peng, G. Yu, *Adv. Funct. Mater.* **2015**, *25*, 1219.

[270] S. Zeng, H. Chen, F. Cai, Y. Kang, M. Chen, Q. Li, *J. Mater. Chem. A* **2015**, *3*, 23864.

[271] D. H. Kim, M. Abidian, D. C. Martin, *Journal of Biomedical Materials Research, Part A* **2004**, *71*, 577.

[272] D.-H. Kim, J. A. Wiler, D. J. Anderson, D. R. Kipke, D. C. Martin, *Acta Biomater.* **2010**, *6*, 57.

[273] J. Hur, K. Im, S. W. Kim, J. Kim, D. Y. Chung, T. H. Kim, K. H. Jo, J. H. Hahn, Z. Bao, S. Hwang, N. Park, *ACS Nano* **2014**, *8*, 10066.

[274] S. M. Richardson-Burns, J. L. Hendricks, B. Foster, L. K. Povlich, D.-H. Kim, D. C. Martin, *Biomaterials* **2007**, *28*, 1539.

[275] E. Castagnola, A. Ansaldo, E. Maggiolini, G. N. Angotzi, M. Skrap, D. Ricci, L. Fadiga, *ACS Nano* **2013**, *7*, 3887.

[276] B. Lu, H. Yuk, S. Lin, N. Jian, K. Qu, J. Xu, X. Zhao, *Nat. Commun.* **2019**, *10*, 1043.

[277] V. R. Feig, H. Tran, M. Lee, Z. Bao, *Nat. Commun.* **2018**, *9*, 2740.

[278] S. Yang, L. Jang, S. Kim, J. Yang, K. Yang, S. W. Cho, J. Y. Lee, *Macromol. Biosci.* **2016**, *16*, 1653.

[279] J. Kang, J. B. H. Tok, Z. Bao, *Nat. Electron.* **2019**, *2*, 144.

[280] Y. Cao, T. G. Morrissey, E. Acome, S. I. Allec, B. M. Wong, C. Keplinger, C. Wang, *Adv. Mater.* **2017**, *29*, 1605099.

[281] Y. Cao, Y. J. Tan, S. Li, W. W. Lee, H. Guo, Y. Cai, C. Wang, B. C. K. Tee, *Nat. Electron.* **2019**, *2*, 75.

[282] J. Kang, D. Son, G. N. Wang, Y. Liu, J. Lopez, Y. Kim, J. Y. Oh, T. Katsumata, J. Mun, Y. Lee, L. Jin, J. B. Tok, Z. Bao, *Adv. Mater.* **2018**, *30*, 1706846.

[283] B. Zhang, P. Zhang, H. Zhang, C. Yan, Z. Zheng, B. Wu, Y. Yu, *Macromol. Rapid Commun.* **2017**, *38*, 1700110.

[284] C. H. Li, C. Wang, C. Keplinger, J. L. Zuo, L. Jin, Y. Sun, P. Zheng, Y. Cao, F. Lissel, C. Linder, X. Z. You, Z. Bao, *Nat. Chem.* **2016**, *8*, 618.

[285] W. Schmolke, N. Perner, S. Seiffert, *Macromolecules* **2015**, *48*, 8781.

[286] S. K. Kang, J. Koo, Y. K. Lee, J. A. Rogers, *Acc. Chem. Res.* **2018**, *51*, 988.

[287] S. W. Hwang, H. Tao, D. H. Kim, H. Cheng, J. K. Song, E. Rill, M. A. Brenckle, B. Panilaitis, S. M. Won, Y. S. Kim, Y. M. Song, K. J. Yu, A. Ameen, R. Li, Y. Su, M. Yang, D. L. Kaplan, M. R. Zakin, M. J. Slepian, Y. Huang, F. G. Omenetto, J. A. Rogers, *Science* **2012**, *337*, 1640.

[288] C. M. Boutry, L. Beker, Y. Kaizawa, C. Vassos, H. Tran, A. C. Hinckley, R. Pfattner, S. Niu, J. Li, J. Claverie, Z. Wang, J. Chang, P. M. Fox, Z. Bao, *Nat. Biomed. Eng.* **2019**, *3*, 47.

[289] C. M. Boutry, Y. Kaizawa, B. C. Schroeder, A. Chortos, A. Legrand, Z. Wang, J. Chang, P. Fox, Z. Bao, *Nat. Electron.* **2018**, *1*, 314.

[290] D. Lu, T. L. Liu, J. K. Chang, D. Peng, Y. Zhang, J. Shin, T. Hang, W. Bai, Q. Yang, J. A. Rogers, *Adv. Mater*., http://doi.org/10.1002/adma.201902739

[291] X. Chen, Y. J. Park, M. Kang, S. K. Kang, J. Koo, S. M. Shinde, J. Shin, S. Jeon, G. Park, Y. Yan, M. R. MacEwan, W. Z. Ray, K. M. Lee, J. A. Rogers, J. H. Ahn, *Nat. Commun.* **2018**, *9*, 1690.

[292] S. E. Shaheen, R. Radspinner, N. Peyghambarian, G. E. Jabbour, *Appl. Phys. Lett.* **2001**, *79*, 2996.

[293] A. Kamyshny, S. Magdassi, *Small* **2014**, *10*, 3515.

[294] B. Nie, R. Li, J. Cao, J. D. Brandt, T. Pan, *Adv. Mater.* **2015**, *27*, 6055.

[295] M. Gao, L. Li, Y. Song, *J. Mater. Chem. C* **2017**, *5*, 2971.

[296] R. D. Farahani, M. Dube, D. Therriault, *Adv. Mater.* **2016**, *28*, 5794.

[297] J. Y. Oh, S. Rondeau-Gagne, Y. C. Chiu, A. Chortos, F. Lissel, G. N. Wang, B. C. Schroeder, T. Kurosawa, J. Lopez, T. Katsumata, J. Xu, C. Zhu, X. Gu, W. G. Bae, Y. Kim, L. Jin, J. W. Chung, J. B. Tok, Z. Bao, *Nature* **2016**, *539*, 411.

[298] E. Bihar, S. Wustoni, A. M. Pappa, K. N. Salama, D. Baran, S. Inal, *npj Flexible Electronics* **2018**, *2*, 30.

[299] S. Ma, F. Ribeiro, K. Powell, J. Lutian, C. Moller, T. Large, J. Holbery, *ACS Appl. Mater. Interfaces* **2015**, *7*, 21628.

[300] S. E. Burns, P. Cain, J. Mills, J. Wang, H. Sirringhaus, *MRS Bull.* **2011**, *28*, 829.

[301] K. Tian, J. Bae, S. E. Bakarich, C. Yang, R. D. Gately, G. M. Spinks, M. In Het Panhuis, Z. Suo, J. J. Vlassak, *Adv. Mater.* **2017**, *29*, 1604827.

[302] J. Wang, T. Lu, M. Yang, D. Sun, Y. Xia, T. Wang, *Sci. Adv.* **2019**, *5*, eaau8769.

[303] Z. Chen, D. Zhao, B. Liu, G. Nian, X. Li, J. Yin, S. Qu, W. Yang, *Adv. Funct. Mater.* **2019**, *29*, 1900971.

[304] D. J. Finn, M. Lotya, J. N. Coleman, *ACS Appl. Mater. Interfaces* **2015**, *7*, 9254.

[305] S. Azoubel, S. Magdassi, *Carbon* **2010**, *48*, 3346.

[306] T. Sekitani, Y. Noguchi, K. Hata, T. Fukushima, T. Aida, T. Someya, *Science* **2008**, *321*, 1468.

[307] F. Bonaccorso, A. Bartolotta, J. N. Coleman, C. Backes, *Adv. Mater.* **2016**, *28*, 6136.

[308] C. J. Zhang, L. McKeon, M. P. Kremer, S. H. Park, O. Ronan, A. Seral-Ascaso, S. Barwich, C. O. Coileain, N. McEvoy, H. C. Nerl, B. Anasori, J. N. Coleman, Y. Gogotsi, V. Nicolosi, *Nat. Commun.* **2019**, *10*, 1795.

[309] W. C. Huang, H. Y. Lai, L. W. Kuo, C. H. Liao, P. H. Chang, T. C. Liu, S. Y. Chen, Y. Y. Chen, *Adv. Mater.* **2015**, *27*, 4186.

[310] Z. Xie, R. Avila, Y. Huang, J. A. Rogers, *Adv. Mater.*, http://doi.org/10.1002/adma.201902767

[311] J. Kim, A. Banks, Z. Xie, S. Y. Heo, P. Gutruf, J. W. Lee, S. Xu, K.-I. Jang, F. Liu, G. Brown, J. Choi, J. H. Kim, X. Feng, Y. Huang, U. Paik, J. A. Rogers, *Adv. Funct. Mater.* **2015**, *25*, 4761.

[312] Q. Guo, J. Koo, Z. Xie, R. Avila, X. Yu, X. Ning, H. Zhang, X. Liang, S. B. Kim, Y. Yan, M. R. MacEwan, H. M. Lee, A. Song, Z. Di, Y. Huang, Y. Mei, J. A. Rogers, *Adv. Funct. Mater.*, http://doi.org/-10.1002/adfm.201905451

[313] L. Lu, P. Gutruf, L. Xia, D. L. Bhatti, X. Wang, A. Vazquez-Guardado, X. Ning, X. Shen, T. Sang, R. Ma, G. Pakeltis, G. Sobczak, H. Zhang, D. O. Seo, M. Xue, L. Yin, D. Chanda, X. Sheng, M. R. Bruchas, J. A. Rogers, *Proc. Natl. Acad. Sci. U. S. A.* **2018**, *115*, 1374.

[314] Z. Yan, F. Zhang, F. Liu, M. Han, D. Ou, Y. Liu, Q. Lin, X. Guo, H. Fu, Z. Xie, M. Gao, Y. Huang, J. Kim, Y. Qiu, K. Nan, J. Kim, P. Gutruf, H. Luo, A. Zhao, K. C. Hwang, Y. Huang, Y. Zhang, J. A. Rogers, *Sci. Adv.* **2016**, *2*, e1601014.

[315] Y. R. Jeong, J. Kim, Z. Xie, Y. Xue, S. M. Won, G. Lee, S. W. Jin, S. Y. Hong, X. Feng, Y. Huang, J. A. Rogers, J. S. Ha, *NPG Asia Mater.* **2017**, *9*, 443.

[316] B. S. Kim, K. Y. Shin, J. B. Pyo, J. Lee, J. G. Son, S. S. Lee, J. H. Park, *ACS Appl. Mater. Interfaces* **2016**, *8*, 2582.

[317] M. Kaltenbrunner, M. S. White, E. D. Glowacki, T. Sekitani, T. Someya, N. S. Sariciftci, S. Bauer, *Nat. Commun.* **2012**, *3*, 770.

[318] Q. Zheng, H. Zhang, B. Shi, X. Xue, Z. Liu, Y. Jin, Y. Ma, Y. Zou, X. Wang, Z. An, W. Tang, W. Zhang, F. Yang, Y. Liu, X. Lang, Z. Xu, Z. Li, Z. L. Wang, *ACS Nano* **2016**, *10*, 6510.

[319] K. Parida, J. Xiong, X. Zhou, P. S. Lee, *Nano Energy* **2019**, *59*, 237.

[320] Q. Zheng, Y. Zou, Y. Zhang, Z. Liu, B. Shi, X. Wang, Y. Jin, H. Ouyang, Z. Li, Z. L. Wang, *Sci. Adv.* **2016**, *2*, e1501478.

[321] A. Branner, R. A. Normann, *Brain Res. Bull.* **2000**, *51*, 293.

[322] E. Roh, B. U. Hwang, D. Kim, B. Y. Kim, N. E. Lee, *Acs Nano* **2015**, *9*, 6252.

[323] J. Park, S. Choi, A. H. Janardhan, S.-Y. Lee, S. Raut, J. Soares, K. Shin, S. Yang, C. Lee, K.-W. Kang, *Sci. Transl. Med.* **2016**, *8*, 344ra86.

Figure Captions

Figure 2. Schematic of skin anatomy and the summarization of various physiological signals accessible from epidermal sensors.

Figure 2. Epidermal bioelectronic sensors. **a)** Representative epidermal physical sensors including a triboelectric motion sensor (top left), a flexible multifunctional sensor for skin temperature, heart rate, physical activity and UV light monitoring (top right), a wireless epidermal sensor for on-skin temperature and pressure mapping (bottom left, scale bar, 8 mm), and a stretchable mechano-acoustic sensing platform for cardiovascular diagnostics (bottom right). Reproduced with permission.[14, 68] Copyright 2017, American Chemical Society; Copyright 2018, AAAS. Reproduced under the terms of Creative Commons Attribution NonCommercial License 4.0.[16, 20] Copyright 2016, AAAS; Copyright 2016, AAAS. **b)** Representative epidermal electrical (electrophysiological) sensors including a CNT-based tether-free ECG sensor (top left), a stretchable and breathable electronic fabric for ECG/EMG measurement (top right), and an ultrathin epidermal sensor for long-term, high fidelity EEG recording (bottom). Reproduced under the terms of Creative Commons Attribution 4.0 International License. [24, 29] Copyright 2014, Nature Publishing Group; Copyright 2014, Nature Publishing Group. Reproduced with permission.[25] Copyright 2015, National Academy of Sciences USA. **c)** Representative epidermal chemical sensors including a wearable and disposable epidermal strip for selective screening of biomarkers in sweat (top left), a skin-interfaced microfluidic/electronic system for simultaneous detection of metabolites and sweating rate (top right), an ultra-flexible organic pulse oximeter (bottom left), and a miniaturized skin-mountable pulse oximeter (bottom right). Reproduced under the terms of Creative Commons Attribution NonCommercial License 4.0.[35, 50, 54] Copyright 2017, AAAS; Copyright 2019, AAAS; Copyright 2016, AAAS; Reproduced with permission.[55] Copyright 2017, Wiley-VCH.

Figure 3. Epidermal stimulating devices. **a)** Photograph of an array of transcutaneous electrical stimulation electrodes (left) and the resulting neuromuscular voltage response (right). Reproduced with permission.[9] Copyright 2016, Wiley-VCH. **b)** Photographs of an epidermal stimulating platform showing its stretchability (left) and conformability to human body (right). Reproduced with permission.[113] Copyright 2018, Nature Publishing Group. **c)** Schematics of the iontophoresis mechanism for sweat induction and on-site analysis. **d)** Photographs of an autonomous sweat extraction and ion screening platform. Reproduced with permission.[63] Copyright 2017, National Academy of Sciences USA. **e)** Illustration and photograph of a tattoo-based wearable iontophoretic-biosensing system. Reproduced with permission.[34] Copyright 2016, American Chemical Society.

Figure 4. Material requirements for epidermal Interfaces. **a)** Photographs of a hydrogel patch adhered to human skin with the assist of the silk adhesive (left) and an ECG electrode with the conductive silk gel as interfacial coating (right). Reproduced with permission.[23] Copyright 2018, Wiley-VCH. **b)** Photographs highlighting the importance of adhesive modulation. The peeling force generated when removing the modified adhesive is much lower than the conventional ECG adhesive. Reproduced under the terms of Creative Commons Attribution 4.0 International License.[72] Copyright 2019, AAAS. **c)** Photograph of a porous silicone-based sweat sensor attached on human skin (left) and SEM image of an elastomeric silicone sponge. Reproduced with permission.[28, 48] Copyright 2014, Wiley-VCH. Copyright 2018, Wiley-VCH. **d)** SEM image of a microperforated soft silicone substrate with serpentine Au mesh electrode patterned on top (left); SEM tilted view of a microperforated soft silicone substrate laminated on a skin replica (right). Reproduced with permission.[73] Copyright 2019, Nature Publishing Group. **e)** Optical microscope image of nanomesh conductors conformally bonded with the uneven skin surface (left) and SEM image showing the epidermal nanomesh conductors is not blocking the sweat pore (right). Reproduced with permission.[27] Copyright 2017, Nature Publishing Group. **f)** Photograph of an electrophysiological sensor with porous graphene as electrodes

(left) and SEM image of the laser-induced porous graphene (right). Reproduced with permission.[28] Copyright 2018, Wiley-VCH.

Figure 5. Schematics depicting neural signals recorded at different length scales. **a)** LFP generated by a small cluster of subcortical neurons with equipotential lines being depicted. **b)** Extracellular potential generated by an individual neuron with equipotential lines being depicted. **c)** Action potential across a neuron's membrane activated during the depolarization process.

Figure 6. Material requirements for neural interfaces. **a)** Photograph of a silicon-based Utah electrode array for chronic intracortical neural recording and stimulation. Reproduced with permission.[321] Copyright 2000, Elsevier. **b)** Photograph of a cortex-conformable electrode array on 25μm thick PI substrate. Reproduced under the terms of Creative Commons Attribution 4.0 International License.[180] Copyright 2014, Nature Publishing Group. **c)** Photograph of a nanowire-based stretchable electrode grid embedded in PDMS. Reproduced under the terms of Creative Commons Attribution NonCommercial License.[99] Copyright 2018, Wiley-VCH. **d)** 3D printed living responsive hydrogel for chemical detection. Reproduced with permission.[104] Copyright 2018, Wiley-VCH. **e)** Equivalent circuit model of electrode-tissue interface. The figure is illustrated in the signal recording condition. Reproduced under the terms of Creative Commons Attribution License 4.0.[5] Copyright 2017, AAAS. **f)** Laser pyrolysis induced porous graphene array as low impedance neural interfaces. Reproduced under the terms of Creative Commons Attribution 4.0 International License.[109] Copyright 2016, Nature Publishing Group. **g)** Schematic of the experimental sample for water penetration testing. Here the bio-fluids barrier is the SiO_2/HfO_2 bilayer (left); SEM image of a 100 nm thick thermal SiO_2 layer on PI substrate (right).[115] Reproduced with permission. Copyright 2018, Wiley-VCH.

Figure 7. Metallic NMs-based bioelectronic interfaces. **a)** SEM image of buckled NMs (left) and photograph showing the deformability of the buckled NMs on PDMS substrate (right). Reproduced

with permission.[117] Copyright 2008, National Academy of Sciences USA. **b)** Micrographs of the filamentary serpentine (FS) mesh with (left) and without (right) the exertion of 30% strain. Reproduced with permission.[125] Copyright 2013, Wiley-VCH. **c)** Micrograph of a multifunctional epidermal electronic system fabricated via NMs-based electronics. Reproduced with permission.[66] Copyright 2011, AAAS. **d)** Photograph of the wireless epidermal electronic systems illustrating their sizes and physical form factors. Reproduced under the terms of Creative Commons Attribution 4.0 International License.[72] Copyright 2019, AAAS. **e)** Photograph of three sets of large-area epidermal electrodes array fabricated on silicon wafer (left) and the magnified view of an individual fractal electrode (right). **f)** Photograph of a large-area epidermal electrodes array laminated on the forearm. Reproduced with permission.[73] Copyright 2019, Nature Publishing Group.

Figure 8. Metallic NWs and their analogues for bioelectronic interfaces. **a)** Photograph of a soft articular heater based on AgNWs-SBS composite; Crosssectional-SEM of the composite electrode (inset). Reproduced with permission.[322] Copyright 2015, American Chemical Society. **b)** Photographs showing the elasticity of a AgNWs-SBS epicardial mesh (left); photograph of the mesh encircling a 3D printed heart model (right). Reproduced with permission.[323] Copyright 2016, AAAS. **c)** Cross-sectional view of the soft neural probe and the magnified view of the AgNWs coating layer (left); schematic depicting simultaneous neural recording and optical stimulation in a mosue spinal cord (right). Reproduced under the terms of Creative Commons Attribution NonCommercial License 4.0.[147] Copyright 2017, AAAS. **d)** Schematic of the functional modules and AgNF antenna/interconnect on the smart contact lens. Reproduced under the terms of Creative Commons Attribution NonCommercial License 4.0.[36] Copyright 2018, AAAS. **e)** SEM image and backscattered electron image (inset) of Ag-Au core-sheath nanowires (left); EDS elemental mapping of the nanowire revealing the distribution of Au and Ag and its core-sheath structure. Scale bars, 5 μm and 200 nm (inset). Reproduced with permission.[113] Copyright 2018, Nature Publishing Group. **f)** SEM image (left) and illustration (middle) of the vertically aligned AuNWs and photograph (right)

of a freestanding "Janus" film. Scale bars, 500 nm and 1cm. Reproduced with permission.[156] Copyright 2018, American Chemical Society.

Figure 9. Graphene-based bioelectronic interfaces. **a)** Photograph of the highly flexible graphene microelectrode for neural implantation (top left); micrograph of electrode array (top right); Graph comparing the recorded spiking activity from brain using Au electrode and doped graphene electrode (bottom). Reproduced under the terms of Creative Commons Attribution 4.0 International License.[180] Copyright 2014, Nature Publishing Group. **b)** Photograph of the flexible porous graphene electrode array placed at the surface of mouse cortex for in vivo cortical sensing (left); SEM image of the porous graphene electrode (right). Scale bar, 100 μm. **c)** Cyclic Voltammetry of the porous graphene electrode demonstrating high charge transfer capacity compared to Au electrode. Reproduced under the terms of Creative Commons Attribution 4.0 International License.[109] Copyright 2016, Nature Publishing Group. **d)** Photograph of the rat brain sized graphene microelectrodes array and the magnified image showing the transparency of graphene electrode. Scale bar, 500 mm. **e)** Fluorescence image of the transparent graphene micro-electrode implanted onto the cerebral cortex of the mouse (left). Scale bar, 500 μm; fluorescence image of the Pt electrode implanted into the cerebral cortex of the mouse for comparison (right). Scale bar, 750 μm. Reproduced under the terms of Creative Commons Attribution 4.0 International License. [90] Copyright 2014, Nature Publishing Group.

Figure 10. MXene-based bioelectronic interfaces. **a)** From left to right: atomic structure of MXene; photograph of delaminated MXene dispersed in water; freestanding MXene film prepared by vacuum filtration; cross-sectional SEM image of a MXene film; TEM image of a single-layer MXene flake. Reproduced with permission.[192] Copyright 2017, Nature Publishing Group. **b)** Schematic of in vivo neural recordings using MXene electrodes. MXene/Au intracortical arrays electrode were implanted into the cortex. **c)** Schematic and microscopy image of the MXene/Au intracortical electrode array (left); diagram comparing the number of unique spikes observed by adjacent Mxene and Au

electrodes (right). Reproduced with permission.[198] Copyright 2018, American Chemical Society. **d)** Schematic of Mxene based transistor biosensor for the detection of dopamine (left); SEM image showing the multilayer structure of MXene (right). **e)** Schematic diagram showing the working principle of the MXene transistor to record action potentials of neurons. Reproduced with permission.[202] Copyright 2016, Wiley-VCH.

Figure 11. Conductive polymer-based bioelectronic interfaces. **a)** Chemical structure of PEDOT:PSS. Reproduced under the terms of Creative Commons Attribution 4.0 International License.[223] Copyright 2016, Nature Publishing Group. **b)** Optical micrograph of the OECT probe conformally wrapping around a curvilinear surface and the magnified view of the transistor structure (left). Scale bars, 1 mm and 10 μm. Recorded neural spikes from an OECT transistor (pink), a surface electrode (blue) and 12 penetrating electrodes (black) (right). Reproduced under the terms of Creative Commons Attribution 4.0 International License.[233] Copyright 2013, Nature Publishing Group. **c)** Illustrations of the glucose sensing mechanism and the enzyme-free gel electrode as the gate of glucose sensing OECTs. Reproduced with permission.[238] Copyright 2018, Wiley-VCH. **d)** Schematic revealing the ionic liquid facilitated phase separation in PEDOT:PSS. Reproduced under the terms of Creative Commons Attribution NonCommercial License 4.0.[242] Copyright 2017, AAAS.

Figure 12. Ionically conductive hydrogel-based bioelectronic interfaces. **a)** Hydrogel coated electrode demonstrating the reduction in the local strain field as indicated in the particle image velocimetry. Reproduced under the terms of Creative Commons Attribution 4.0 International License.[259] Copyright 2017, Nature Publishing Group. **b)** Schematic depicting the working mechanism of the implanted hydrogel electrode based on the formation of an EDL capacitor across the interface of the hydrogel and the metallic electrode. Reproduced with permission.[103] Copyright 2019, Elsevier. **c)** Schematic and photograph of the salt/PEG ATPS based interface for in vivo electrostimulation of the skeletal muscle of a mice (top). Scale bar, 1 cm; comparison of localized

heating when high current is injected from different electrodes (bottom). Reproduced with permission.[105] Copyright 2018, Wiley-VCH. **d)** Schematic of the hydrogel fiber electrode used for simultaneous neural recording and optical stimulation. **e)** Photographs of the hydrogel fiber electrode with the laser switched off and on and photograph of the mouse implanted with the hydrogel fiber electrode. Reproduced with permission.[103] Copyright 2019, Elsevier.

Figure 13. Electrically conductive hydrogel-based bioelectronic interfaces. **a)** Micrographs of the flexible micro-electrode coated with PEDOT-CNT nanocomposite and encapsulated with human fibrin-based hydrogel. Reproduced with permission.[275] Copyright 2013, American Chemical Society. **b)** Schematic of the fabrication process of the interpenetrating hydrogel network, formed by infiltrating a loosely crosslinked PEDOT:PSS network with a polyacrylic acid-based secondary polymer scaffold. **c)** Various geometries, shapes, and designs of the PEDOT:PSS hydrogel (left). Scale bars, 1 cm; PEDOT:PSS hydrogel with micropatterned surface (middle). Scale bar, 100 μm; the hydrogel can be stretched to 250% without damage (right). Reproduced under the terms of Creative Commons Attribution 4.0 International License.[277] Copyright 2018, Nature Publishing Group. **d)** Illustration of stepwise fabrication process of the PEDOT:PSS hydrogel through photolithography, dry etching and water exchanging. **e)** Photograph of a freestanding micropatterned PEDOT:PSS hydrogel electrode array and the zoomed-in image. Scale bars, 2 mm and 200 μm. Reproduced with permission.[93] Copyright 2019, Nature Publishing Group.

Figure 14. Research trends for future soft bioelectronic interfaces. **a)** Schematic of the self-healing process of a transparent, stretchable and self-healable ionic conductor. Reproduced with permission.[280] Copyright 2017, Wiley-VCH. **b)** Photographs showing a transient electronic module disintegrating in DI water. Reproduced with permission.[287] Copyright 2012, AAAS. **c)** 3D printed hydrogel on elastomeric substrate serving as stretchable conductors. Reproduced under the terms of Creative Commons Attribution NonCommercial License 4.0.[302] Copyright 2019, AAAS. **d)**

Schematic of the formulated MXene ink suitable for both extrusion printing and inkjet printing. Reproduced under the terms of Creative Commons Attribution 4.0 International License.[308] Copyright 2019, Nature Publishing Group. **e)** Exploded-view schematic and photograph of a miniaturized flexible NFC antenna. Reproduced with permission.[311] Copyright 2015, Wiley-VCH. **f)** Photograph of a stretchable and transparent antenna base on AgNW electrodes.[316] Copyright 2016, American Chemical Society.

Author Biographies

Dace Gao received his B.Eng. from Zhejiang University, China (2016). He is currently a Ph.D. student under the supervision of Prof. Pooi See Lee at the School of Materials Science and Engineering in Nanyang Technological University, Singapore. His research interests include soft electronics and iontronics for human-machine interface applications.

Kaushik Parida received his master's degree from Indian Institute of Technology Bombay, India. He received his Ph.D. under the supervision of Prof. Pooi See Lee at the School of Materials Science and Engineering in Nanyang Technological University, Singapore. He is currently a Research Fellow at Nanyang Technological University. His research focuses on deformable electronics, piezoelectric and triboelectric energy harvesters.

Pooi See Lee received her Ph.D. degree from National University of Singapore in 2002 in the field of semiconductor materials. In 2004, she joined the School of Materials Science and Engineering at Nanyang Technological University where she is currently a Full Professor. Her research focuses on hybrid nanomaterials for flexible and stretchable electronics, energy harvesting and storage, wearable technology and human-machine interface. She was awarded the National Research Foundation Investigatorship in 2015 and the Nanyang Research Award 2016. Prof. Lee also won the Nanyang Award for Innovation and Entrepreneurship in 2017.

Table of Contents

Keyword: bioelectronics

D. Gao, Dr. K. Parida, Prof. P. S. Lee*

Emerging Soft Conductors for Bioelectronic Interfaces

Soft and biocompatible electronic systems are beginning to revolutionize future health care. This review provides a full spectrum of recently developed soft conductors with target applications in epidermal and implantable bioelectronics, summarizes the achievements being made so far, and addresses the challenges to be solved to further advance the development of next-generation bioelectronic interfaces.